STATISTICAL ERROR ANALYSIS OF A DOA ESTIMATOR FOR A PCL SYSTEM USING THE CRAMER-RAO BOUND THEOREM

THESIS

Kerim SAY, First Lieutenant, TUAF

AFIT/GE/ENG/02M-23

DEPARTMENT OF THE AIR FORCE

AIR UNIVERSITY

AIR FORCE INSTITUTE OF TECHNOLOGY

Wright-Patterson Air Force Base, Ohio

Report Documentation Page

Report Date	Report Type	Dates Covered (from... to)
15 Mar 02	Final	Jun 01 - Mar 02

Title and Subtitle
Statistical Error Analysis of a DOA Estimator for a PCL System Using the Cramer-RAO Bound Theorem

Contract Number

Grant Number

Program Element Number

Author(s)
1st Lt TUAF Kerim Say

Project Number

Task Number

Work Unit Number

Performing Organization Name(s) and Address(es)
Air Force Institute of Technology Graduate School of Engineering and Management (AFIT/EN) 2950 P Street, Bldg 640 WPAFB, OH 45433-7765

Performing Organization Report Number
AFIT/GE/ENG/02M-23

Sponsoring/Monitoring Agency Name(s) and Address(es)
Dr. Paul Howland NATO C3 Agency P.O. Box 174 The Netherlands

Sponsor/Monitor's Acronym(s)

Sponsor/Monitor's Report Number(s)

Distribution/Availability Statement
Approved for public release, distribution unlimited

Supplementary Notes
The original document contains color images.

Abstract
Direction of Arrival (DOA) estimation of signals has been a popular research area in Signal Processing. DOA estimation also has a significant role in the object location process of Passive Coherent Location (PCL) systems. The purpose of this research is to analyze the DOA estimation errors in a PCL system. The performance of DOA estimators is studied using the Cramer-Rao Bound (CRB) Theorem. The CRB provides a lower bound on the variance of unbiased DOA estimators. Since variance is a desirable property for measuring the accuracy of an estimator, the CRB gives a good indication about the performance of an estimator. Previous DOA estimators configured with array antennas used the array antenna manifold, or the properties of the array antenna structure, to estimate signal DOA. Conventional DOA estimators use arbitrary signal (AS) structures. Constant Modulus (CM) DOA estimators restrict the input signals to a family of constant envelope signals, and when there are multiple signals in the environment, CM DOA estimators are able to separate signals from each other using the CM signal property. CM estimators then estimate the DOA for each signal individually. This research compares the CRB for AS and CM DOA estimators for a selected system. The CRB is also computed for this system when single and multiple and moving objects are present. The CRBAS and CRBCM are found to be different for the multiple signal case and moving object cases.

Subject Terms
Passive Radar, Passive Coherent Location System, Passive Sensor Location System, Bistatic Radar, Multistatic Radar, Cramer-Rao Bound, Diretion of Arrival, DOA Estimator, Array Antennas, Statistical Error Analysis

Report Classification unclassified	**Classification of this page** unclassified
Classification of Abstract unclassified	**Limitation of Abstract** UU
Number of Pages 111	

The views expressed in this document are those of the author and do not reflect the official policy or position of the United States Air Force, Department of Defense, United States Government, the corresponding agencies of any other government, NATO, or any other defense organization.

This document represents the results of research based on information obtained solely from open sources. No agency, whether United States Government or otherwise, provided any threat system parameters, or weapons systems performance data in support of the research documented herein.

AFIT/GE/ENG/02M-23

STATISTICAL ERROR ANALYSIS OF A DOA ESTIMATOR FOR A PCL SYSTEM USING THE CRAMER-RAO BOUND THEOREM

THESIS

Presented to the Faculty

Graduate School of Engineering and Management

Air Force Institute of Technology

Air University

Air Education and Training Command

In Partial Fulfillment of the Requirements for the

Degree of Master of Science in Electrical Engineering

Kerim SAY, B.S.

First Lieutenant, TUAF

March 2002

AFIT/GE/ENG/02M-23

STATISTICAL ERROR ANALYSIS OF A DOA ESTIMATOR FOR A PCL SYSTEM USING THE CRAMER-RAO BOUND THEOREM

Kerim SAY, B.S.

First Lieutenant, TUAF

Approved:

Maj. Roger L. Claypoole, Jr., PhD. Committee Chairman	15 MAR 02 Date
Andrew J. Terzuoli, PhD. Committee Member	15 Mar 2002 Date
Michael A. Temple, PhD. Committee Member	15 Mar 02 Date

Acknowledgements

I would like to thank my thesis advisor Maj. Roger L. Claypoole, Jr. for his support and guidance throughout this research. I am grateful for the friendly working environment that he created. The contributions of my committee Dr. Andrew J. Terzuoli and Dr. Michael A. Temple were also invaluable and certainly appreciated. I especially wish to thank my sponsor Dr. Paul E. Howland, who made contributions in the PCL area, for his support from great distances. I also would like to thank Dr. Erdoğan Dilaveroğlu from Uludağ University, Bursa/Turkey and Mr. Nicholas J. Willis for their advice and support.

The support and love of my family and my girlfriend were one of the major keystones in completing this research. Despite the great geographical distances, they were always there for me. I have enjoyed the sincere and professional working environment in AFIT. Therefore, I would like to extend my thanks to my colleagues from the U.S. Military Services, to the family of international officers, and especially to the Turkish Air Force officers and their families for keeping the spirit and motivation high. I want to take the opportunity to thank Lt. Ahmet Özçetin and Lt. Barış Çalıkoğlu for their professionalism and true friendship during our study sessions. I cannot finish without thanking all my true friends both here and back in Turkey; their friendship is and always will be invaluable to me.

Table of Contents

List of Figures

Notation

Scalars, Vectors, Matrices

Scalars are denoted by upper or lower case letters, as the scalars x or J.

Vectors are denoted by underlined letters, as the vector $\underline{x}$ made up of components x_i.

Matrices are denoted by upper case letters in boldface type, as the matrix **A** made up of elements A_{ij} (i^{th} row, j^{th} column).

E[.] is the expectation operator.

.* is array multiplication operator.

Superscripts

^ : Estimated, Computed, or Measured Value (not true value).

$^{-1}$: Matrix Inverse.

* : Vector or Matrix Conjugate.

^{T} : Vector or Matrix Transpose.

^{H} : Vector or Matrix Hermitian.

$\bar{}$: Real part.

~ : Imaginary Part.

Acronym List

Abbreviation	Acronym
ACMA	Algebraic Constant Modulus Algorithm
AFIT	Air Force Institute of Technology
BVR	Beyond Visual Range
CBF	Conventional Beam Forming
CM	Constant Modulus
CPI	Coherent Processing Interval
CRB	Cramer-Rao Bound
CW	Continuous Wave
DOA	Direction of Arrival
DoD	Department of Defense
ESA	Electronically Steered (Scanned) Array
FEBA	Forward Edge of Battle Area
IEEE	Institute of Electrical and Electronics Engineers
LOS	Line of Sight
ML	Maximum Likelihood
MLE	Maximum Likelihood Estimate
MSE	Mean Squared Error
MUSIC	Multiple Signal Characterization
MV	Minimum Variance
MVUB	Minimum Variance Unbiased
PCL	Passive Coherent Location
PDF	Probability Density Function
ULA	Uniform Linear Array

Abstract

Direction of Arrival (DOA) estimation of signals has been a popular research area in Signal Processing. DOA estimation also has a significant role in the object location process of Passive Coherent Location (PCL) systems. PCL systems have been in open literature since 1986 and their applications are not as clearly understood as the DOA estimation problem. However, they are the focus of many current research efforts and show much promise.

The purpose of this research is to analyze the DOA estimation errors in a PCL system. The performance of DOA estimators is studied using the Cramer-Rao Bound (CRB) Theorem. The CRB provides a lower bound on the variance of unbiased DOA estimators. Since variance is a desirable property for measuring the accuracy of an estimator, the CRB gives a good indication about the performance of an estimator.

Previous DOA estimators configured with array antennas used the array antenna manifold, or the properties of the array antenna structure, to estimate signal DOA. Conventional DOA estimators use arbitrary signal (AS) structures. Constant Modulus (CM) DOA estimators restrict the input signals to a family of constant envelope signals, and when there are multiple signals in the environment, CM DOA estimators are able to separate signals from each other

using the CM signal property. CM estimators then estimate the DOA for each signal individually.

This research compares the CRB for AS and CM DOA estimators for a selected system. The CRB is also computed for this system when single, multiple and moving objects are present. The CRB_{AS} and CRB_{CM} are found to be different for the multiple signal case and moving object cases.

STATISTICAL ERROR ANALYSIS OF A DOA ESTIMATOR FOR A PCL SYSTEM USING THE CRAMER-RAO BOUND THEOREM

1 . INTRODUCTION

1.1 Background

The leading countries in history, the super powers of their own time, have always showed great interest in scientific research and development and its applications in military matters. The lifetime of their superiority was related to how long they were able to maintain their position as scientific leaders.

Political uncertainties before WWII sent a message of the upcoming conflict and every nation was aware that there were going to be many firsts during this war, like the first use of the *Radio Detection and Ranging* (RADAR) systems. After airpower entered the warfare arena, early detection of airborne objects became of great interest, due to the importance of quick reaction against enemy airpower [1]. In the last century there have been numerous research and development efforts in different aspects of radar systems, causing the "lose sight, lose fight" concept to go *Beyond Visual Range* (BVR) of human eye. Today, there are many different types of radar systems for many different purposes and uses.

Passive Coherent Location (PCL) and the related terms are explained in Chapter 2 but basically it can be thought as a passive radar system which is composed of only a receiver unit. Most of the conventional radar concepts still apply to PCL because the illumination of the object still takes place; not by a

transmitter which is designed for this purpose but by a transmitter that is already in that environment. Advantages and disadvantages of PCL systems are discussed in Chapter 2.

1.2 Problem Statement

Monostatsic radars follow the generalizations and equations that are applicable to bistatic radar. Monostatic object location errors are functions of transmitted pulse width, antenna half power beam width, and signal-to-noise ratio [2].

There are inherent errors in object location caused by bistatic geometry in addition to the errors that are caused in monostatic radars. The most basic system architecture scenario of a PCL system is the bistatic case, which is illustrated in Figure 1. θ_T is the *transmit angle* and is the angle from the reference direction to the line between the transmitter and the object, and θ_R is the *receive angle* and is the angle from the reference direction to the line between the receiver and the object. Object location errors that apply to monostatic radars also apply to bistatic radars but object location errors in bistatic radars have additional dependence on the receive angle, θ_R [3].

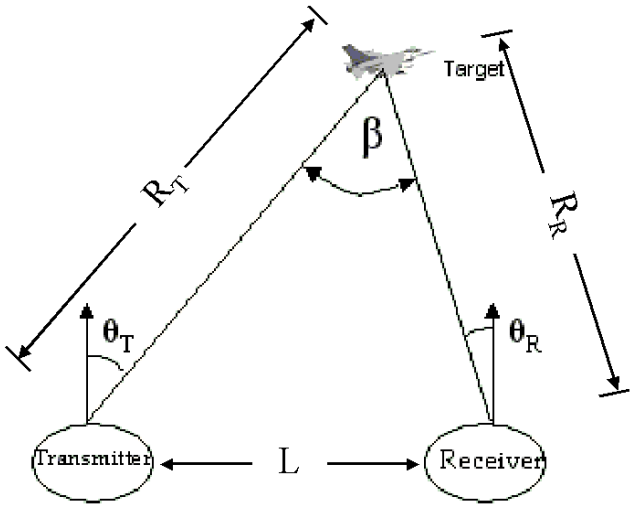

Figure 1. Transmit and Receive Angles (θ_T, θ_R).

To demonstrate the dependence of object location errors on the receive angle θ_R, let's introduce a basic object location technique for a bistatic system from [3]. Measuring the total range from the transmitter to object (R_T) and from the object to receiver (R_R) places the object on an *isorange ellipsoid* as shown in Figure 2. The range from the transmitter to an arbitrary point on this isorange ellipsoid plus the range from the same point to the receiver is the *Range Sum* (R_T+R_R). This range sum is constant for all points on an isorange ellipsoid. The foci points of the ellipsoid are the locations of the receiver and the transmitter sites.

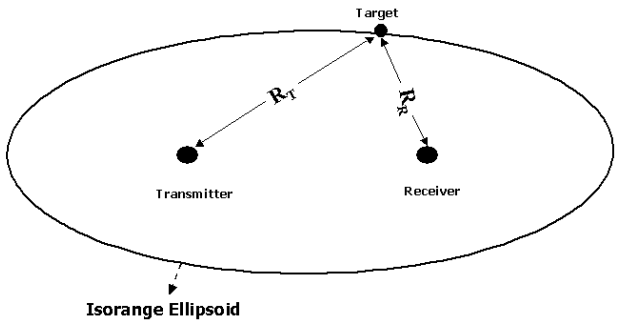

Figure 2. Isorange Ellipsoid.

Given range sum (R_T+R_R) and receive angle (θ_R), R_R is calculated by:

$$R_R = \frac{\left(R_T + R_R\right)^2 - L^2}{2\left(R_T + R_R + L\sin\left(\theta_R\right)\right)} \qquad (1)$$

where L is the baseline distance. The object is declared to be at range R_R and its direction is determined via θ_R.

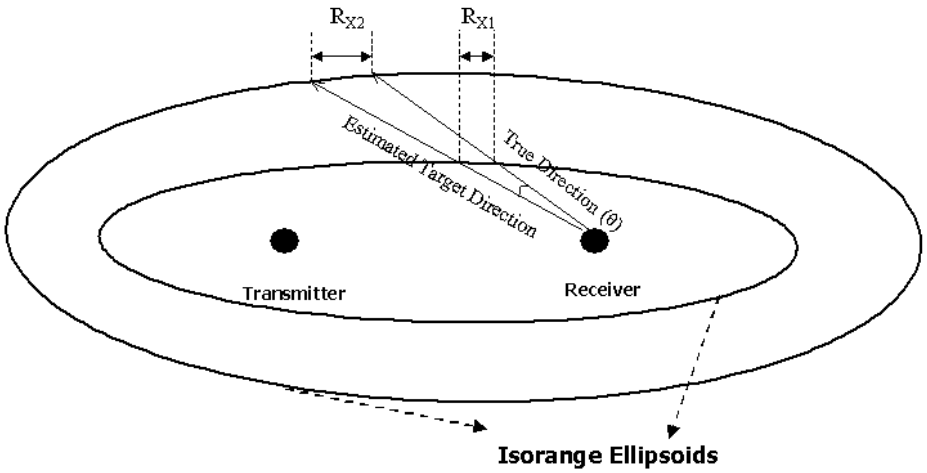

Figure 3. Isorange Ellipsoids and increasing contribution of same amount of DOA estimation error to object location with the increase in range sum.

There are many object location methods in PCL systems, with each based on different object measurements. The most basic object location technique is done by range sum measurement and DOA estimation. In Figure 3 two different isorange ellipsoids are shown for two different range sums. DOA estimation helps us determine on which point of the isorange ellipsoid the object is located. Figure 3 illustrates that for smaller range sums the error in DOA estimation has a smaller contribution to object location errors and as the object range increases the

same amount of angular error in DOA estimation leads to an increase in object location errors. When the estimated object direction is off from true object direction by some error then the spatial error in object location can be represented by R_{X1} and R_{X2}, assuming that range sum is measured correctly. R_{X1} and R_{X2} in Figure 3 are cross-range values and they demonstrate the increasing contribution of same amount of DOA estimation error to object location with the increase in object range sum.

In Figure 5, the root sum square errors are plotted versus receiver look angle (θ_R) for a bistatic system. The contribution of different kinds of object location errors for different receive angles are clearly seen. When the object is on the extended baseline shown in Figure 4 (the straight-line that passes through the transmitter and receiver, excluding the line segment between the transmitter and the receiver), transmit and receive angles are equal. This means that when an object is on the extended baseline, θ_T which is equal to θ_R, and this causes the object location errors to converge to the monostatic case [3].

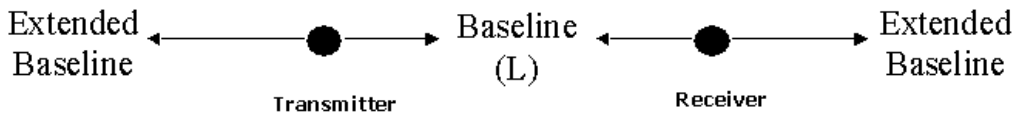

Figure 4. Baseline, and extended baseline.

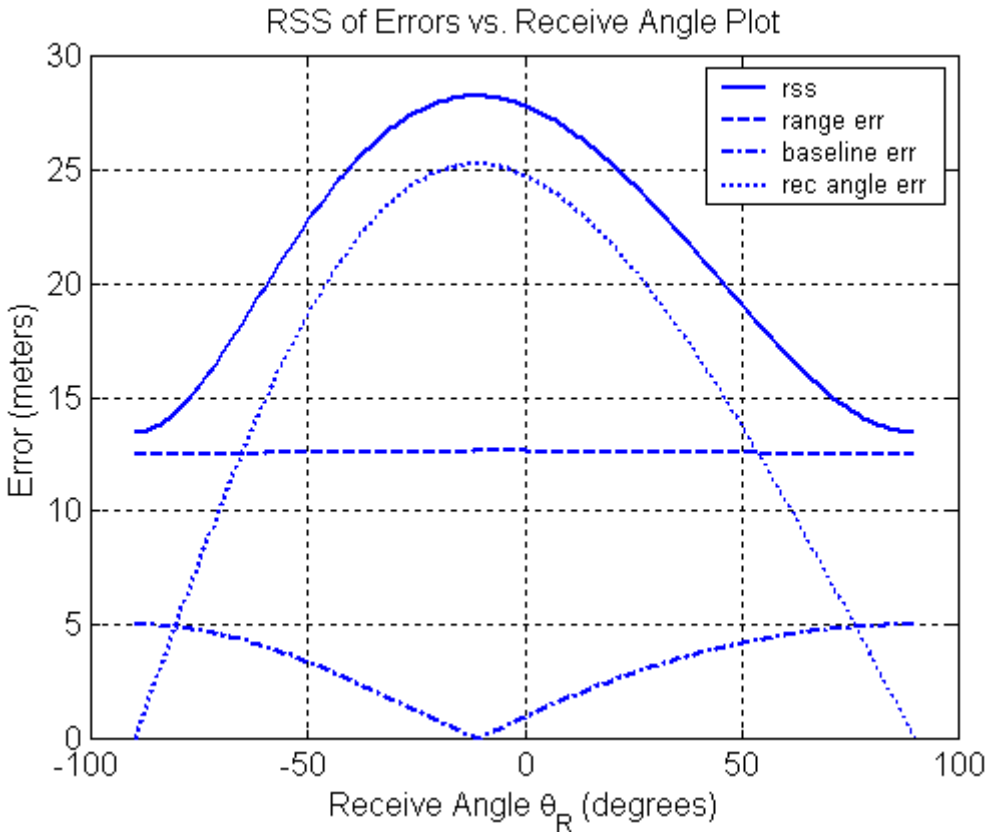

Figure 5. Root Sum Square (RSS) of range sum, baseline, and receive angle errors for the following conditions: R_T+R_R =100km, baseline distance (L) = 10 km [3].

The receive angle, θ_R, is determined by *Direction of Arrival* (DOA) estimation. As seen in Figure 5, the receive angle errors have the greatest contribution to total object location error over a wide range of receive angles. As the receive angle approaches +/- 90°, the contribution of receive angle error to total object location error is less than other errors. Section 1.5 introduces the system used in this thesis and the antenna is chosen to be an array antenna. Due to array antenna characteristics, reception using the array antenna is chosen to be in the approximate region from -70° to 70°. This region is where receive angle has the greatest contribution to total object location errors.

Keeping in mind the content of Figure 3 and Figure 5, clearly any increase in DOA estimation accuracy (receive angle estimation) leads to more accurate results in object location. The curves in Figure 5 are obtained by applying the root sum square (RSS) concept on bistatic object location technique. It is important to note that object location is not determined in this fashion for all PCL systems. However, these figures effectively illustrate the importance of accuracy in DOA estimation for a more precise estimate of object location. Since DOA estimation plays a major role in object location of PCL systems, the accuracy of DOA estimation is the primary emphasis of this thesis.

1.3 Scope

Error analysis of PCL systems is a very broad research area. There are electromagnetic based issues, signal processing based issues, hardware related issues, software related issues, etc. This thesis focuses on the signal processing side of the problem and performs statistical error analysis. As mentioned above, this analysis is performed on the most essential part of object location, the DOA estimation.

The problem is considered in two-dimensions (object altitudes are ignored). When the problem is reduced to two-dimensions, the ellipsoids in three-dimensional cases become ellipses in two-dimensional scenarios. All objects are at zero altitude and the DOA estimation problem is in azimuth only.

1.4 Approach/Methodology

Different statistical approaches in spectral estimation have introduced different algorithms in signal processing for estimating signal DOA. The performance of these algorithms is commonly measured using the variance of the DOA estimate. The *Cramer-Rao Bound* (CRB) is a statistical theorem that places a lower bound on this variance for any unbiased estimator, given the probability density function of the error is the same among those estimators [4, 5].

DOA estimation of different signals using an array antenna has become a common approach. Most algorithms such as *Multiple Signal Characterization* (MUSIC), *Maximum Likelihood Estimation* (MLE) [6] and *Conventional Beam Forming* (CBF) use the properties of array antennas or their structure and have the same statistical error probability distribution function. This is explained in more detail in Chapter 3.

Improvements in spectral estimation enabled the use of signal properties in DOA estimation, in addition to, the array manifold or properties of the array structure. In [7] an algorithm for *Constant Modulus* (CM) signals has been introduced (signals with constant envelope using phase or frequency modulation). An *Algebraic Constant Modulus Algorithm* (ACMA) uses the constant modulus property of signals and makes a source separation among signals having the CM property; the DOA estimation problem is decoupled in

multiple object scenarios, which is usually the case in real-world applications. The CM DOA estimators have a different CRB and this is explained in Chapter 3.

This thesis discusses the derivation and calculation of the CRB for estimators using common algorithms over a wider class of signals (arbitrary signals) and the CRB for estimators using CM algorithms (CM signals). Therefore, to make a distinction between the two, the CRB for *Arbitrary Signals* (AS) is denoted as CRB_{AS} and the CRB for *Constant Modulus* (CM) signals is denoted as CRB_{CM}.

The difference in the CRB of arbitrary signals and CM signals is demonstrated by calculating the CRB for different scenarios. The correlation of incoming signals is taken into account throughout the calculations. Changes in the CRB with respect to the correlation level of the signals is shown for CRB_{AS}.

1.5 System Description

The CRB is directly related to a system architecture; thus, a basic system model is established for calculating the CRB. Since all the algorithms mentioned above use array antennas, the model consists of an *Uniform Linear Array* (ULA) antenna with 16 elements and element spacing of $\lambda/2$. In each *Coherent Processing Interval* (CPI), 512 realizations (snap shots) are considered.

1.6 Assumptions

To make some approximations and simplify the problem at hand, this research is based on the following assumptions:

- This research assumes the interfering noise $\underline{e}(t)$ is circular Gaussian distributed white noise with zero mean ($E[\underline{e}(t)]=0$) and $E[\underline{e}(t)\underline{e}^H(t)] = \sigma\mathbf{I}$, where $\underline{e}(t)$ is a noise vector and $\mathbf{I}$ is the identity matrix. This is a reasonable assumption to model the noise in the environment.
- Objects are at zero altitude and DOA estimation is performed in azimuth only. This assumption simplifies the problem being faced in the real world. Therefore, the results obtained using this assumption form a baseline to extend the results to the real world scenarios.
- Object SNR remains constant during a Coherent Processing Interval (CPI). This is a reasonable assumption.
- Signal DOA remains constant during a CPI. This is a reasonable assumption because the real-world objects can be maneuvering objects. But it is a good starting point.
- The antenna is calibrated so that the array response for each DOA is known. This is a good assumption and is consistent with real-world applications.
- When calculating CRB_{CM}, all signals are assumed to be CM signals.

- Object ranges are assumed to be far enough for the signal wave fronts to be considered as plane waves. This is a reasonable assumption since this is usually the case in radar application due to the desired object detection ranges.

2 . BACKGROUND

The purpose of this chapter is to explain the Passive Coherent Location (PCL) system and its related issues. The basic terms related to PCL are explained thoroughly, and the position of a PCL system in today's Radar world is made clear.

Therefore, this chapter first discusses developments in radar, during which basic concepts that are needed for a good understanding of a PCL system are introduced. Second, the PCL system is explained, including PCL system definition, operation, characteristics, and advantages and disadvantages in both general and military applications. Next, the Cramer Rao Lower Bound Theorem is explained. Finally, phased array antennas are introduced because of the need to establish a basic understanding of the "big picture" of system description and system operation.

2.1 Development of RADAR and Basic Terms

When *Radio Detection and Ranging* (RADAR) systems are the topic, the detection of aircraft or airborne objects is the typical consideration. However, when radar was first developed the primary objects were typically naval vessels. After Hertz showed that radio waves could be reflected from metallic objects, and formed the basis for the concept of radar [8], Hulsmeyer built the first

operational radar in 1904 to detect ships [9]. Hulsmeyer's radar was *monostatic* (collocated receiving and transmitting sites).

Some coincidences also contributed to the development of radar. In 1922, Taylor and Young detected a change in the signal as a ship passed between a transmitter and receiver located on opposite sides of a river [10]. This example from history is completely compatible with today's *Continuous Wave* **(**CW**)** radar. CW Radars transmit continuously and receive while transmitting [1]. Although it is possible to build a CW radar with a collocated receiver and transmitter, CW radar applications are much easier to implement with a bistatic design than the monostatic design.

In the very early stages of radar development, detecting ships by radar was the primary concern because unlike the aircraft of that time, ships were made of metal. It wasn't until the late 1920's that aircraft manufacturers changed aircraft designs and started using metal on the fuselage and the wings (versus a wooden structure with fabric redundant cover) [1]. After this change in aviation design, detection of aircraft by radar became possible. Each country began showing interest in military radar applications for aircraft detection because of the political imbalance, which lead the world into the Second World War (WW II). The revolution in technology changed the tactics of war that would be fought. Meanwhile, aviation as a military power became of primary importance. These reasons caused radar advancement to exceed a natural development line and drew a great deal of attention to this field.

In *bistatic radars*, the transmitter and the receiver are separated, but the distance between the transmitter and the receiver is known (Figure 6). The distance between the transmitter and the receiver sites is called the *baseline distance* (L); requirements on the length of the baseline distance are vague in most texts. The IEEE description of bistatic radar also does not completely describe this baseline distance [3]. Skolnik provides better explanation; he argues that the distance should change relative to the object distance. A baseline can be relatively small for objects that are close in range. On the other hand it must be larger for the long-range objects. A different way of describing this baseline requirement is the need for two different electromagnetic paths for the propagation of the transmitted signal from transmitter to the object and propagation of the object echo from the object to the receiver [11].

Bistatic angle (β) is equal to the difference between the transmit and the receive angles θ_T and θ_R. θ_T and θ_R are defined in Section 1.2.

$$\beta = \theta_T - \theta_R \qquad (2)$$

Monostatic radar can be considered as a special case of bistatic radar with R_T equal to R_R, θ_T equal to θ_R, and L = 0. Since θ_T equals θ_R, β is equal to zero in monostatic radar. In bistatic radar applications, the bistatic angle becomes zero as the object approaches the extended baseline; this is called *over the shoulder operation*.

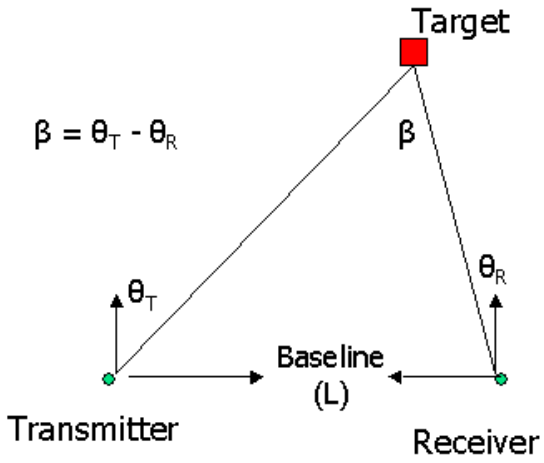

Figure 6. Bistatic Geometry and Bistatic Angle (β).

Most of the earliest radars were bistatic. In some early applications, systems were built to detect objects on the baseline between the transmitter and the receiver. This special case is called the *forward scatter* case (or forward scatter geometry). In a forward scatter case, the object echo, which is scattered forward from the object towards the receiver, is of interest rather than the object echo that is reflected back towards the transmitter. Initially, bistatic radars that could detect objects crossing the baseline using the forward scatter from the objects were developed, and they were called forward scatter fences. Japan, the Soviet Union, and France had approximately 200 of these forward scatter fences before and during WW II [3]. After forward scatter fences, use of bistatic radar was extended out of the baseline area. The Klein Heidelberg device, the first bistatic-of-opportunity system, was used by Germans in WW II [12].

Object detection and location is a much more complicated task in bistatic radars, as compared to monostatic radars. Thus, upon the invention of the duplexer, a device enabling the use of a single antenna for both transmission and reception by avoiding transmitter and receiver interference, monostatic radars gained greater popularity over bistatic radars, especially after WW II [13]. This lead to a drastic reduction in bistatic radar research.

Bistatic radar establishes a basic understanding for *multistatic* radars. When more than one receiver or more than one transmitter is used for object detection, and object detection is done coherently by establishing a network between the receiver sites, the system established is called a *multistatic system* [2]. Each transmitter and receiver pair of a multistatic system is a bistatic system. Creating a network of these basic bistatic elements turns these separate bistatic systems into a multistatic system.

Each radar measurement from a different transmitter-receiver pair (or basic bistatic element) is sent to a central station where data processing is performed. There is a natural trade-off between the coverage area of the multistatic system and the object estimates. Creating a larger common coverage area of the bistatic elements of a multistatic system can enhance object estimates, but this reduces the total coverage area of the multistatic system. If a wider coverage area is desired, then the basic bistatic elements must be spread apart, thus reducing the common coverage area. This in turn degrades the object estimation [3].

2.2 Passive Coherent Location System

There was a turn-around on the reduction of bistatic radar research around 1980s. Some applications of bistatic radar became really popular, e.g., semi-active missiles. Improvements in destroying enemy radars lead to the development of *anti-radiation missiles* (ARM). Bistatic radars are less susceptible to ARMs by locating the receiver close to the Forward Edge of Battle Area (FEBA) and the transmitter further away in a more secure environment, well out of ARMs reach. Basically in some scenarios bistatic radars have advantages over monostatic radars. This realization made the bistatic radars an interesting research topic once again.

Bistatic radars use regular radar transmitters designed for radar applications. As the researches on bistatic radars kept going new ideas such as using different transmitters were considered and that is how idea of *Passive Coherent Location* (PCL) was born.

PCL systems use ambient radio waves as a source of illumination in order to detect and track objects. The most common type of radio waves, available all around the world for this purpose, are television and FM radio broadcasts, even though they might differ somewhat from one country to another. A PCL system can be either multistatic or bistatic, depending on the kind of network and number of transmitters and receivers used in the system. The most basic form of a PCL system is the bistatic case when only one transmitter and receiver are used

for object detection and tracking [2]. Figure 7 shows the basic architecture of a PCL system.

2.2.1 Types of PCL

There are three types of PCL systems, classified with respect to the kinds of signal that they utilize to obtain object estimations. These are Narrow band PCL, Wide band PCL, and Pulsed PCL [14].

Narrow band PCL uses the narrow video carrier or audio carrier portion of a TV waveform where most of the signal energy is contained. This type of PCL enables Doppler and/or DOA measurements.

Wide band PCL uses the modulation spectrum of an FM waveform, which has a broader band. The methods used in Wide band PCL enable range and/or DOA measurements. In some cases Doppler measurements are also obtained.

Pulsed PCL system uses pulsed waveforms from pulsed radars.

2.2.2 System Operation

Most PCL systems receive a direct signal from the transmitter and another signal scattered from the object. Thus the correlation between the scattered signal from the object and direct (reference) signal will give the object's range estimate. If the reference signal is distorted by any means, this will present some deviation from the original object information. As Howland states in [2], "Accurate bearing information can be obtained using two or more antennas, using techniques such as phase interferometry, amplitude monopulse, conventional beam forming, and super resolution."

There are times when the direct signal from the transmitter interferes with the beam looking in the object direction and the receiving object information. When this occurs one of the simplest methods to get rid of this direct signal interference is to use the reference signal to cancel it out. The Adaptive beam forming technique can be used to null out most interference that might be encountered [15].

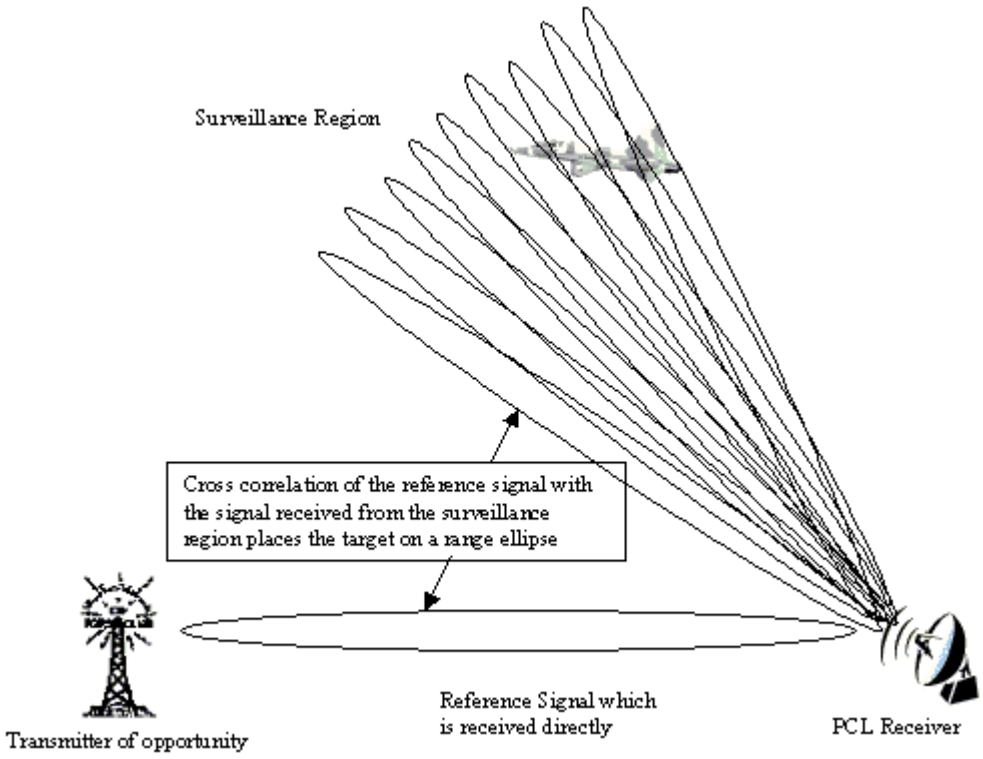

Figure 7. PCL System.

2.2.3 Characteristics of PCL

PCL is called a "coherent" system because it uses both the phase and the amplitude of the received waveform to obtain object estimates. PCL measures range, Doppler, and DOA parameters of the object when bistatic architecture is

used. In Multistatic cases, Time Difference of Arrival (TDOA) and Differential Doppler measurements are also of interest [2].

A PCL system uses a non-cooperative transmitter, which means the system has no control of the transmitter. Thus, these transmitters are also called transmitters of opportunity. A system can be designed to use different waveforms, but it is restricted to use whichever waveform exists in its environment.

Because PCL is bistatic, the transmitter and the receiver must both have clear line of sight (LOS) to the object. This requirement has to be taken into consideration for the system deployment. Because there is no control on the transmitter of opportunity, a receiver must be placed to satisfy this requirement.

Since PCL uses TV and FM radio broadcasts, which are not designed for radar processing purposes, these waveforms have poor radar ambiguity function [14]. For that reason, a PCL system must use a non-linear estimation or optimization algorithm to resolve object range, bearing, heading and velocity, as opposed to conventional radars [16].

A PCL system differs from a conventional monostatic radar system by the frequency spectrum it uses, and its bistatic or multistatic geometry [14]. Multistatic geometry enables additional object data, and as a result of this much more accurate object location estimates can be performed. A PCL system must operate in VHF and/or UHF frequency range in units of MHz; this is the frequency range used for all TV and FM radio transmissions. Most conventional

radars operate in the GHz range. Therefore, processing techniques that are used with today's conventional radar must be modified; this is an arduous task, which can be done only by the extensive use of digital processing.

2.2.4 Advantages of PCL

PCL is potentially a low cost system. It uses transmitters of opportunity as sources of illumination; the radiation sources are already out there in the environment. This saves PCL users the money that will be spent on the transmitter [16]. On the other hand, the receiver must be more complex than conventional radar to compensate for operating on a "free" transmitter, but all of the modifications can be done in software. The hardware requirements for the PCL system are the same as the equipment contained in the receiver unit of conventional radar; however, this equipment has to be designed to operate in the frequency spectrum that PCL uses.

Therefore, emphasis is on the software in PCL systems. Software does the correlation between the reference signal and the scattered signal to estimate the range, the Doppler processing, and the digital beam forming. The future improvements of the system seem to be in more robust software rather than new hardware requirements. The possible mid-life upgrade on a PCL system will most probably be cost effective.

The frequency separation among PCL systems is not as big an issue as it is in conventional radars [2]. Conventional radars are designed to transmit and receive at one or more frequencies. Today there are numerous radar designs,

and most of these radars are likely to have the same operating frequencies, thus causing an interference problem among radars using similar frequency ranges. This is not the case in PCL. VHF and UHF frequencies have many users with frequency allocation for each user; more than one PCL receiver can operate out of the same transmitter in multistatic cases. The interference problems in PCL occur by the reception of a different transmitter or scattering of different transmitter broadcasts from different objects operating at the same frequency. Once a PCL system is deployed to an area, and its set-up is complete, these kinds of interferences can be experienced. Appropriate receiver placement to exploit the terrain can be used to prevent interfering transmitter broadcasts, but object returns from these transmitter signals are harder to eliminate. These returns must be compensated for in the software.

2.2.5 Disadvantages of PCL

The most essential disadvantage of a PCL system is having no control over the transmitting site. This can be considered in two ways. The first is having no physical control over the transmitter: when to transmit, etc. The second is having no control on the transmission: the broadcast frequency, average power, the transmitted waveform, etc. Since commercial broadcasts are not designed for radar processing, they have a poor ambiguity function.

Other disadvantages are caused by the bistatic nature of the system. In order to detect an object in a surveillance region both the transmitter and the

receiver must have line of site to the desired surveillance region. When terrain is a factor this might cause severe limitations for low altitude objects.

There are also some limitations on the PCL antenna. Small antenna size is preferred due to the efforts of making the system low cost, mobile, and difficult to detect. The trade off for a smaller antenna size is reduced detection range, besides a degraded spatial resolution.

Some PCL receivers have very high receiver noise figures. This reduces thermal noise-limited detection ranges usually by a factor of two, or even more. Interference of Galactic noise is one of the reasons for this reduction. In [1], Skolnik uses the term cosmic noise instead of Galactic noise, and describes it as a continuous background caused by electromagnetic radiations from extraterrestrial sources in our own galaxy, extragalactic sources, and radio stars. Galactic noise decreases with increasing frequency. Hence, it is negligible at frequencies above UHF. However, the frequency range of most PCL systems is still affected by the Galactic noise; this contributes to the increased noise figure of the PCL receivers. Having other transmitters, or the original transmitter of opportunity in the surveillance region can also contribute to the higher noise figure in PCL receivers [14].

After giving the definition to PCL, mentioning its characteristics, advantages, and disadvantages now it is time to touch on the CRB theorem which is used in this thesis for characterizing the general performance of the DOA estimators used for PCL purposes.

2.3 Cramer-Rao Lower Bound (CRLB, CRB)

The analysis of DOA estimation uses the statistical technique Cramer-Rao Bound (CRB), which determines the best achievable estimate using the lower bound on the error variance. Therefore, the statistics of the measurement errors must be known or modeled.

In this research the Fisher information matrix depends on the likelihood function, which is expressed in terms of variance of errors in the each phase measurement of all the array antenna elements, σ. Therefore, when the Fisher matrix is inverted, the result of the CRB is a function of the measurement error variance, σ.

For this reason, CRB enables the evaluation criteria for the marginal measurement errors. From that point, accuracy of an estimate of an object's direction can be determined depending upon measurement errors and the original direction of the object.

When a parameter is being estimated, the properties of the estimator – such as variance, or bias- are usually of great concern. Greater insight for the estimator provides better insight about the actual estimate of the parameter of interest, in particular the reliability and accuracy of the estimate. More detailed discussion on these terms is available in [4, 5].

2.3.1 Unbiased Estimators

If the expected value of the estimator output is the true value of the parameter of interest then this estimator is *unbiased*. Mathematically an estimator $\hat{\theta}$ is unbiased if:

$$E\left[\hat{\theta}\right]=\theta, \quad a<\theta<b \tag{3}$$

where θ is the unknown parameter, (a,b) is the range of possible values for θ, $\hat{\theta}$ is an estimator for the parameter θ, and E[.] is the expected value operator.

2.3.2 Minimum Variance Unbiased (MVUB) Estimator

Trying to design or select an estimator from a family of estimators is difficult. Because of this some criteria are needed to compare how optimal each estimator is. *Mean Square Error* (MSE) between the estimate $\hat{\theta}$ and the true value θ is one of them and it is defined as:

$$\text{mse}\left(\hat{\theta}\right) = E\left[\left(\hat{\theta}-\theta\right)^2\right] \tag{4}$$

MSE can also be rewritten as:

$$\text{mse}\left(\hat{\theta}\right) = E\left\{\left[\left(\hat{\theta}-E\left[\hat{\theta}\right]\right)+\left(E\left[\hat{\theta}\right]-\theta\right)\right]^2\right\} \tag{5}$$

$$\text{mse}\left(\hat{\theta}\right) = E\left\{\left(\hat{\theta}-E\left[\hat{\theta}\right]\right)^2\right\} + 2\left(E\left[\hat{\theta}\right]-\mu_{\hat{\theta}}\right)\left(E\left[\hat{\theta}\right]-\theta\right) + \left(\mu_{\hat{\theta}}-\theta\right)^2 \tag{6}$$

$$\text{mse}\left(\hat{\theta}\right) = \text{var}\left(\hat{\theta}\right) + \text{bias}^2\left(\hat{\theta}\right) \tag{7}$$

where $\mu_{\hat{\theta}} = E\left[\hat{\theta}\right]$.

Since $\mu_{\hat{\theta}}$-$E\left[\hat{\theta}\right]$=0, the whole second term in Equation (6) goes to zero and the remaining part can be written as a function of the variance and the bias of the estimator.

In an unbiased estimator, the bias$^2(\hat{\theta})$ term in Equation (7) is zero. In this case, MSE is only a function of the variance and is minimized by minimizing the variance for the unbiased estimators.

In order to test whether an estimator is unbiased or not, its expected value is checked. If the expected value of an estimator is equal to the unknown parameter θ, then this estimator is unbiased as in Section 2.3.1. The discussion of *Minimum Variance* (MV) is restricted to the class of unbiased estimators.

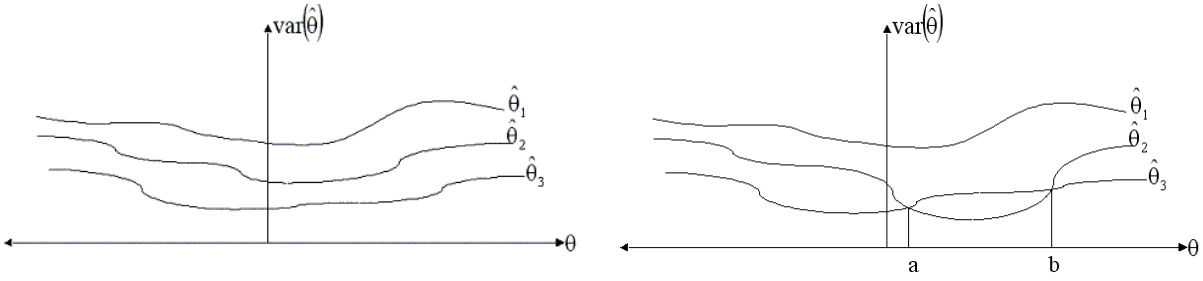

(a) (b)

Figure 8. Minimum Variance Estimators [4].

Figure 8a shows the variance of three different unbiased estimators. Since estimator $\hat{\theta}_3$ has the lowest variance for all θ in Figure 8a, it is the MV estimator. On the other hand in Figure 8b $\hat{\theta}_3$ is the MV estimator when θ<a and θ>b, and $\hat{\theta}_2$

is the MV estimator when $a < \theta < b$. In this case, there is no single MV estimator for all θ.

A *Minimum Variance Unbiased* (MVUB) estimator is an unbiased estimator that has the minimum variance for all the unknown parameter θ. Sometimes no MVUB estimator can be found in the search for an estimator. MVUB estimators do not always exist. The MSE of an MVUB estimator is equal to its variance.

2.3.3 Likelihood, Log-likelihood, and Score Functions

Observed data enables the estimation of the unknown parameter. Since observed data is dependent on the pdf of the data, estimation starts with the determination of the pdf for that data. If the pdf of the observed data is independent of the desired parameter, then that parameter cannot be estimated using that set of data. The pdf of a random variable X parameterized by the unknown parameter θ is denoted as $f_\theta(X)$.

A simple example makes it easier to understand this concept. Let x be the observed or measured data, n be additive white gaussian noise with zero mean and variance σ^2, and θ be the unknown parameter. The relation between these terms are formulized as

$$x[t] = \psi + n[t].$$

In this case a good estimator for θ is $\hat{\theta} = x[t]$. Since $E\{\hat{\theta}\} = E\{x[t]\} = \theta$, $\hat{\theta}$ is an unbiased estimator. Its variance is σ^2 and the accuracy of the estimator gets better as σ^2 decreases and the pdf is $f_\psi(x) = \frac{1}{\sqrt{2\pi\sigma^2}} \exp\left[-\frac{1}{2\sigma^2}(x[t]-\psi)^2\right]$.

"When the pdf is viewed as a function of the unknown parameter (with **x** - the data- fixed) it is termed the *Likelihood Function*" [4]. Since X is a random variable the change in X is random. Fixing X is done via inputting a set of observation data to the joint pdf of X and θ ($f_\theta(X)$). $\hat{x}$ is denoted as the observed data and the mathematical representation of the likelihood function is:

$$l\left(\theta,\hat{X}\right) = f_\theta\left(\hat{X}\right) \tag{8}$$

and the *Log-Likelihood Function* is simply the natural log of the likelihood function:

$$L\left(\theta,\hat{X}\right) = \ln\left[l\left(\theta,\hat{X}\right)\right] = \ln\left[\ f_\theta\left(\hat{X}\right)\ \right]. \tag{9}$$

Differentiating the log-likelihood function with respect to θ gives the *score function* [5], whose mathematical representation is

$$s\left(\theta,\hat{X}\right) = \frac{\partial}{\partial\theta}L\left(\theta,\hat{X}\right) = \frac{\partial}{\partial\theta}\ln\left[l\left(\theta,\hat{X}\right)\right] \tag{10}$$

The maximum likelihood estimate (MLE) of $\hat{\theta}$ is found by setting the score function equal to zero and solving for $\hat{\theta}$.

$$s\left(\hat{\theta},\hat{X}\right) = 0 \tag{11}$$

This is equivalent to finding the maximum of $f_\theta\left(\hat{\mathbf{X}}\right)$.

Using x instead of $\hat{x}$, which represents the observed data is usually done for notational convenience and this notation is also used in this thesis.

2.3.4 Cramer-Rao Bound Theorem

The *Cramer-Rao Bound* is a lower bound on the covariance matrix of any unbiased estimator of parameter θ. Thus, no unbiased estimator can exist whose variance is lower than the CRB for each value that θ can take in the parameter space. An unbiased estimator that attains the CRB is by definition the MVUB estimator. Thus, the CRB is a great aid to determine if an unbiased estimator is the MVUB. It sets a benchmark against which we can compare the performance of an unbiased estimator.

As mentioned above, values of $\hat{\theta}$ that makes the score function equal to zero are Maximum Likelihood (ML) estimates for θ. The score function has mean zero; in [4] this is called the *Regularity Condition* and mathematically:

$$E\left[s(\theta,\mathbf{X})\right] = E\left[\frac{\partial}{\partial\theta}\ln f_\theta(\mathbf{X})\right] = \int_{-\infty}^{\infty} dx\, f_\theta(\mathbf{X})\ \frac{\partial}{\partial\theta}\ln\left(f_\theta(\mathbf{X})\right)$$

$$= \int_{-\infty}^{\infty} dx\, f_\theta(\mathbf{X})\ \frac{1}{f_\theta(\mathbf{X})}\ \frac{\partial}{\partial\theta}\left(f_\theta(\mathbf{X})\right) = \frac{\partial}{\partial\theta}\int_{-\infty}^{\infty} f_\theta(\mathbf{X})\, dx\ = \frac{\partial}{\partial\theta}1 = 0 \qquad (12)$$

The *Fisher Information Matrix* ($\mathbf{J}(\theta)$) is the covariance matrix of the score function:

$$\mathbf{J}(\theta) = E\left[s(\theta,\mathbf{X})s^T(\theta,\mathbf{X})\right] = E\left[\frac{\partial}{\partial\theta}\ln f_\theta(\mathbf{X})\left(\frac{\partial}{\partial\theta}\ln f_\theta(\mathbf{X})\right)^T\right] \qquad (13)$$

Some simplifications in (13) lead to another formula for the Fisher Information matrix [5]:

$$\mathbf{J}(\theta) = -\mathrm{E}\left[\frac{\partial}{\partial\theta}\left(\frac{\partial}{\partial\theta}\ln f_\theta(\mathbf{X})\right)^{\mathrm{T}}\right] \tag{14}$$

The individual elements of the Fisher Information matrix can be found by:

$$\begin{aligned} J_{ij} &= \mathrm{E}\left[\frac{\partial}{\partial\theta_i}\ln f_\theta(\mathbf{X})\frac{\partial}{\partial\theta_j}\ln f_\theta(\mathbf{X})\right] \\ &= \mathrm{E}\left[-\frac{\partial^2}{\partial\theta_i\partial\theta_j}\ln f_\theta(\mathbf{X})\right] \end{aligned} \tag{15}$$

The Cramer-Rao Bound theorem indicates that each diagonal element of the covariance matrix ($\mathbf{C}_{\hat{\theta}}$) of an unbiased estimator $\hat{\theta}$ is greater than or equal to the corresponding element of the matrix obtained by inversing the Fisher Information matrix. This also means that $\mathbf{J}(\theta)$ has to be invertible. That is,

$$\mathbf{C}_{\hat{\theta}} \geq \mathbf{J}^{-1}(\theta) \tag{16}$$

The (i,i) element of $\mathbf{C}_{\hat{\theta}}$ is the mean-squared error of the $\hat{\theta}_i$ estimate of the unknown parameter θ_i and the (i,i) element of $\mathbf{J}^{-1}(\theta)$ lower bounds it:

$$\mathrm{C}_{\hat{\theta}_{ii}} = \mathrm{E}\left[\left(\hat{\theta} - \theta\right)^2\right] \geq \mathrm{J}_{ii}^{-1}(\theta). \tag{17}$$

An *efficient estimator* is an unbiased estimator whose covariance matrix is equal to the inverse of Fisher Information matrix [5]:

$$\mathbf{C}_{\hat{\theta}} = \mathbf{J}^{-1}(\theta). \tag{18}$$

Each efficient estimator is the MVUB estimator but the opposite is not true.

2.4 Phased Array Antennas

Phased Array Antennas are mounted on a steady platform and their beam is steered electronically instead of moving the platform of the antenna to mechanically change the direction of the beam. Controlling the phase difference of the radiating elements both at transmission and reception does the electronic steering (Figure 9). Therefore in some literature these antennas are also called *Electronically Steered Array Antennas* (ESAs).

[1, 17, 18, 19] present more detailed information on phased array antennas; here the relation between the phase delay between the radiating elements and the desired angle of transmission/reception is shown.

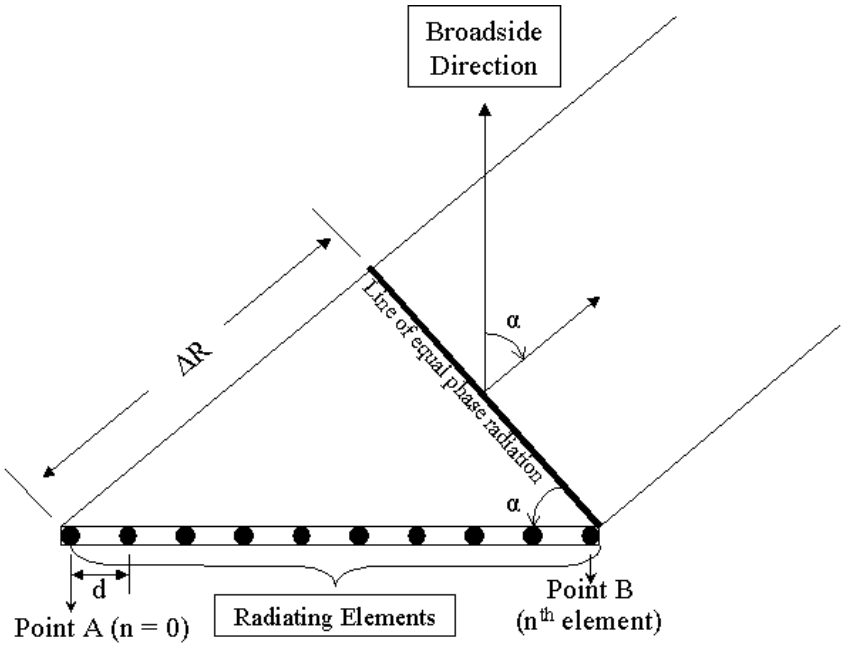

Figure 9. Phased Array Antenna [17].

In Figure 9, it can be seen that the radiating element in point A must lead the other radiating elements. Each element leads the one that is located on its

right side (because of the way it is illustrated in Figure 9). When all the elements of an array antenna are uniformly separated, this type of antenna is called *Uniform Linear Array* (ULA). In a ULA the phase difference between any of the two elements located next to each other is the same.

The total change in phase over a distance of one wavelength (λ) is 2π. The ratio of 2π to λ gives the phase per unit distance. Phase difference ($\Delta\Phi$) over a specific distance (ΔR) is:

$$\Delta\Phi = \frac{2\pi}{\lambda}\Delta R \qquad (19)$$

As can be seen from Figure 9, ΔR is equal to $\Delta R = (n-1)\times d\,\mathbf{sin}(\alpha)$. Substituting this into (19) yields:

$$\Delta\Phi = \frac{2\pi}{\lambda}\times(n-1)d\ \mathbf{sin}(\alpha) \qquad (20)$$

where α is the angle off broadside of the antenna, the angle between the antenna broadside direction and the direction that the main beam is pointing at.

$\Delta\Phi$ is the total phase difference between the first and last elements. Element to element phase difference is the same between all the elements of a ULA and it can be calculated by (20) by substituting 2 for n. Result of this is the phase difference between the first and the second elements, which is equal to the phase differences between all the adjacent elements.

The phase differences calculated using the formulas above hold in theory but in real life this might not be the case. The near field interaction of the radiating elements (also called mutual coupling of the elements) affects the

radiation pattern. Therefore each antenna must be calibrated in order to steer the beam to the exact angle off the antenna broadside direction.

2.5 Summary

This chapter explained the terms required for a better understanding of PCL systems and discussed PCL characteristics, advantages, and disadvantages. The CRB theorem was discussed, and the use of array antennas in the DOA estimation applications was shown. All of these sections mentioned above provide insight for the methodology outlined in Chapter 3.

3 . METHODOLOGY

As mentioned in Section 2.4 the phase differences between the elements under noise free conditions results with Equation (20). But the noise measured along with the signals affects the measured phase differences between the array elements and therefore, additive noise contributing to the measurements causes the error in DOA estimation when using array antennas. In order to determine the CRB for an estimator, the statistical distribution of the error or pdf of the interfering noise must be known. If these statistics are unknown, then they must be modeled as accurately as possible.

3.1 System Model

As mentioned shortly in Chapter 1 a Uniform Linear Array (ULA) antenna is modeled whose element spacing is half a wavelength or $\lambda/2$. The number of antenna elements is m =16; the number of realizations (or snap shots) N = 512. n is the number of signals impinging on the antenna.

Figure 10 illustrates how the DOA angles are referenced throughout this thesis. 0° represent the antenna broadside direction; the angle is measured in a clockwise fashion, 90°represents a one quarter rotation to the right, while -90° is a rotation to the left. Thus, -90° and 90° can also be referred as 90° left and 90° right.

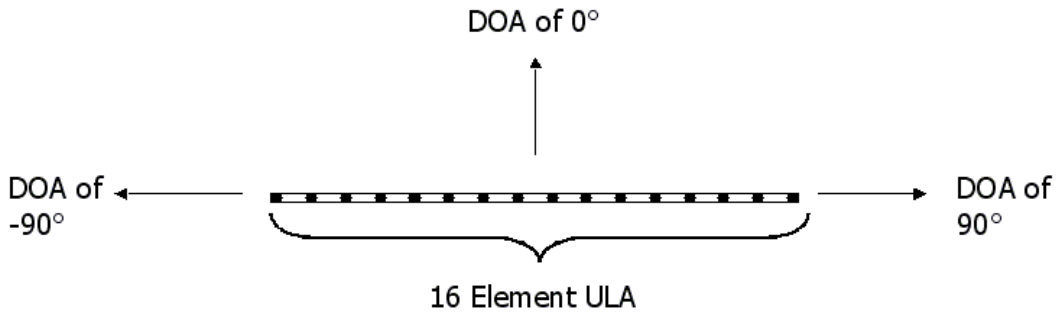

Figure 10. Direction of Arrival Angles with respect to the antenna.

3.2 Derivation of CRB for Arbitrary Signals (CRB_{AS})

Derivation of CRB_{AS} for DOA follows [6]. Measured data can be modeled by,

$$\underline{y}(t) = \mathbf{A}(\underline{\theta}_R)\underline{x}(t) + \underline{e}(t) \qquad t = 1, 2, \cdots, N \tag{21}$$

where

$\underline{y}(t)$ is a m-by-1 data vector including measurement noise,

$\underline{x}(t)$ is a n-by-1 vector and its elements are signal amplitudes,

$\underline{e}(t)$ is the m-by-1 noise vector,

A is a m-by-n array response matrix, which is given by Equation (22).

$$\mathbf{A}(\underline{\theta}_R) = \left[\underline{a}(\theta_{R1}) \ \cdots \ \underline{a}(\theta_{Rn})\right] \tag{22}$$

Each $\underline{a}(\theta_{Ri})$ in Equation (22) is a steering vector of the i^{th} signal and contains the phase delays of the corresponding elements; $\underline{\theta}_R$ is a n-element receive angle (DOA) vector whose elements are real parameters $[\theta_{R1}, \ldots, \theta_{Rn}]^T$. One must be cautious with notation. θ all by itself represents the unknown parameters, as

mentioned in the definition of CRB in Section 2.3, and θ_R represents the DOA or receive angle.

Figure 11 shows how additive noise affects the measured signal in one channel of the array. The in-coming signal is corrupted by an in-phase (real part, $\bar{e}_i(t)$) and quadrature (imaginary part, $\tilde{e}_i(t)$) component of the noise ($e_i(t)$ indicates the i^{th} element of noise vector $\underline{e}(t)$). The resultant phase error is ψ_e which causes DOA estimates to deviate from the true value.

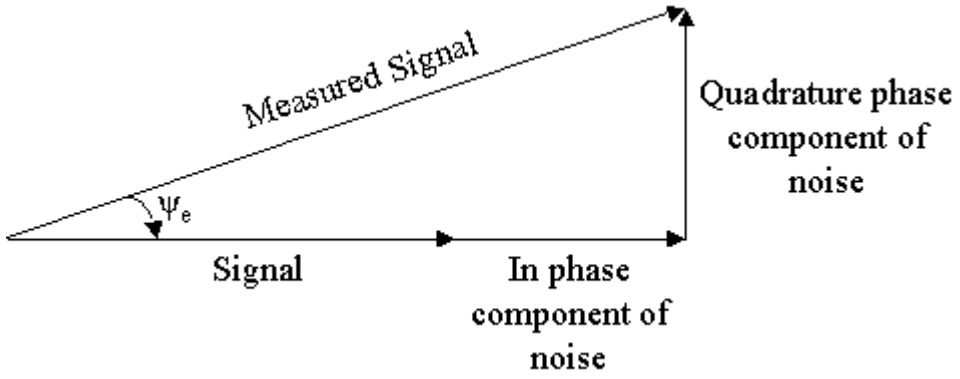

Figure 11. In Phase and Quadrature components of additive noise [16].

From Equation (21) $\underline{e}(t)$ can be written as in Equation (23):

$$\underline{e}(t) = \underline{y}(t) - \mathbf{A}\underline{x}(t) \qquad (23)$$

In Section 1.6, each noise vector $\underline{e}(t)$ is assumed to have a circular Gaussian distribution with zero-mean and covariance $\sigma\mathbf{I}$. (For more information on circular Gaussian distributions see [20]). Therefore, random matrix $\mathbf{E}_c$ which is formed from N random vectors and given by Equation (24), is circular Gaussian distributed (subscript "c" denotes circular):

$$\mathbf{E}_C = \left[\, \underline{e}(1), \underline{e}(2), \cdots, \underline{e}(N) \,\right] \tag{24}$$

Since $\underline{e}(t) = \underline{\bar{e}}(t) + j\underline{\tilde{e}}(t)$ and both $\underline{\bar{e}}(t)$ and $\underline{\tilde{e}}(t)$ are real-valued, a real random matrix $\mathbf{E}_R$ can be formed as in Equation (25), and each random vector, either $\underline{\bar{e}}(t)$ or $\underline{\tilde{e}}(t)$ forming $\mathbf{E}_R$, has a Gaussian distribution with zero mean and covariance of $(\sigma/2)\mathbf{I}$ (subscript "R" denotes real):

$$\mathbf{E}_R = \left[\bar{\mathbf{E}}, \tilde{\mathbf{E}}\right] = \left[\underline{\bar{e}}(1), \underline{\bar{e}}(2), \cdots, \underline{\bar{e}}(N), \underline{\tilde{e}}(1), \underline{\tilde{e}}(2), \cdots, \underline{\tilde{e}}(N)\right] \tag{25}$$

Since the real and the imaginary parts are statistically independent, the multidimensional Gaussian pdf [21] for the measured data $\underline{y}(t)$ is dependent on the set of unknown parameters $\underline{\theta}$ and can be written as in Equation (26):

$$\begin{aligned} F_{\underline{\theta}}(\mathbf{Y}) &= \prod_{t=1}^{N} P\left(\underline{Y}(t) \le \underline{y}(t), \underline{\theta}\right) = \prod_{t=1}^{N} P\left(\underline{\bar{Y}}(t) + j\underline{\tilde{Y}}(t) \le \underline{\bar{y}}(t) + j\underline{\tilde{y}}(t), \underline{\theta}\right) \\ &= \prod_{t=1}^{N} P\left(\underline{\bar{Y}}(t) \le \underline{\bar{y}}(t), \underline{\theta}\right) \prod_{t=1}^{N} P\left(\underline{\tilde{Y}}(t) \le \underline{\tilde{y}}(t), \underline{\theta}\right) = F_{\underline{\theta}}\left(\bar{\mathbf{Y}}\right) F_{\underline{\theta}}\left(\tilde{\mathbf{Y}}\right) \end{aligned}$$

$$f_{\underline{\theta}}(\mathbf{Y}) = \nabla_Y F_{\underline{\theta}}(\mathbf{Y}) = \nabla_{\bar{Y}} F_{\underline{\theta}}\left(\bar{\mathbf{Y}}\right) \times \nabla_{\tilde{Y}} F_{\underline{\theta}}\left(\tilde{\mathbf{Y}}\right) = f_{\underline{\theta}}\left(\bar{\mathbf{Y}}\right) \times f_{\underline{\theta}}\left(\tilde{\mathbf{Y}}\right)$$

$$\begin{aligned} f_{\underline{\theta}}(\mathbf{Y}) = {} & (2\pi)^{-Nm/2} \left\{\det(\mathbf{K})\right\}^{-N/2} \exp\left\{-\frac{1}{2}\sum_{t=1}^{N}\left(\underline{\bar{y}}(t) - \mathbf{A}\underline{\bar{x}}(t)\right)^T \mathbf{K}^{-1}\left(\underline{\bar{y}}(t) - \mathbf{A}\underline{\bar{x}}(t)\right)\right\} \\ & \times (2\pi)^{-Nm/2} \left\{\det(\mathbf{K})\right\}^{-N/2} \exp\left\{-\frac{1}{2}\sum_{t=1}^{N}\left(\underline{\tilde{y}}(t) - \mathbf{A}\underline{\tilde{x}}(t)\right)^T \mathbf{K}^{-1}\left(\underline{\tilde{y}}(t) - \mathbf{A}\underline{\tilde{x}}(t)\right)\right\} \end{aligned} \tag{26}$$

Since covariance matrix $\mathbf{K}$ is given as $(\sigma/2)\mathbf{I}$ for each $\underline{\bar{y}}(t)$ and $\underline{\tilde{y}}(t)$, Equation (26) takes the form of:

$$f_{\underline{\theta}}(\mathbf{Y})=(2\pi)^{-Nm}\left(\frac{\sigma}{2}\right)^{-Nm}\exp\left\{-\frac{1}{\sigma}\left(\sum_{t=1}^{N}\left(\underline{\overline{y}}(t)-\mathbf{A}\underline{\overline{x}}(t)\right)^{T}\left(\underline{\overline{y}}(t)-\mathbf{A}\underline{\overline{x}}(t)\right)+\sum_{t=1}^{N}\left(\underline{\tilde{y}}(t)-\mathbf{A}\underline{\tilde{x}}(t)\right)^{T}\left(\underline{\tilde{y}}(t)-\mathbf{A}\underline{\tilde{x}}(t)\right)\right)\right\}$$

$$f_{\underline{\theta}}(\mathbf{Y})=(2\pi)^{-Nm}\left(\frac{\sigma}{2}\right)^{-Nm}\exp\left\{-\frac{1}{\sigma}\sum_{t=1}^{N}\left(\underline{y}(t)-\mathbf{A}\underline{x}(t)\right)^{H}\left(\underline{y}(t)-\mathbf{A}\underline{x}(t)\right)\right\} \quad (27)$$

The likelihood and log-likelihood functions simply become,

$$l(\underline{\theta},\mathbf{Y})=(2\pi)^{-Nm}\left(\frac{\sigma}{2}\right)^{-Nm}\exp\left\{-\frac{1}{\sigma}\sum_{t=1}^{N}\underline{e}(t)^{H}\,\underline{e}(t)\right\} \quad (28)$$

$$L(\underline{\theta},\mathbf{Y})=\ln\left\{l(\underline{\theta},\mathbf{Y})\right\}=\text{const - Nm}\ln(\sigma)\ -\ \frac{1}{\sigma}\sum_{t=1}^{N}\underline{e}(t)^{H}\,\underline{e}(t) \quad (29)$$

where the vector of unknown parameters $\underline{\theta} = [\sigma\ \ \underline{\overline{x}}^{T}(t)\ \ \underline{\tilde{x}}^{T}(t)\ \ \underline{\theta}_R]^T$.

The derivation of CRB_{AS} follows from [6]. The derivate of the log-likelihood function $L(\underline{\theta},\mathbf{Y})$ is taken with respect to the unknown parameters σ, $\underline{\overline{x}}^{T}(t)$, $\underline{\tilde{x}}^{T}(t)$, $\underline{\theta}_R$ in Equations (30), (31), (32), and (33):

$$s(\sigma,\mathbf{Y})=\frac{\partial}{\partial\sigma}L(\underline{\theta},\mathbf{Y})=-\frac{mN}{\sigma}+\frac{1}{\sigma^{2}}\sum_{t=1}^{N}\underline{e}^{H}(t)\,\underline{e}(t) \quad (30)$$

$$\begin{aligned}s(\underline{\overline{x}}(k),\mathbf{Y})&=\frac{\partial}{\partial\underline{\overline{x}}(k)}L(\underline{\theta},\mathbf{Y})=\frac{1}{\sigma}\left[\mathbf{A}^{H}\underline{e}(k)+\mathbf{A}^{T}\underline{e}^{*}(k)\right]\\&=\frac{2}{\sigma}\mathbf{Re}\left\{\mathbf{A}^{H}\underline{e}(k)\right\}\qquad\qquad k=1,\cdots,N\end{aligned} \quad (31)$$

$$\begin{aligned}s(\underline{\tilde{x}}(k),\mathbf{Y})&=\frac{\partial}{\partial\underline{\tilde{x}}(k)}L(\underline{\theta},\mathbf{Y})=\frac{1}{\sigma}\left[-j\mathbf{A}^{H}\underline{e}(k)+j\mathbf{A}^{T}\underline{e}^{*}(k)\right]\\&=\frac{2}{\sigma}\mathbf{Im}\left\{\mathbf{A}^{H}\underline{e}(k)\right\}\qquad\qquad k=1,\cdots,N\end{aligned} \quad (32)$$

$$s(\theta_{Ri}, \mathbf{Y}) = \frac{\partial}{\partial \theta_{Ri}} L(\underline{\theta}, \mathbf{Y}) = \frac{2}{\sigma} \sum_{t=1}^{N} \mathbf{Re}\left\{ \underline{x}^{H}(t) \frac{d\mathbf{A}^{H}}{d\theta_{Ri}} \underline{e}(t) \right\} \qquad (33)$$

$$i = 1, \cdots, n$$

Define new matrices, **D** and **X** as:

$$\mathbf{D} = [\underline{d}(\theta_{R1}), \cdots, \underline{d}(\theta_{Rn})] = \left[\frac{d\underline{a}(\theta_{R1})}{d\theta_{R1}}, \cdots, \frac{d\underline{a}(\theta_{Rn})}{d\theta_{Rn}} \right]$$

$$\mathbf{X}(t) = \mathrm{diag}(\underline{x}(t)) = \begin{bmatrix} x_1(t) & & 0 \\ & \ddots & \\ 0 & & x_n(t) \end{bmatrix}$$

Using **D** and **X**, Equation (33) can be rewritten as:

$$s(\underline{\theta}_R, \mathbf{Y}) = \frac{\partial}{\partial \underline{\theta}_R} L(\underline{\theta}, \mathbf{Y}) = \frac{2}{\sigma} \sum_{t=1}^{N} \mathbf{Re}\left\{ \mathbf{X}^{H}(t) \mathbf{D}^{H} \underline{e}(t) \right\} \qquad (34)$$

CRB_{AS} is given by:

$$\mathbf{J}^{-1} = \left\{ E\left[s(\underline{\theta}, \mathbf{Y}) s^{T}(\underline{\theta}, \mathbf{Y}) \right] \right\}^{-1} \qquad (35)$$

where $s(\theta, \mathbf{Y})$ is called the *score function*, and **J** is the *Fisher Information matrix* as explained in Section 2.3. The score function is given by Equation (10).

The derivation of the Fisher Information matrix is shown below. The covariance of $s(\underline{\theta}, \mathbf{Y})$ must be computed. The first step is to compute the correlation of each unknown parameter with itself, and with the other unknown parameters.

$$E\left[s(\sigma,\mathbf{Y})^2\right]=E\left[\left(-\frac{mN}{\sigma}+\frac{1}{\sigma^2}\sum_{t=1}^{N}\underline{e}^H(t)\underline{e}(t)\right)^2\right]$$
$$=\frac{m^2N^2}{\sigma^2}-\frac{2mN}{\sigma^3}\sum_{t=1}^{N}E\left[\underline{e}^H(t)\underline{e}(t)\right]+\frac{1}{\sigma^4}\sum_{t=1}^{N}\sum_{s=1}^{N}E\left[\underline{e}^H(t)\underline{e}(t)\underline{e}^H(s)\underline{e}(s)\right]$$

Since $E\left[\underline{e}^H(t)\ \underline{e}(t)\right]=m\sigma$ and $\underline{e}(t)$ independent of $\underline{e}(s)$ for all $s\neq t$

$$E\left[\underline{e}^H(t)\ \underline{e}(t)\ \underline{e}^H(s)\ \underline{e}(s)\right]=\begin{cases}m^2\sigma^2 & \text{for } t\neq s\\ m(m+1)\sigma^2 & \text{for } t=s\end{cases}$$

(for proof see PRF 1 in Appendix A), $E[s(\sigma,\mathbf{Y})^2]$ takes the form of:

$$E\left[s(\sigma,\mathbf{Y})^2\right]=\frac{m^2N^2}{\sigma^2}-\frac{2m^2N^2}{\sigma^2}+\frac{Nm}{\sigma^2}\left[(N-1)m+(m+1)\right]=\frac{mN}{\sigma^2}\qquad(36)$$

Using $E\left[\underline{e}^H(t)\ \underline{e}(t)\ \underline{e}^H(s)\right]=0$ (See Appendix A for proof), $s(\sigma,\mathbf{Y})$ is uncorrelated with the other score functions for the remaining unknown parameters.

To simplify the equations written below, transformations between the real and imaginary parts of different complex variables, which are given in Appendix A for all t and s, are used.

$E\left[s\left(\underline{\bar{x}}(k),\mathbf{Y}\right)\ s^T\left(\underline{\bar{x}}(p),\mathbf{Y}\right)\right]$ is found below using (31).

$$E\left[s\left(\underline{\bar{x}}(k),\mathbf{Y}\right)\ s^T\left(\underline{\bar{x}}(p),\mathbf{Y}\right)\right]=E\left[\frac{2}{\sigma}\mathrm{Re}\left\{\mathbf{A}^H\underline{e}(k)\right\}\frac{2}{\sigma}\mathrm{Re}\left\{\underline{e}^T(p)\mathbf{A}^*\right\}\right]$$
$$=\frac{4}{\sigma^2}\frac{1}{2}\left(\mathrm{Re}\left\{\mathbf{A}^HE\left[\underline{e}(k)\ \underline{e}^T(p)\right]\mathbf{A}^*\right\}+\mathrm{Re}\left\{\mathbf{A}^HE\left[\underline{e}(k)\underline{e}^H(p)\right]\mathbf{A}\right\}\right)\qquad(37)$$

$$E\left[\underline{e}(t)\ \underline{e}^T(s)\right]=0\qquad(38)$$

$$E\left[\underline{e}(t)\ \underline{e}^{H}(s)\right]=\sigma\mathbf{I} \tag{39}$$

Substituting Equations (38) and(39) in Equation (37) leads to Equation (40).

$$E\left[s(\underline{\bar{x}}(k),\mathbf{Y})s^{T}(\underline{\bar{x}}(p),\mathbf{Y})\right]=\frac{2}{\sigma}\mathbf{Re}\left\{\mathbf{A}^{H}\mathbf{A}\right\}\delta_{k,p} \tag{40}$$

$E\left[s(\underline{\bar{x}}(k),\mathbf{Y})s^{T}(\underline{\tilde{x}}(p),\mathbf{Y})\right]$ is found in a similar manner from Equations (31), and (32).

$$\begin{aligned}E\left[s(\underline{\bar{x}}(k),\mathbf{Y})s^{T}(\underline{\tilde{x}}(p),\mathbf{Y})\right]&=E\left[\frac{2}{\sigma}\mathbf{Re}\left\{\mathbf{A}^{H}\underline{e}(k)\right\}\frac{2}{\sigma}\mathbf{Im}\left\{\underline{e}^{T}(p)\mathbf{A}^{*}\right\}\right]\\&=\frac{2}{\sigma^{2}}\left(\mathbf{Im}\left\{\mathbf{A}^{H}E\left[\underline{e}(k)\underline{e}^{T}(p)\right]\mathbf{A}^{*}\right\}-\mathbf{Im}\left\{\mathbf{A}^{H}E\left[\underline{e}(k)\underline{e}^{H}(p)\right]\mathbf{A}\right\}\right)\end{aligned} \tag{41}$$

Substituting Equations (38) and(39) in Equation (41) leads to Equation (42).

$$E\left[s(\underline{\bar{x}}(k),\mathbf{Y})s^{T}(\underline{\tilde{x}}(p),\mathbf{Y})\right]=-\frac{2}{\sigma}\mathbf{Im}\left\{\mathbf{A}^{H}\mathbf{A}\right\}\delta_{k,p} \tag{42}$$

$E\left[s(\underline{\bar{x}}(k),\mathbf{Y})s^{T}(\underline{\theta}_{R},\mathbf{Y})\right]$ is found below using Equations (31), and (34).

$$\begin{aligned}E\left[s(\underline{\bar{x}}(k),\mathbf{Y})s^{T}(\underline{\theta}_{R},\mathbf{Y})\right]&=E\left[\frac{4}{\sigma^{2}}\mathbf{Re}\left\{\mathbf{A}^{H}\underline{e}(k)\right\}\sum_{t=1}^{N}\mathbf{Re}\left\{\underline{e}^{T}(t)\mathbf{D}^{*}\mathbf{X}^{*}(t)\right\}\right]\\&=\frac{2}{\sigma^{2}}\sum_{t=1}^{N}\left(\mathbf{Re}\left\{\mathbf{A}^{H}E\left[\underline{e}(k)\underline{e}^{T}(t)\right]\mathbf{D}^{*}\mathbf{X}^{*}(t)\right\}+\mathbf{Re}\left\{\mathbf{A}^{H}E\left[\underline{e}(k)\underline{e}^{H}(t)\right]\mathbf{D}\mathbf{X}(t)\right\}\right)\end{aligned} \tag{43}$$

Once again using Equations (38) and (39), Equation (43) simplifies to Equation (44).

$$E\left[s(\underline{\bar{x}}(k),\mathbf{Y})s^{T}(\underline{\theta}_{R},\mathbf{Y})\right]=\frac{2}{\sigma^{2}}\mathbf{Re}\left\{\mathbf{A}^{H}\mathbf{D}\mathbf{X}(k)\right\} \tag{44}$$

$E\left[s(\underline{\tilde{x}}(k),\mathbf{Y})\ s^{T}(\underline{\tilde{x}}(k),\mathbf{Y})\right]$, and $E\left[s(\underline{\tilde{x}}(k),\mathbf{Y})\ s^{T}(\underline{\theta}_{R},\mathbf{Y})\right]$, which are obtained in the same manner that $E\left[s(\underline{\bar{x}}(k),\mathbf{Y})\ s^{T}(\underline{\bar{x}}(k),\mathbf{Y})\right]$, and

$E\left[s\left(\underline{\bar{x}}(k),\mathbf{Y}\right)\ s^{T}\left(\underline{\theta}_{R},\mathbf{Y}\right)\right]$ are obtained in Equations (40), and (44), are given below in Equations (45), and (46).

$$E\left[s(\underline{\tilde{x}}(k),\mathbf{Y})s^{T}(\underline{\tilde{x}}(p),\mathbf{Y})\right]=\frac{2}{\sigma^{2}}\mathbf{Re}\left\{\mathbf{A}^{H}E\left[\underline{e}(k)\underline{e}^{T}(p)\right]\mathbf{A}\right\}=\frac{2}{\sigma}\mathbf{Re}\left\{\mathbf{A}^{H}\mathbf{A}\right\}\delta_{k,p} \quad (45)$$

$$E\left[s(\underline{\tilde{x}}(k),\mathbf{Y})s^{T}(\underline{\theta}_{R},\mathbf{Y})\right]=-\frac{2}{\sigma}\mathbf{Im}\left\{\mathbf{X}^{H}(k)\mathbf{D}^{H}\mathbf{A}\right\}^{T}=\frac{2}{\sigma}\mathbf{Im}\left\{\mathbf{A}^{H}\mathbf{D}\mathbf{X}(k)\right\} \quad (46)$$

$E\left[s\left(\underline{\theta}_{R},\mathbf{Y}\right)\ s^{T}\left(\underline{\theta}_{R},\mathbf{Y}\right)\right]$ is shown as the last step.

$$E\left[s(\underline{\theta}_{R},\mathbf{Y})s^{T}(\underline{\theta}_{R},\mathbf{Y})\right]=E\left[\frac{4}{\sigma^{2}}\sum_{t=1}^{N}\sum_{s=1}^{N}\mathbf{Re}\left\{\mathbf{X}^{H}(t)\mathbf{D}^{H}\underline{e}(t)\right\}\mathbf{Re}\left\{\underline{e}^{T}(s)\mathbf{D}^{*}\mathbf{X}^{*}(s)\right\}\right]$$
$$=\frac{2}{\sigma^{2}}\sum_{t=1}^{N}\sum_{s=1}^{N}\left(\mathbf{Re}\left\{\mathbf{X}^{H}(t)\mathbf{D}^{H}E\left[\underline{e}(t)\underline{e}^{T}(s)\right]\mathbf{D}^{*}\mathbf{X}^{*}(s)\right\}+\mathbf{Re}\left\{\mathbf{X}^{H}(t)\mathbf{D}^{H}E\left[\underline{e}(t)\underline{e}^{H}(s)\right]\mathbf{D}\mathbf{X}(s)\right\}\right)$$

Substituting Equations (38) and (39) leads to Equation (47).

$$E\left[s(\underline{\theta}_{R},\mathbf{Y})s^{T}(\underline{\theta}_{R},\mathbf{Y})\right]=\frac{2}{\sigma}\sum_{t=1}^{N}\mathbf{Re}\left\{\mathbf{X}^{H}(t)\mathbf{D}^{H}\mathbf{D}\mathbf{X}(t)\right\} \quad (47)$$

Now the complete Fisher Information matrix can be constructed:

$$\mathbf{J}^{-1}=\begin{bmatrix} E\left[s(\sigma,\mathbf{Y})^{2}\right] & & & 0 & & \\ & E\left[s(\underline{\bar{x}}(1),\mathbf{Y})\,s^{T}(\underline{\bar{x}}(1),\mathbf{Y})\right] & E\left[s(\underline{\bar{x}}(1),\mathbf{Y})\,s^{T}(\underline{\tilde{x}}(1),\mathbf{Y})\right] & & & E\left[s(\underline{\bar{x}}(1),\mathbf{Y})\,s^{T}(\underline{\theta}_{R},\mathbf{Y})\right] \\ & E\left[s(\underline{\tilde{x}}(1),\mathbf{Y})\,s^{T}(\underline{\bar{x}}(1),\mathbf{Y})\right] & E\left[s(\underline{\tilde{x}}(1),\mathbf{Y})\,s^{T}(\underline{\tilde{x}}(1),\mathbf{Y})\right] & & & E\left[s(\underline{\tilde{x}}(1),\mathbf{Y})\,s^{T}(\underline{\theta}_{R},\mathbf{Y})\right] \\ & & & \ddots & & \vdots \\ & & & E\left[s(\underline{\bar{x}}(N),\mathbf{Y})\,s^{T}(\underline{\bar{x}}(N),\mathbf{Y})\right] & E\left[s(\underline{\bar{x}}(N),\mathbf{Y})\,s^{T}(\underline{\tilde{x}}(N),\mathbf{Y})\right] & E\left[s(\underline{\bar{x}}(N),\mathbf{Y})\,s^{T}(\underline{\theta}_{R},\mathbf{Y})\right] \\ 0 & & & E\left[s(\underline{\tilde{x}}(N),\mathbf{Y})\,s^{T}(\underline{\bar{x}}(N),\mathbf{Y})\right] & E\left[s(\underline{\tilde{x}}(N),\mathbf{Y})\,s^{T}(\underline{\tilde{x}}(N),\mathbf{Y})\right] & E\left[s(\underline{\tilde{x}}(N),\mathbf{Y})\,s^{T}(\underline{\theta}_{R},\mathbf{Y})\right] \\ & \left(E\left[s(\underline{\bar{x}}(1),\mathbf{Y})\,s^{T}(\underline{\theta}_{R},\mathbf{Y})\right]\right)^{T} & \left(E\left[s(\underline{\tilde{x}}(1),\mathbf{Y})\,s^{T}(\underline{\theta}_{R},\mathbf{Y})\right]\right)^{T} & \cdots & \left(E\left[s(\underline{\bar{x}}(N),\mathbf{Y})\,s^{T}(\underline{\theta}_{R},\mathbf{Y})\right]\right)^{T} & \left(E\left[s(\underline{\tilde{x}}(N),\mathbf{Y})\,s^{T}(\underline{\theta}_{R},\mathbf{Y})\right]\right)^{T} & E\left[s(\underline{\theta}_{R},\mathbf{Y})\,s^{T}(\underline{\theta}_{R},\mathbf{Y})\right] \end{bmatrix} \quad (48)$$

The following terms are introduced for notational convenience.

$$\mathbf{\Gamma} = \frac{2}{\sigma}\sum_{t=1}^{N} \mathbf{Re}\left\{\mathbf{X}^{H}(t)\mathbf{D}^{H}\mathbf{D}\mathbf{X}(t)\right\}$$

$$\mathbf{var}_{CR}(\sigma) = \frac{\sigma^2}{mN}$$

$$\mathbf{H} = \frac{2}{\sigma}\mathbf{A}^{H}\mathbf{A}$$

$$\mathbf{G} = \mathbf{H}^{-1}$$

$$\Delta_k = \frac{2}{\sigma}\mathbf{A}^{H}\mathbf{D}\mathbf{X}(k)$$

G is defined with respect to **H** and they are related in an inverse sense. This special relation between **H** and **G** becomes useful while inverting the Fisher Information matrix. Simply $\mathbf{G} \overset{\Delta}{=} \mathbf{H}^{-1}$, but the following relation also holds (for proof see PRF 3 in Appendix A).

$$\begin{bmatrix} \overline{H} & -\widetilde{H} \\ \widetilde{H} & \overline{H} \end{bmatrix}^{-1} = \begin{bmatrix} \overline{G} & -\widetilde{G} \\ \widetilde{G} & \overline{G} \end{bmatrix}$$

The **H** matrix is Hermitian and therefore its imaginary part must be skew-symmetric $\widetilde{\mathbf{H}}^{T} = -\widetilde{\mathbf{H}}$.

J($\underline{\theta}$) introduced in Equation (48) can be rewritten by using the newly defined terms:

$$\mathbf{J}^{-1} = \begin{bmatrix} \mathbf{var}_{CR}^{-1}(\sigma) & & & & 0 & \\ & \overline{\mathbf{H}} & -\widetilde{\mathbf{H}} & & & \overline{\Delta}_1 \\ & \widetilde{\mathbf{H}} & \overline{\mathbf{H}} & & & \widetilde{\Delta}_1 \\ & & & \ddots & & \vdots \\ & & & & \overline{\mathbf{H}} \; -\widetilde{\mathbf{H}} & \overline{\Delta}_N \\ 0 & & & & \widetilde{\mathbf{H}} \quad \overline{\mathbf{H}} & \widetilde{\Delta}_N \\ & \overline{\Delta}_1^{T} & \widetilde{\Delta}_1^{T} & \cdots & \overline{\Delta}_N^{T} \; \widetilde{\Delta}_N^{T} & \mathbf{\Gamma} \end{bmatrix} \qquad (49)$$

In order to obtain the CRB as a function of DOA angles ($\underline{\theta}_R$), $\mathbf{J}(\underline{\theta}_R)$ is needed. $\mathbf{J}(\underline{\theta}_R)$ is found in (50) by partitioning $\mathbf{J}^{-1}$.

$$\mathbf{J}\left(\underline{\theta}_R\right)=\mathbf{\Gamma}-\left[\begin{array}{cccc}\overline{\Delta}_1^T & \tilde{\Delta}_1^T & \cdots & \overline{\Delta}_N^T \;\; \tilde{\Delta}_N^T\end{array}\right]\left[\begin{array}{ccc}\overline{\mathbf{G}} & -\tilde{\mathbf{G}} & \\ \tilde{\mathbf{G}} & \overline{\mathbf{G}} & \\ & & \ddots \\ 0 & & \end{array}\right.\left.\begin{array}{c}0\\ \\ \\ \overline{\mathbf{G}} \;\; -\tilde{\mathbf{G}}\\ \tilde{\mathbf{G}} \;\; \overline{\mathbf{G}}\end{array}\right]\left[\begin{array}{c}\overline{\Delta}_1\\ \tilde{\Delta}_1\\ \vdots\\ \overline{\Delta}_1\\ \tilde{\Delta}_1\end{array}\right] \qquad (50)$$

Using $\left[\begin{array}{cc}\overline{\mathbf{G}} & -\tilde{\mathbf{G}}\\ \tilde{\mathbf{G}} & \overline{\mathbf{G}}\end{array}\right]\left[\begin{array}{c}\overline{\mathbf{\Delta}}\\ \tilde{\mathbf{\Delta}}\end{array}\right]=\left[\begin{array}{c}\overline{\mathbf{G}}\,\overline{\mathbf{\Delta}}-\tilde{\mathbf{G}}\,\tilde{\mathbf{\Delta}}\\ \tilde{\mathbf{G}}\,\overline{\mathbf{\Delta}}+\overline{\mathbf{G}}\,\tilde{\mathbf{\Delta}}\end{array}\right]=\left[\begin{array}{c}\mathbf{Re}(\mathbf{G\Delta})\\ \mathbf{Im}(\mathbf{G\Delta})\end{array}\right]$ and $\left[\begin{array}{cc}\overline{\mathbf{\Delta}}^{\mathrm{T}} & \tilde{\mathbf{\Delta}}^{\mathrm{T}}\end{array}\right]\left[\begin{array}{c}\mathbf{Re}(\mathbf{G\Delta})\\ \mathbf{Im}(\mathbf{G\Delta})\end{array}\right]=\mathbf{Re}\left[\mathbf{\Delta}^{\mathrm{H}}\mathbf{G\Delta}\right]$,

Equation (50) takes the form in Equation (51).

$$\begin{aligned}&\mathbf{J}(\underline{\theta}_{\mathrm{R}})=\mathbf{\Gamma}-\sum_{t=1}^{N}\mathbf{Re}\left[\mathbf{\Delta}^{\mathrm{H}}\mathbf{G\Delta}\right]\\ &\mathbf{J}(\underline{\theta}_{\mathrm{R}})=\frac{2}{\sigma}\sum_{t=1}^{N}\mathbf{Re}\left[\mathbf{X}^{\mathrm{H}}(t)\mathbf{D}^{\mathrm{H}}\mathbf{D}\mathbf{X}(t)-\mathbf{X}^{\mathrm{H}}(t)\mathbf{D}^{\mathrm{H}}\mathbf{A}\left(\mathbf{A}^{\mathrm{H}}\mathbf{A}\right)^{-1}\mathbf{A}^{\mathrm{H}}\mathbf{D}\mathbf{X}(t)\right]\end{aligned} \qquad (51)$$

Finally in Equation (52) $\mathbf{J}(\underline{\theta}_R)$ is inverted in order to obtain the formula for $\mathrm{CRB}_{AS}(\underline{\theta}_R)$.

$$\mathrm{CRB}_{\mathrm{AS}}\left(\underline{\theta}_{\mathrm{R}}\right)=\mathbf{J}^{-1}\left(\underline{\theta}_{\mathrm{R}}\right)=\frac{\sigma}{2}\left(\sum_{t=1}^{N}\mathrm{Re}\left[\mathbf{X}^{\mathrm{H}}(t)\mathbf{D}^{\mathrm{H}}\left[\mathbf{I}-\mathbf{A}\left(\mathbf{A}^{\mathrm{H}}\mathbf{A}\right)^{-1}\mathbf{A}^{\mathrm{H}}\right]\mathbf{D}\mathbf{X}(t)\right]\right)^{-1} \qquad (52)$$

For sufficiently large N, the $\mathrm{CRB}_{AS}(\underline{\theta}_R)$ is given by Equation (53) (see Appendix B for proof). The dependence of the CRB_{AS} on $\underline{\theta}_R$ is shown:

$$\mathrm{CRB}_{\mathrm{AS}}\left(\underline{\theta}_{\mathrm{R}}\right)=\frac{\sigma}{2N}\left[\mathbf{Re}\left\{\left(\mathbf{D}^{*}\left[\mathbf{I}-\mathbf{A}\left(\mathbf{A}^{\mathrm{H}}\mathbf{A}\right)^{-1}\mathbf{A}^{\mathrm{H}}\right]\mathbf{D}\right).*\,\mathbf{P}^{\mathrm{T}}\right\}\right]^{-1} \qquad (53)$$

where $\mathbf{P}\overset{\Delta}{=}\mathrm{E}\left[\underline{\mathrm{x}}(t)\;\underline{\mathrm{x}}^{\mathrm{H}}(t)\right]$ and ".* " is array multiplication operator.

Equation (53) implies that when N is sufficiently large, the CRB can be determined depending on σ, **P**, and the true DOA of the signal i (θ_{Ri}) without the need for the eigenvalue decomposition of the covariance matrix **R** of the observation data, y(t). In this case, the CRB for θ_{Ri} is given by (54).

$$\mathrm{CRB}_{AS}(\theta_{Ri}) = \frac{\sigma}{2N}\left[\mathbf{Re}\left\{\left(\mathbf{D}^{*}\left[\mathbf{I}-\mathbf{A}\left(\mathbf{A}^{H}\mathbf{A}\right)^{-1}\mathbf{A}^{H}\right]\mathbf{D}\right).*\mathbf{P}^{T}\right\}\right]^{-1}_{ii} \qquad (54)$$

In our model, the number of realizations N is 512 which makes Equation (54) a good approximation for determining the CRB_{AS} for different DOA and different number of signals with different correlation levels.

3.3 Derivation of the CRB for Constant Modulus Signals ($\mathbf{CRB}_{CM}$)

Constant Modulus signals have constant envelope and these signals are modulated via a change in frequency. Some examples of constant modulus signals include Frequency Modulation (FM), Phase Modulation (PM), Frequency Shift Keying (FSK), and Phase Shift Keying (PSK). The Constant Modulus Algorithm (CMA) was first considered in [22, 23].

Derivation of CRB_{CM} follows [24]. For CM signals, measured data is modeled by,

$$\underline{y}(t) = \mathbf{AB}\underline{s}(t) + \underline{e}(t) \qquad (55)$$

where

$\underline{y}(t)$ is m by 1 measured data vector at time t,

$\mathbf{A} = [\underline{a}(\theta_{R1}), \cdots, \underline{a}(\theta_{Rn})]$ where $\underline{a}(\theta_{Ri})$ is m-by-1 array response vector from direction θ_{Ri}, and $\underline{\theta}_R = [\theta_{R1}, \ldots, \theta_{Rn}]$ is the DOA vector of the signals,

B is n-by-n channel gain matrix and has the amplitudes of the signals ($\underline{\beta} = [\beta_1, \ldots, \beta_n]$) on the main diagonal. Amplitude of the i^{th} signal as received by the antenna is a real parameter and is denoted as β_i,

$\underline{s}(t)$ is an n-by-1 vector of source signals at time t with unit amplitude, equal to$[s_1(t), \ldots, s_n(t)]$,

$\underline{e}(t)$ is an m-by-1 additive noise vector with complex parameters.

Different signal amplitudes are absorbed into the **B** matrix. Therefore the $\underline{s}(t)$ vector only has phase information corresponding to observation time t. Hence, the phase of the i^{th} signal can be written as $s_i(t) = e^{j\Phi_i(t)}$, where $\Phi_i(t)$ is the unknown phase modulation for i^{th} signal. A source vector can be defined as $\underline{\Phi}(t) = [\Phi_1(t), \cdots, \Phi_n(t)]^T$, the phase vector for all signals at time t.

Maintaining assumptions of additive noise as for the AS case, the likelihood function given in Equation (28) also holds true for CM signals except that the form of $\underline{e}(t)$ is different. In each case Likelihood and log-likelihood functions are given in Equations (56), and (57) respectively:

$$l(\underline{\theta}, \mathbf{Y}) = (2\pi)^{-Nm} \left(\frac{\sigma}{2}\right)^{-Nm} \exp\left\{-\frac{1}{\sigma}\sum_{t=1}^{N}\left(\underline{y}(t)^H - \underline{s}^H(t)\,\mathbf{B}^H\mathbf{A}^H\right)\left(\underline{y}(t) - \mathbf{AB}\underline{s}(t)\right)\right\} \quad (56)$$

$$L(\underline{\theta},\mathbf{Y})=\text{const - Nm}\ln(\sigma)-\frac{1}{\sigma}\sum_{t=1}^{N}\left(\underline{y}(t)^{H}-\underline{s}^{H}(t)\,\mathbf{B}^{H}\mathbf{A}^{H}\right)\left(\underline{y}(t)-\mathbf{AB}\underline{s}(t)\right) \qquad (57)$$

Taking derivates of the log-likelihood function with respect to the unknown parameters $\underline{\Phi}(t)$, $\underline{\beta}(t)$, and $\underline{\theta}_R$ leads to the individual score functions. The set of unknown parameters are represented by a vector, denoted as $\underline{\theta}$, where $\underline{\theta}=\left[\underline{\Phi}^{T}(1),\cdots,\underline{\Phi}^{T}(N),\underline{\beta}^{T}(1),\cdots,\underline{\beta}^{T}(N),\underline{\theta}_R^{T}\right]$.

The partial derivative with respect to $\underline{\Phi}(t)$ is found by,

$$s(\underline{\Phi}(t),\mathbf{Y})=\frac{\partial}{\partial\underline{\Phi}(t)}L(\underline{\theta},\mathbf{Y})=\frac{\partial\underline{\bar{x}}(t)}{\partial\underline{\Phi}(t)}\frac{\partial}{\partial\underline{\bar{s}}(t)}L(\underline{\theta},\mathbf{Y})+\frac{\partial\underline{\tilde{x}}(t)}{\partial\underline{\Phi}(t)}\frac{\partial}{\partial\underline{\tilde{s}}(t)}L(\underline{\theta},\mathbf{Y}) \qquad (58)$$

and $\frac{\partial}{\partial\underline{\bar{s}}(t)}L(\underline{\theta},\mathbf{Y})$, $\frac{\partial}{\partial\underline{\tilde{s}}(t)}L(\underline{\theta},\mathbf{Y})$ follows from Equations (31), and (32).

$$\frac{\partial}{\partial\underline{\bar{s}}(t)}L(\underline{\theta},\mathbf{Y})=\frac{2}{\sigma}\mathbf{Re}\left\{\mathbf{B}^{H}\mathbf{A}^{H}\underline{e}(t)\right\}$$

$$\frac{\partial}{\partial\underline{\tilde{s}}(t)}L(\underline{\theta},\mathbf{Y})=\frac{2}{\sigma}\mathbf{Im}\left\{\mathbf{B}^{H}\mathbf{A}^{H}\underline{e}(t)\right\}$$

Since the $\underline{s}(t)$ vector only carries phase information (the observed signal amplitudes are contained in the matrix **B**), its real and the imaginary parts are $\underline{\bar{s}}(t)=\mathbf{Re}\{\underline{s}(t)\}=\mathbf{cos}(\underline{\Phi}(t))$, and $\underline{\tilde{s}}(t)=\mathbf{Im}\{\underline{s}(t)\}=\mathbf{sin}(\underline{\Phi}(t))$. Therefore $\frac{\partial\underline{\bar{s}}(t)}{\partial\underline{\Phi}(t)}$ and $\frac{\partial\underline{\tilde{s}}(t)}{\partial\underline{\Phi}(t)}$ are simply found as:

$$\frac{\partial\underline{\bar{s}}(t)}{\partial\underline{\Phi}(t)}=-\sin(\underline{\Phi}(t)),\quad\frac{\partial\underline{\tilde{s}}(t)}{\partial\underline{\Phi}(t)}=\cos(\underline{\Phi}(t))$$

Let $\mathbf{X_t}$ be a matrix that has $\underline{s}(t)$ on its main diagonal, $\mathbf{S}_t \stackrel{\Delta}{=} \mathrm{diag}(\underline{s}(t))$; then $\frac{\partial \underline{\bar{s}}(t)}{\partial \underline{\Phi}(t)}$, and $\frac{\partial \underline{\tilde{s}}(t)}{\partial \underline{\Phi}(t)}$ can be written in terms of $\mathbf{S}_t$.

$$\frac{\partial \underline{\bar{s}}(t)}{\partial \underline{\Phi}(t)} = -\mathbf{Im}\{\mathbf{S}_t\}$$
$$\frac{\partial \underline{\tilde{s}}(t)}{\partial \underline{\Phi}(t)} = \mathbf{Re}\{\mathbf{S}_t\}$$

Then Equation (58) becomes,

$$s(\underline{\Phi}(k), \mathbf{Y}) = \frac{\partial}{\partial \underline{\Phi}(k)} L(\underline{\theta}, \mathbf{Y}) = \frac{2}{\sigma}\left(-\mathbf{Im}\{\mathbf{X}_k\}\mathbf{Re}\{\mathbf{B}^H\mathbf{A}^H\underline{e}(k)\} + \mathbf{Re}\{\mathbf{X}_k\}\mathbf{Im}\{\mathbf{B}^H\mathbf{A}^H\underline{e}(k)\}\right)$$

$$s(\underline{\Phi}(t), \mathbf{Y}) = \frac{2}{\sigma}\mathbf{Im}\{\mathbf{S}_t^H\mathbf{B}^H\mathbf{A}^H\underline{e}(t)\} \quad (59)$$

$s(\underline{\theta}_R, \mathbf{Y})$ is found with a similar manner as Equation (34)

$$s(\underline{\theta}_R, \mathbf{Y}) = \frac{\partial}{\partial \underline{\theta}_R} L(\underline{\theta}, \mathbf{Y}) = \frac{2}{\sigma}\sum_{t=1}^{N}\mathbf{Re}\{\mathbf{S}_t^H\mathbf{B}^H\mathbf{D}^H\underline{e}(t)\} \quad (60)$$

where $\mathbf{D} = [\underline{d}(\theta_{R1}), \cdots, \underline{d}(\theta_{Rn})] = \left[\frac{d\underline{a}(\theta_{R1})}{d\theta_{R1}}, \cdots, \frac{d\underline{a}(\theta_{Rn})}{d\theta_{Rn}}\right]$.

$s(\underline{\beta}, \mathbf{Y})$ is obtained from [6].

$$s(\underline{\beta}, \mathbf{Y}) = \frac{\partial}{\partial \underline{\beta}} L(\underline{\theta}, \mathbf{Y}) = \frac{2}{\sigma}\sum_{t=1}^{N}\mathbf{Re}\{\mathbf{S}_t^H\mathbf{A}^H\underline{e}(t)\} \quad (61)$$

Fisher Information matrix can be derived as,

$$\mathbf{J}=\begin{bmatrix} \mathbf{H}_1 & & 0 & \boldsymbol{\Delta}_1^{\mathrm{T}} & \mathbf{E}_1^{\mathrm{T}} \\ & \ddots & & \vdots & \vdots \\ 0 & & \mathbf{H}_N & \boldsymbol{\Delta}_N^{\mathrm{T}} & \mathbf{E}_N^{\mathrm{T}} \\ \boldsymbol{\Delta}_1 & \cdots & \boldsymbol{\Delta}_N & \boldsymbol{\Gamma} & \boldsymbol{\Lambda}^{\mathrm{T}} \\ \mathbf{E}_1 & \cdots & \mathbf{E}_N & \boldsymbol{\Lambda} & \mathbf{M} \end{bmatrix} \tag{62}$$

where

$$\mathbf{H}_t \overset{\Delta}{=} \mathrm{E}\left[s(\underline{\Phi}(t),\mathbf{Y})\,s^{\mathrm{T}}(\underline{\Phi}(t),\mathbf{Y})\right]=\frac{2}{\sigma}\mathbf{Re}\left\{\mathbf{S}_t^{\mathrm{H}}\mathbf{B}^{\mathrm{H}}\mathbf{A}^{\mathrm{H}}\mathbf{A}\mathbf{B}\mathbf{S}_t\right\} \tag{63}$$

$$\boldsymbol{\Delta}_t \overset{\Delta}{=} \mathrm{E}\left[s(\underline{\theta}_R,\mathbf{Y})\,s^{\mathrm{T}}(\underline{\Phi}(t),\mathbf{Y})\right]=-\frac{2}{\sigma}\mathbf{Im}\left\{\mathbf{S}_t^{\mathrm{H}}\mathbf{B}^{\mathrm{H}}\mathbf{D}^{\mathrm{H}}\mathbf{A}\mathbf{B}\mathbf{S}_t\right\} \tag{64}$$

$$\mathbf{E}_t \overset{\Delta}{=} \mathrm{E}\left[s(\underline{\beta},\mathbf{Y})\,s^{\mathrm{T}}(\underline{\Phi}(t),\mathbf{Y})\right]=-\frac{2}{\sigma}\mathbf{Im}\left\{\mathbf{S}_t^{\mathrm{H}}\mathbf{A}^{\mathrm{H}}\mathbf{A}\mathbf{B}\mathbf{S}_t\right\} \tag{65}$$

$$\boldsymbol{\Gamma} \overset{\Delta}{=} \mathrm{E}\left[s(\underline{\theta}_R,\mathbf{Y})\,s^{\mathrm{T}}(\underline{\theta}_R,\mathbf{Y})\right]=-\frac{2}{\sigma}\sum_{t=1}^{N}\mathbf{Re}\left\{\mathbf{S}_t^{\mathrm{H}}\mathbf{B}^{\mathrm{H}}\mathbf{D}^{\mathrm{H}}\mathbf{D}\mathbf{B}\mathbf{S}_t\right\} \tag{66}$$

$$\boldsymbol{\Lambda} \overset{\Delta}{=} \mathrm{E}\left[s(\underline{\beta},\mathbf{Y})\,s^{\mathrm{T}}(\underline{\theta}_R,\mathbf{Y})\right]=-\frac{2}{\sigma}\sum_{t=1}^{N}\mathbf{Re}\left\{\mathbf{S}_t^{\mathrm{H}}\mathbf{A}^{\mathrm{H}}\mathbf{D}\mathbf{B}\mathbf{S}_t\right\} \tag{67}$$

$$\mathbf{M} \overset{\Delta}{=} \mathrm{E}\left[s(\underline{\beta},\mathbf{Y})\,s^{\mathrm{T}}(\underline{\beta},\mathbf{Y})\right]=-\frac{2}{\sigma}\sum_{t=1}^{N}\mathbf{Re}\left\{\mathbf{S}_t^{\mathrm{H}}\mathbf{A}^{\mathrm{H}}\mathbf{A}\mathbf{S}_t\right\} \tag{68}$$

Inversion of the Fisher Information matrix is carried out in block-partitioned form using Schur complement formulas and the Woodbury identity as in [24]. The CRB for DOA of CM signals is given by:

$$\mathrm{CRB}_{\mathrm{CM}}(\underline{\theta}_R)=\mathrm{diag}\left(\boldsymbol{\Psi}_{11}-\boldsymbol{\Psi}_{12}\boldsymbol{\Psi}_{22}^{-1}\boldsymbol{\Psi}_{21}\right)^{-1} \tag{69}$$

where

$$\boldsymbol{\Psi}=\begin{bmatrix}\boldsymbol{\Psi}_{11} & \boldsymbol{\Psi}_{12}\\ \boldsymbol{\Psi}_{21} & \boldsymbol{\Psi}_{22}\end{bmatrix}=\begin{bmatrix}\boldsymbol{\Gamma} & \boldsymbol{\Lambda}^{\mathrm{T}}\\ \boldsymbol{\Lambda} & \mathbf{M}\end{bmatrix}-\begin{bmatrix}\boldsymbol{\Xi}_{11} & \boldsymbol{\Xi}_{12}\\ \boldsymbol{\Xi}_{21} & \boldsymbol{\Xi}_{22}\end{bmatrix}$$

$$\boldsymbol{\Xi}_{11} = \sum_{t=1}^{N} \boldsymbol{\Delta}_t \mathbf{H}_t^{-1} \boldsymbol{\Delta}_t^T$$

$$\boldsymbol{\Xi}_{21} = \sum_{t=1}^{N} \mathbf{E}_t \mathbf{H}_t^{-1} \boldsymbol{\Delta}_t^T$$

$$\boldsymbol{\Xi}_{12} = \sum_{t=1}^{N} \boldsymbol{\Delta}_t \mathbf{H}_t^{-1} \mathbf{E}_t^T$$

$$\boldsymbol{\Xi}_{22} = \sum_{t=1}^{N} \mathbf{E}_t \mathbf{H}_t^{-1} \mathbf{E}_t^T$$

3.4 CRB Calculation

The CRBs for different scenarios are calculated and plotted by using Matlab® software to illustrate performance under different conditions. The first scenario is where only one object is assumed to exist in the surveillance region. The CRB for different object locations in azimuth (θ_R) and different SNR levels is observed.

The second scenario includes two objects. One of the objects simulates a moving object and its DOA changes between Coherent Processing Intervals (CPIs) and as it moves from one angular location in azimuth to another. The second object remains stationary at a fixed location in azimuth throughout all CPIs. A stationary object does not necessarily imply the object is a non-maneuvering object; it implies the object does not change location in azimuth. The CRB for both objects is plotted separately on different figures.

Interference from multiple transmitters in the surveillance region is one of issue in PCL systems. Thus, to observe the effects of having a transmitter in the

surveillance region on the bounds of the object echo signals, a third scenario is introduced and includes two object echo signals and a direct signal from a transmitter of opportunity in the surveillance area. The transmitter is simulated by choosing a relatively high SNR level compared to the SNR levels of the object signals, and having zero Doppler shift. The object signals are chosen to be a moving object and a stationary object as in the second scenario. Last but not least, fourth scenario observes the CRB of the moving target for AS and CM cases for different transmitter of opportunity DOAs. This experiment should yield additional insight into antenna placement and orientation.

Correlation between object returns is also implemented for the arbitrary signal case. The matrix **P**, defined in Equation (70), includes the correlation of the signals. In the case when two objects have the same SNR values and they are uncorrelated, the correlation coefficient, $\rho = 0$. For fully correlated signals, $\rho = 1$.

$$\mathbf{P} = \begin{bmatrix} 1 & \rho \\ \rho & 1 \end{bmatrix} \tag{70}$$

SNR variation is implemented by assigning new values of σ. Signal power is assumed to be 1 Watt and the relation between the σ and the SNR level is given in Equation (71) for SNR expressed in dB:

$$\sigma = \frac{1}{10^{SNR/10}} \tag{71}$$

Dimensions of **P** change according to the number of signals being received. To illustrate how the cross correlation of multiple signals for different numeric SNR levels take place, a matrix **P** for three signals is given in Equation (72) (See Appendix C for proof). Signal one has been normalized to 1 watt.

$$\mathbf{P}=\begin{bmatrix} 1 & \rho_{12}\sqrt{\frac{SNR_2}{SNR_1}} & \rho_{13}\sqrt{\frac{SNR_3}{SNR_1}} \\ \rho_{12}\sqrt{\frac{SNR_2}{SNR_1}} & \frac{SNR_2}{SNR_1} & \rho_{23}\frac{\sqrt{SNR_3SNR_2}}{SNR_1} \\ \rho_{13}\sqrt{\frac{SNR_3}{SNR_1}} & \rho_{23}\frac{\sqrt{SNR_3SNR_2}}{SNR_1} & \frac{SNR_3}{SNR_1} \end{bmatrix} \tag{72}$$

3.5 Summary

This chapter explained and showed the derivation of CRB_{AS} and CRB_{CM}. The implementation of correlation between two signals is also explained and expanded to multiple correlated signals for AS case. The formulas given here are used for the CRB calculations.

Equation (54) which is approximated for sufficiently large number of realizations (N) is used for the CRB_{AS} calculations.

$$\mathrm{CRB}_{\mathrm{AS}}(\theta_{\mathrm{Ri}})=\frac{\sigma}{2N}\left[\mathbf{Re}\left\{\left(\mathbf{D}^{*}\left[\mathbf{I}-\mathbf{A}\left(\mathbf{A}^{\mathrm{H}}\mathbf{A}\right)^{-1}\mathbf{A}^{\mathrm{H}}\right]\mathbf{D}\right).*\mathbf{P}^{\mathrm{T}}\right\}\right]_{\mathrm{ii}}^{-1} \tag{54}$$

Equation (69) is used for the CRB_{CM} calculations.

$$\mathrm{CRB}_{\mathrm{CM}}(\underline{\theta}_{\mathrm{R}})=\mathrm{diag}\left(\boldsymbol{\Psi}_{11}-\boldsymbol{\Psi}_{12}\boldsymbol{\Psi}_{22}^{-1}\boldsymbol{\Psi}_{21}\right)^{-1} \tag{69}$$

4 . CONTRIBUTIONS OF RESEARCH

This chapter presents results computed for the CRB of Arbitrary Signals and Constant Modulus signals in different scenarios. The CRBs for moving signal sources are plotted versus the true DOA of the moving signal sources, and CRBs of the stationary signal sources are plotted versus angular separation of the stationary signal sources with the moving signal sources. Matlab® software is used for calculating the CRBs and for generating the plots.

4.1 Scenario 1: Single Signal

The simplest case considered includes only one signal impinging on the antenna. This case is studied because it is a good way of evaluating the system performance before moving on to more complicated scenarios. The single signal provides an understanding of basic system performance and gives a reference for comparison when studying more complicated scenarios.

CRB_{AS} and CRB_{CM} are equal to each other when there is only one signal. This is because the CM signal model in Equation (55) can also be represented using the arbitrary signal model given in Equation (21) in the single signal case. Since the pdfs of CM and arbitrary signals are basically identical (differing only in the way that their means are represented), then the single signal case results in identical pdfs for the CM and arbitrary signals.

Figure 12 shows the CRB of a single object. The CRB is a function of the true DOA of the signal, or in other words, it is a function of the angular difference between object location in azimuth and the antenna broadside direction. As the location of the signal source in azimuth shifts away from the antenna broadside direction, there is a nonlinear increase in the CRB. The CRB is symmetric in this case because it is a function of the signal angular location in azimuth, as measured from the antenna broadside direction. For example, a signal source has the same CRB when it is either located at -10° or 10° from antenna broadside (assuming all other parameters such as SNR remain constant).

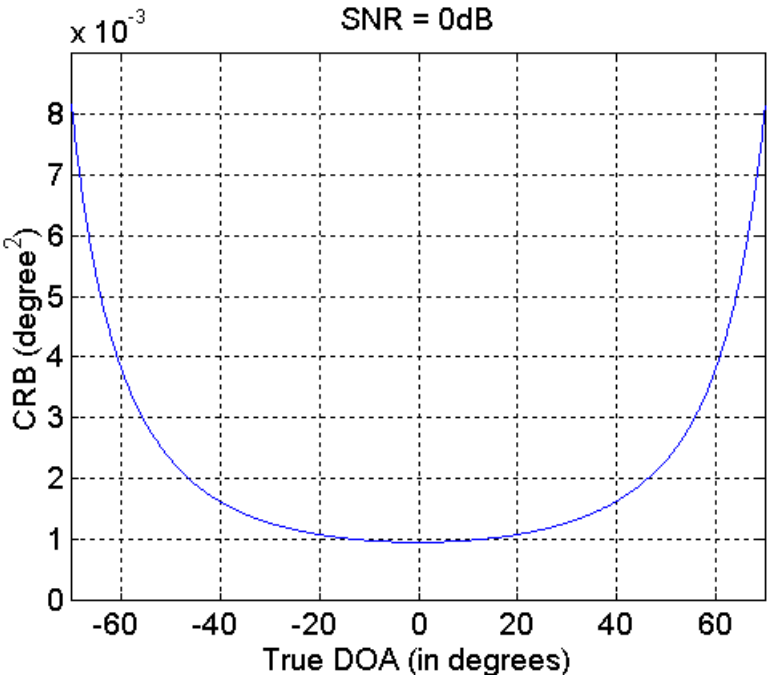

Figure 12. CRB for single signal case when SNR = 0dB.

An increase or decrease in SNR results in a linear change on the CRB in an inverse sense; increasing SNR causes a decrease in the CRB and decreasing SNR causes an increase in the CRB. The effect of SNR changes on the CRB is

demonstrated in Appendix D where the CRBs for –10dB, 10dB, and 20dB SNRs are plotted. The shape of the CRB does not change but there is an increase or a decrease of the CRB amplitude inversely proportional to the change in the SNR. This result is expected; as signal power increases one expects the variance in the DOA estimate to decrease.

4.2 Scenario 2: Two Signal Sources

When receiving multiple one signals, the CRB_{AS} and CRB_{CM} show differing characteristics. This is due to the CM constraint on the received signal type [25].

DOA estimators that utilize signals with the CM property separate the incoming signals using different techniques, and then utilize the signal properties, such as signal phase, in addition to the array antenna manifold, that conventional DOA estimators use. Not only is the phase difference between array antenna elements used to estimate DOA, but also the actual phase information of the incoming signal.

Since the phase of the incoming signal is also processed in CM estimators, a derivative is taken with respect to the signal phase when the Fisher Information matrix is being constructed. The signal phase is added to the vector of unknown parameters when the CM constraint is brought into the estimator. This is the reason why CM estimators have a different CRB than AS estimators.

4.2.1 CRB_{AS} of Two Signal Sources

In Figure 13, the CRB for the so-called "moving object" is illustrated. One signal is a stationary signal source sitting at 0° and the other signal source is a moving signal source. It is called a "moving signal" because the source remains fixed at one angle during 512 realizations of measurement data, after which it is moved to the next DOA where it remains fixed for another 512 snapshots. Basically, the moving object remains fixed during a CPI but is moved to the next DOA angle between CPIs. The stationary signal source remains at the same exact location throughout all CPIs. This is a fair approximation to a moving object scenario; recall from Section 3.2 that the number of realizations must be kept large (in this case, N = 512) for the CRB approximation of Equation (53) to remain valid.

When CRB_{AS} plots are observed it can be seen that the CRB_{AS} out to 70° is relatively high due to the system performance shown in single signal case (see Figure 13 (b)). This is actually seen in the CRB plots for single signal case. As the moving object gets closer to the other signal source, a nonlinear increase in the CRB_{AS} is observed (see Figure 13 (a) and (c)). This is caused by both signals having close DOA angles, thus causing the phase delays between the elements of the array antenna to become very similar. Hence, the array response vectors $\underline{a}(\theta_1)$, and $\underline{a}(\theta_2)$ become more alike as the angular difference between the two signals is reduced in the azimuth plane. When two signals are exactly on the top of each other, the **A** matrix formed by $\underline{a}(\theta_1)$ and $\underline{a}(\theta_2)$ and the **D** matrix formed by

$\frac{\partial}{\partial\theta_1}\underline{a}(\theta_1)$ and $\frac{\partial}{\partial\theta_2}\underline{a}(\theta_2)$, become singular and cause the CRB_{AS} to approach infinity. Therefore, as the DOA of two signals gets close to each other the CRB_{AS} increases. When they are exactly at the same DOA we say that it is unbounded.

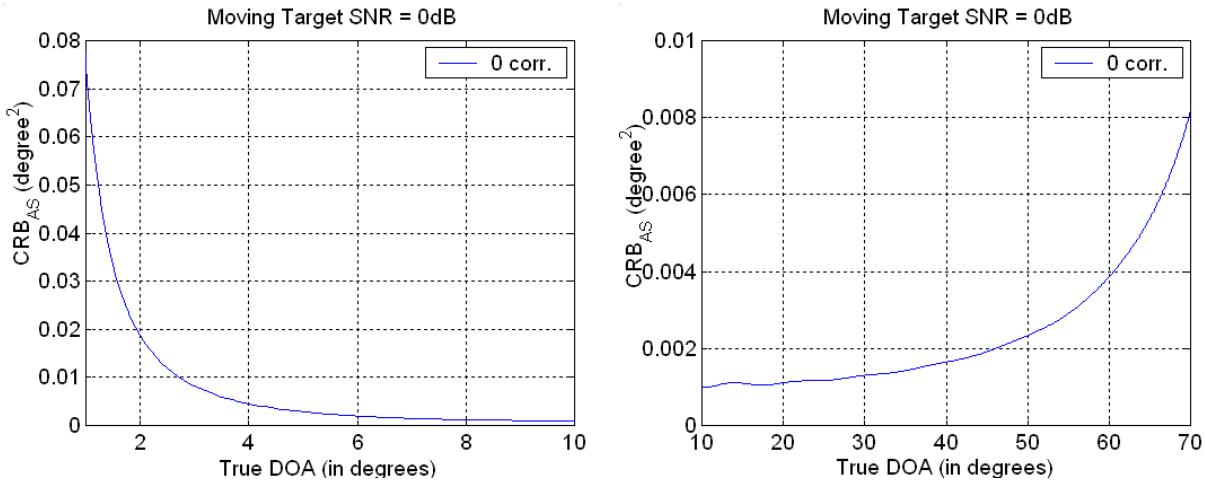

(a) (b)

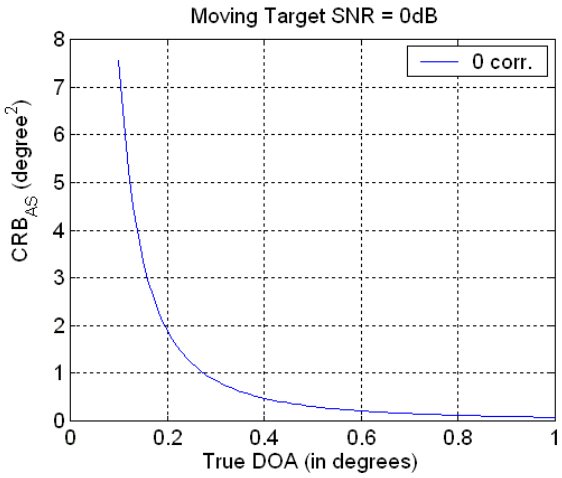

(c)

Figure 13. The CRB_{AS} of a moving object with 0dB SNR with a stationary object of the same SNR located at 0°.

Figure 13 (b) shows the decrease in CRB_{AS} as the moving signal source moves away from 70° off broadside towards broadside. Figure 13 (a) shows the increase in CRB_{AS} in the DOA angle range of 1°-10°. When the moving object is at 1° of DOA its CRB_{AS} is nearly ten times as more than when it is out at 70°. Finally, the DOA range of 0° - 1° is shown in Figure 13 (c) and the increase in CRB_{AS} is shown when two signal sources are very near to each other.

To gain a better understanding of the increase in CRB_{AS} as the angular separation between the signals decrease, the CRB_{AS} of the stationary signal source is plotted versus its angular separation with the moving object in Figure 14. Therefore, the CRB_{AS} of the stationary object is calculated for each DOA of the moving signal and plotted versus the angular separation with the moving signal source.

The CRB_{AS} of the stationary object does not exhibit a monotonic increase or decrease. In Figure 14 (a), the minimum CRB_{AS} of the stationary object is achieved when the moving signal source is furthest away. As the two signal sources get closer in azimuth, the difference between the minimum and maximum points increases. The CRB_{AS} values in Figure 14 (b) and (c) are similar to CRB_{AS} values of the moving object; this is because the **A** and **D** matrices become nearly singular as two signal sources gets closer to each other in azimuth.

Correlation between the arbitrary signals should also be incorporated into our DOA estimate, since the bounds change with respect to the correlation level

of the signals. The effect of correlation between two signals is shown in Appendix E, where bounds for the moving and the stationary signal sources are plotted. The higher the correlation between the arbitrary signals, the higher the bound becomes.

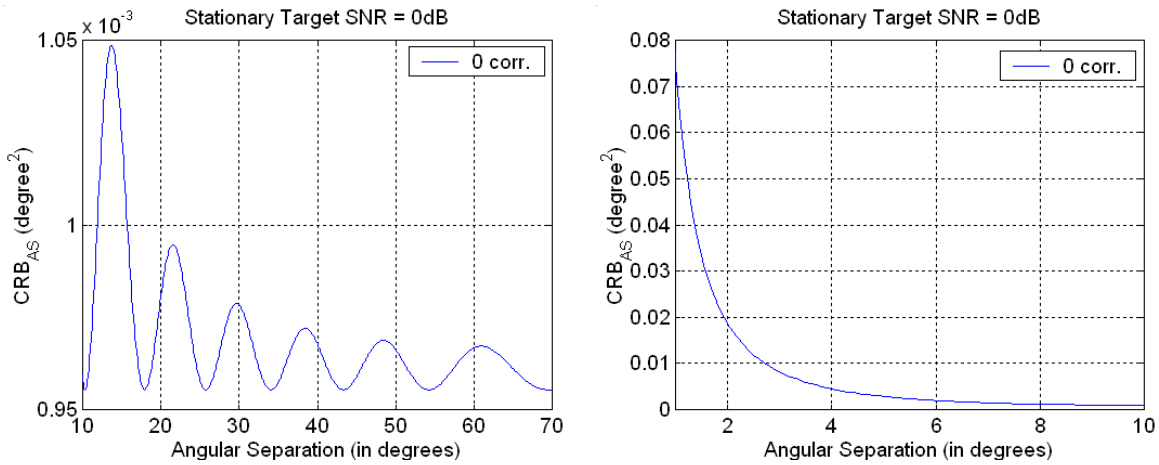

(a) (b)

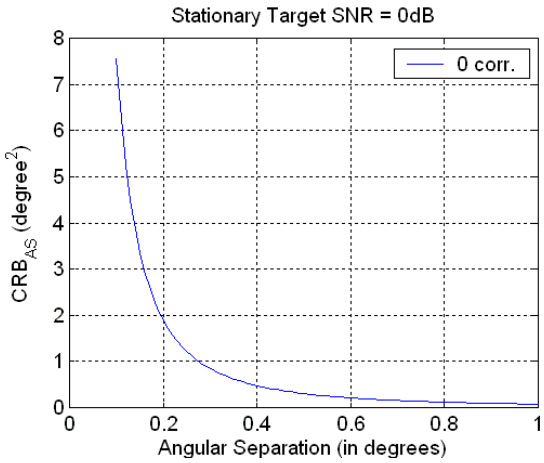

(c)

Figure 14. The CRB_{AS} of a stationary object with 0dB SNR with a moving object of the same SNR.

When the CRB_{AS} in the two signals case is compared with the CRB in single signal case, the bound increases in the antenna broadside direction in the CRB_{AS} of two signals when the DOA of the two signals are near to each other.

4.2.2 CRB_{CM} of Two Signal Sources

As mentioned in Section 3.3, the CM constraint on the signal changes the CRB. In this research the CRB_{CM} is unique because of the effects of the changes in the Doppler shift and the start phase of the signal sources. These parameters are modeled using the FM signal model. Estimators having the CM signal constraint use many signal properties, especially properties of the signal phase. Therefore different effects on the phase of the incoming signals, such as different Doppler, different start phases of the signals, or different information messages being modulated can cause the signals to be distinguished from one another.

As different signal sources get closer to each other in azimuth, the **A** and **D** matrices become singular, but the CRB_{CM} is not as susceptible to reduced angular separation between signal sources in azimuth plane as the CRB_{AS}. This is because of the CM constraint on the signal; a new unknown parameter vector of phase must be added to the unknown parameter vector ($\underline{\theta}$) for arbitrary signals. Hence, the derivative of log-likelihood function with respect to phase vector of the signal sources is found in Equation (59). The correlation of the unknown parameter vector phase with itself and the other unknown parameters given in Equations (63), (64), and (65) makes the Fisher information matrix invertible even when two signal sources are closely located in the azimuth plane.

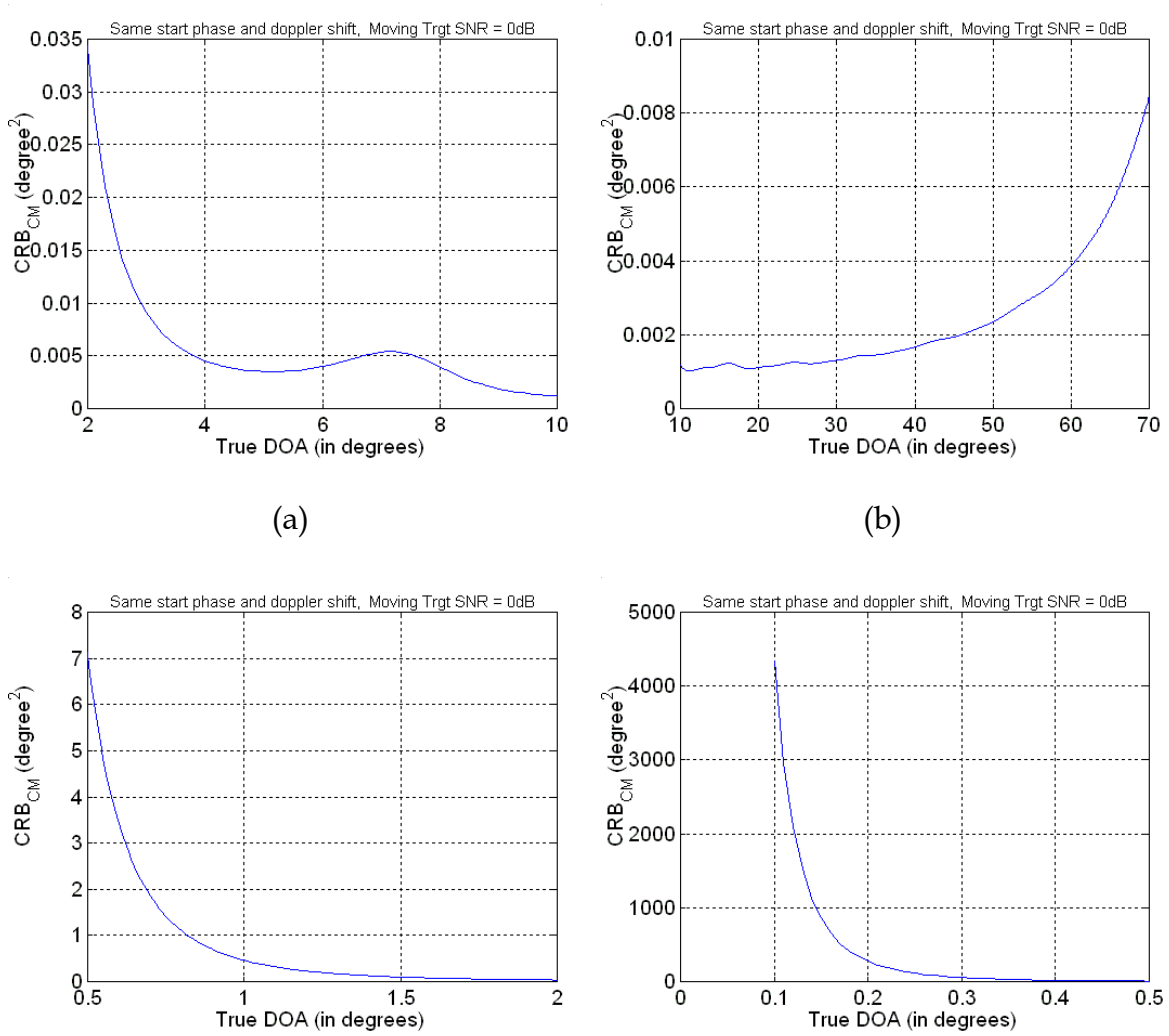

Figure 15. The CRB_{CM} of the moving signal source with 0dB SNR with a stationary signal source of the same SNR when the Start Phases and the Doppler Shifts of the two signal sources are the same.

The CRB_{CM} is also found to be a function of start phase and Doppler shift differences. In Figure 15, the start phase and the Doppler shift of the incoming signals are the same, so this can be thought of the case when the phases of the two incoming signals are fully correlated. Due to the reason, the signal model

used in this thesis assumes identical FM modulation (message) signals for the two signals, and that this FM signal remains constant during the sampling of the data. Therefore, having the same Doppler shift and starting phase for the two signal sources should be considered as a worst-case scenario.

In Figure 15 (b) the CRB_{CM} for the moving object seems to be almost identical to the CRB_{AS} of the moving object within the DOA range of 10° - 70°. The real problem is in the two signals case, especially when the two signals get closer in azimuth; this research now focuses on the region where the signals are relatively close in azimuth. When the moving object is within 10° of the stationary object, its CRB_{CM} is initially lower than CRB_{AS}. But, as the moving object approaches the stationary object at 0°, the increase in the CRB_{CM} is greater than the increase in CRB_{AS}. This is because to the two signals have exactly the same phase properties (due to our initial assumptions of identical starting phase and Doppler).

When the two signals have a starting phase difference and a Doppler shift difference, the CRB_{CM} varies because it can better separate two signals from each other. This is shown in Figure 16 by choosing an arbitrary starting phase and Doppler shift difference between the signals.

Figure 16 (a) shows that when there is a difference in the phase parameters of the two signal sources, the CRB_{CM} of the moving object remains the same as the CRB_{AS} of the moving object in Figure 13 (a) and CRB_{CM} of the moving object in Figure 15 (a) between the DOA range of 10° - 70°. The CRB_{CM}

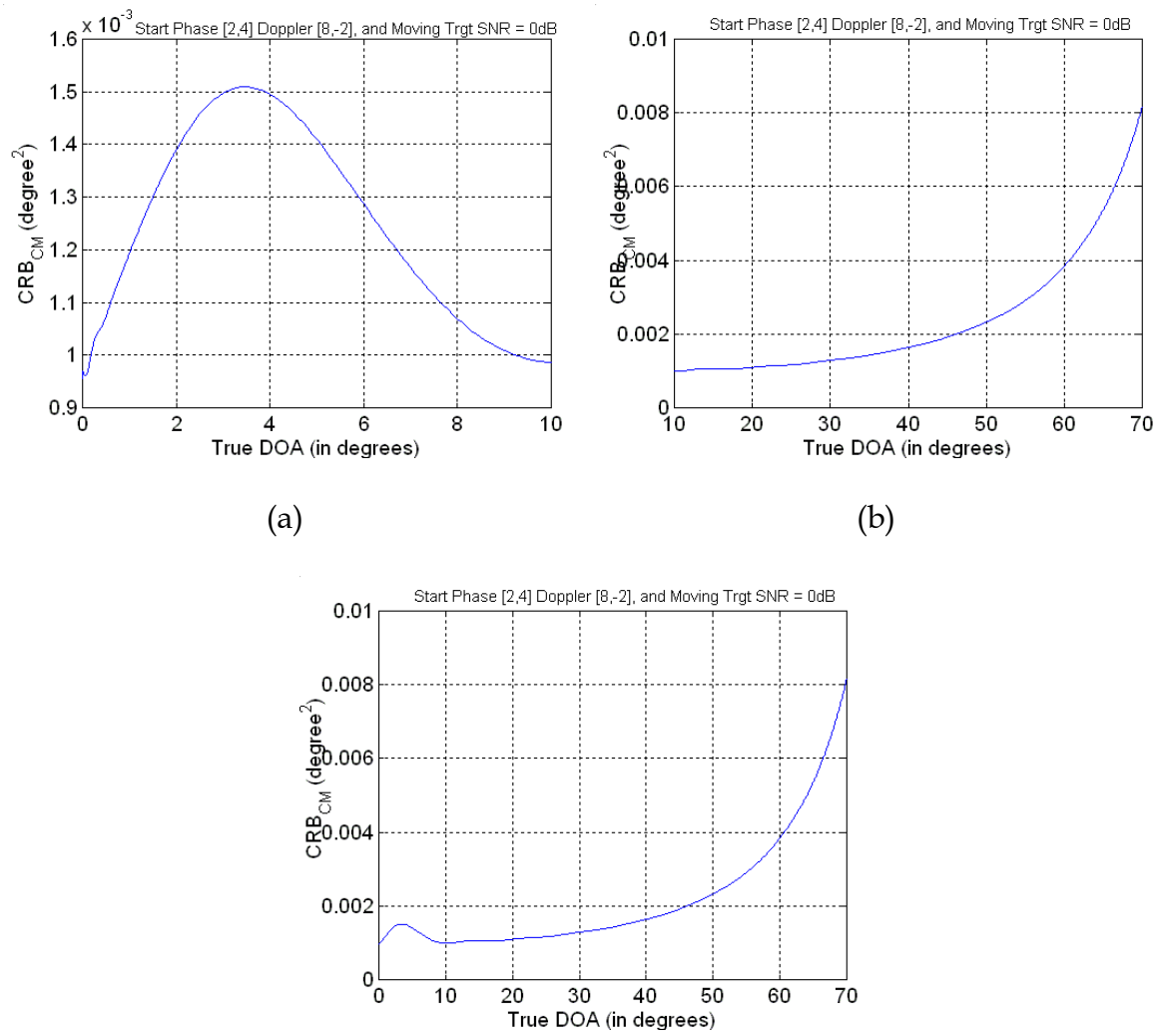

Figure 16. The CRB_{CM} of moving signal source with 0dB SNR with a stationary signal source of the same SNR when Start Phases/Doppler Shifts of the moving, and stationary signal sources are [2,4]/[8,-2] respectively.

in Figure 16 (a) takes a better look at the behavior of the bound for the moving object when the two signals approach each other in azimuth plane. CRB_{CM} does not increase as much when compared with the previous cases and it is the most

robust bound obtained, considering the increase in the CRB of the previous cases (when the two signals became near to each other in azimuth).

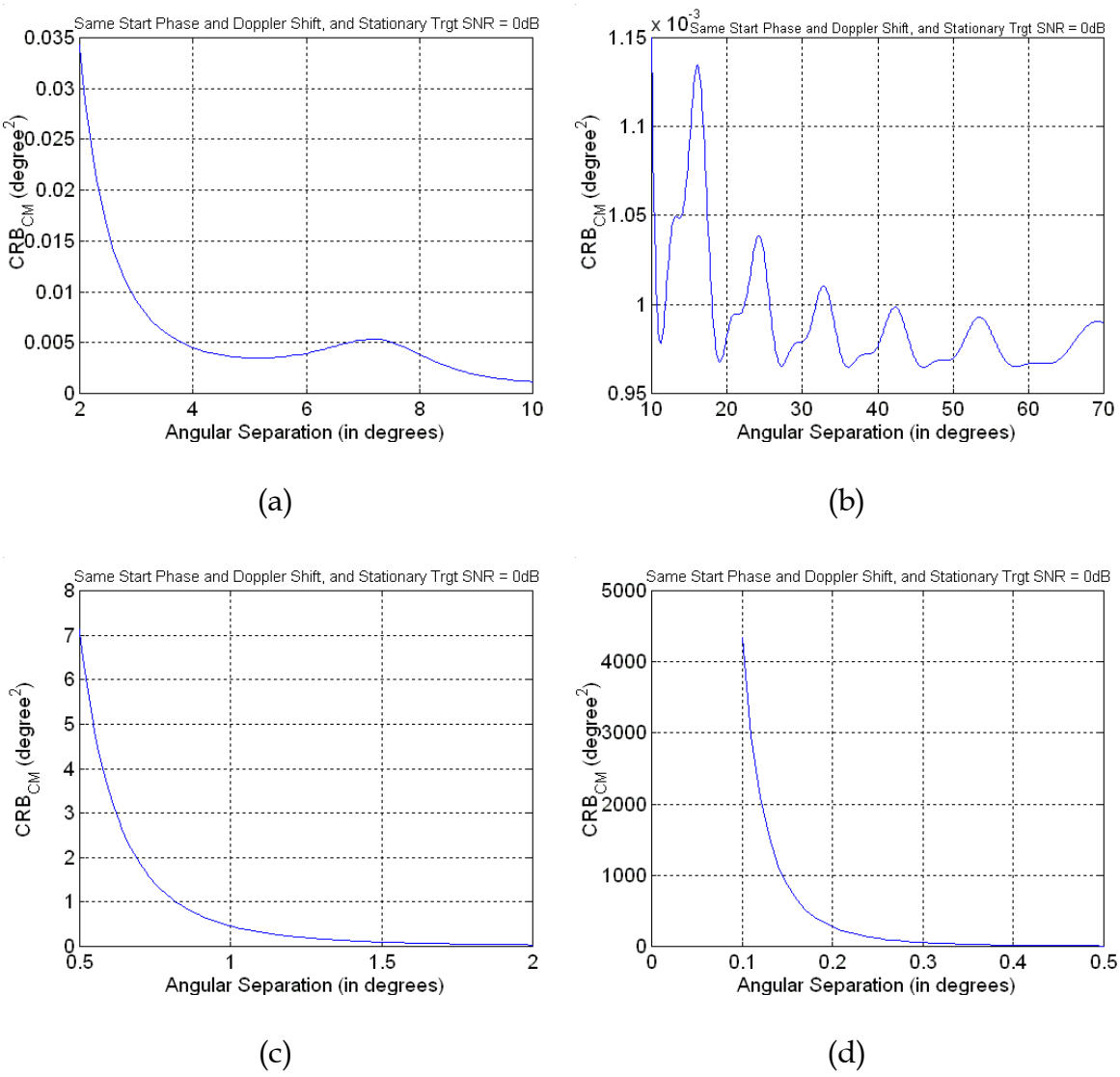

Figure 17. The CRB_{CM} of the stationary signal source with 0dB SNR with a moving signal source of the same SNR when the Start Phases, and the Doppler Shifts of the two signal sources are the same.

The final CRB_{CM} analysis for this case involves the CRB_{CM} of the stationary signal source. Figure 17 shows the worst case scenario for the CM signal estimators when the phase parameters of the two signals are fully correlated. As a result, (just as in the case of the CRB_{AS} of the stationary object) there is not a constant increase in the bound as the separation between the two signal sources gets smaller. After noting the similarity of Figure 15 (a, c, d) with Figure 17 (a, c, d), it becomes apparent that once the separation between the moving and stationary signal sources becomes less than ten degrees, the CRB_{CM} of the stationary object and moving object is identical.

As a result, the CRB_{CM} of both signal sources having identical phase parameters yield similar bounds with the CRB_{AS} when the signal separation is between 10° – 70°. On the other hand, when the angular separation of the two signals in azimuth is less than ten degrees, the CRB_{AS} is lower than the CRB_{CM} for the same phase parameters. It must be remembered that when both of the signals have the same phase parameters, this implies both signals are fully correlated in phase and represents a worst case scenario for CM signals. This is rarely the case in real-world scenarios.

The arbitrary phase parameters used for generating Figure 16 are also used to generate Figure 18. When the separation between the two signal sources are in the 10° - 70° range, the CRB_{AS} behavior illustrated in Figure 14 (a) is similar to the CRB_{CM} response of Figure 18 (b). However, when the signal separation is less than ten degrees, the CRB_{CM} of the stationary object achieves the CRB_{CM} of

the moving object. Note that the plots in Figure 16 (b, c) for the moving signal source are exactly the same as those in Figure 18 (b, c) for the stationary signal source.

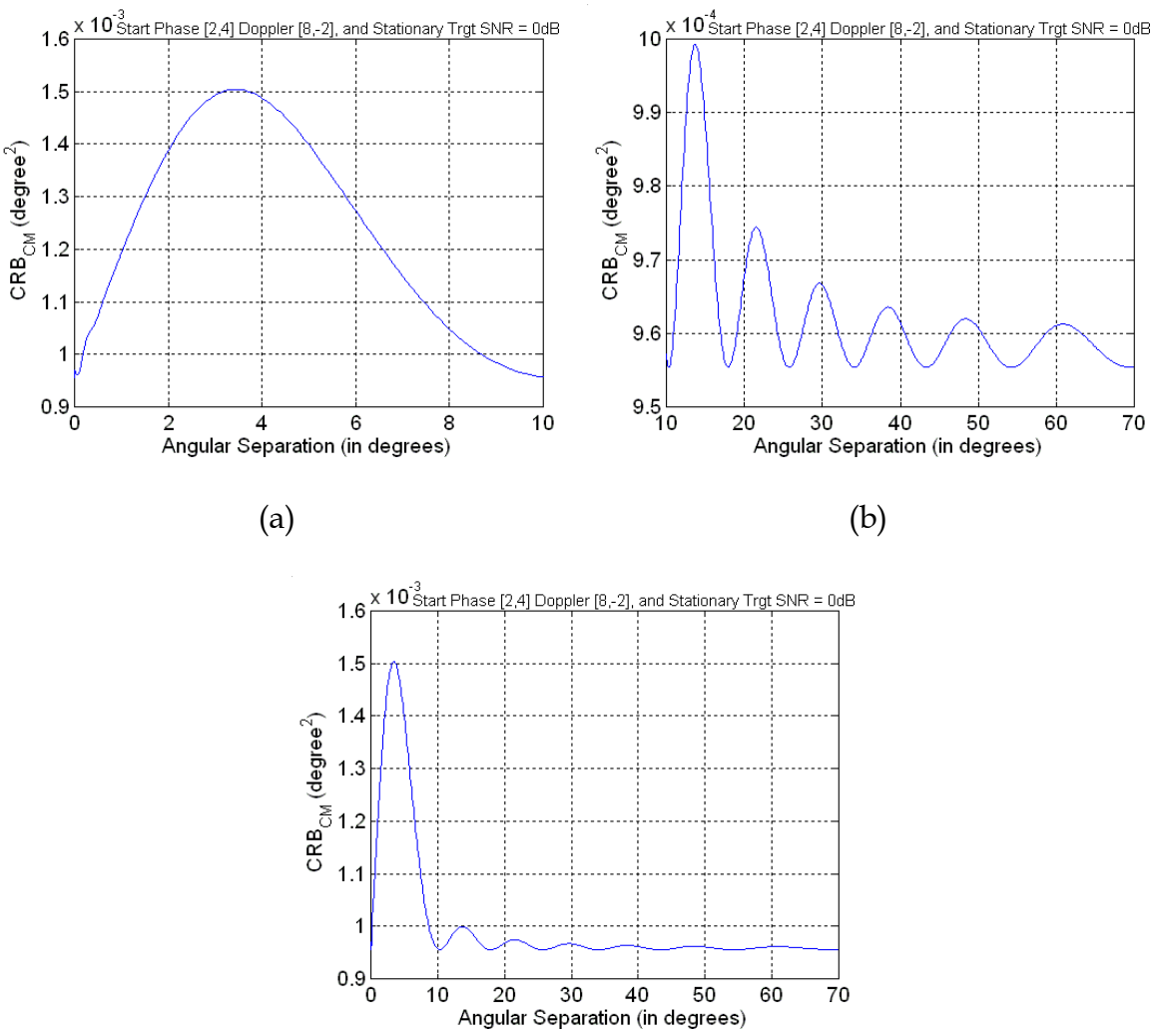

(a) (b)

(c)

Figure 18. The CRB_{CM} of the stationary signal source with 0dB SNR with a moving signal source of the same SNR when Start Phases/Doppler Shifts of the moving, and stationary signal sources are [2,4]/[8,-2] respectively.

The CRB_{CM} of signals with different phase parameters seems to be a lower bound, especially when angular signal separation in azimuth gets smaller. When the angular separation of the signals in azimuth is relatively large (in the 10° - 70° range), the CRB_{CM} of the signals with different phase parameters seems to be slightly lower than if not almost the same as the CRB_{AS} of two signals with zero correlation.

4.3 Scenario 3: Two Signal Sources and a Transmitter of Opportunity (Interferer)

PCL systems can be susceptible to interfering signals in the environment, or even interfering signals from their own transmitters of opportunity. In this section, the effects of a transmitter on the bounds of CM and arbitrary signals are illustrated. Figure 19 shows the CRB_{AS} when all three signals are uncorrelated. Figure 20 shows CRB_{CM} for the phase parameters that are specified on the figures.

4.3.1 CRB_{AS} of Two Signal Sources and a Transmitter of Opportunity (Interferer)

To determine the CRB_{AS} performance for the selected conditions, compare Figure 13 (c) with Figure 19 (b); clearly, a transmitter in the surveillance region does not have a big impact on the CRB_{AS} of the moving signal source when it is in the proximity of the stationary signal source in azimuth plane. This is true in this scenario because the transmitter is further apart from the stationary signal.

When the CRB_{AS} of the moving signal source is observed in the azimuth region near where the transmitter of opportunity is located, the CRB_{AS} of the moving signal source is truly degraded. When the moving object is at 69° its bound is approximately 4 degrees^2, which is approximately equal to 2° standard variation. This value is relatively large, but as the moving object is within 1° of the transmitter, this increase in the bound is crucial.

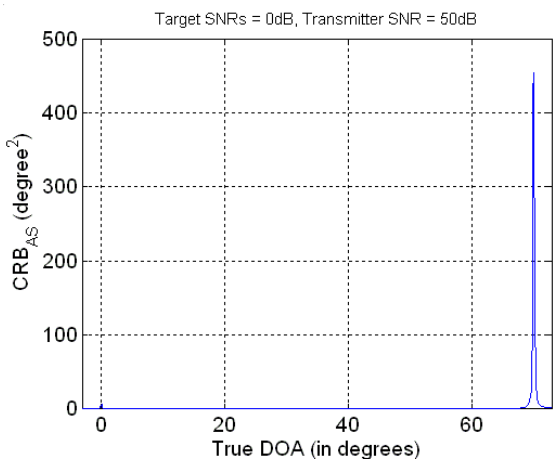

(a)

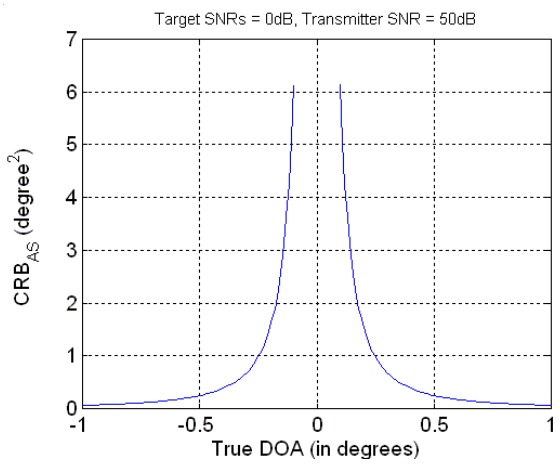

(b)

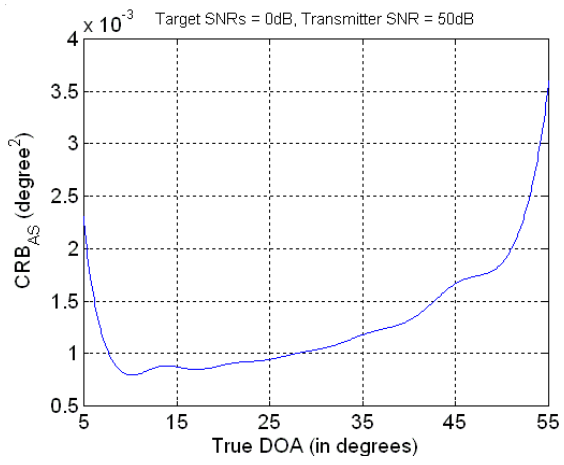

(c)

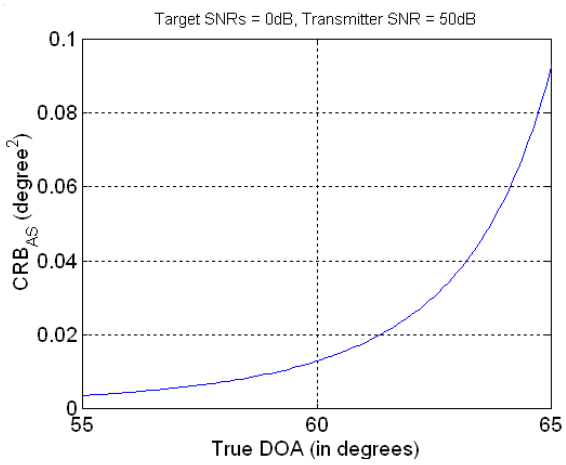

(d)

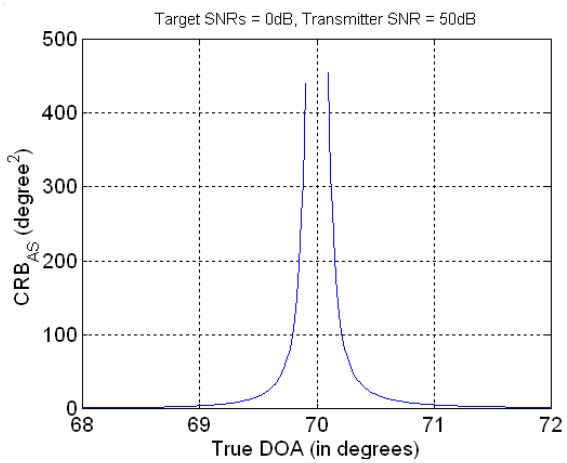

(e)

Figure 19. The CRB_{AS} of the moving signal source with a stationary signal source at 0° and a transmitter of opportunity at 70° when SNR of the moving and stationary signal sources are 0dB and transmitter SNR 50dB.

4.3.2 CRB_{CM} of Two Signal Sources and a Transmitter of Opportunity (Interferer)

The CRB_{CM} of the moving object seems to be a lower bound than CRB_{AS} especially in the proximity of the both stationary signal source and the transmitter in azimuth. As the moving signal source moves away from the antenna broadside, the bound increases due to the array antenna performance; this is shown in Section 4.1.

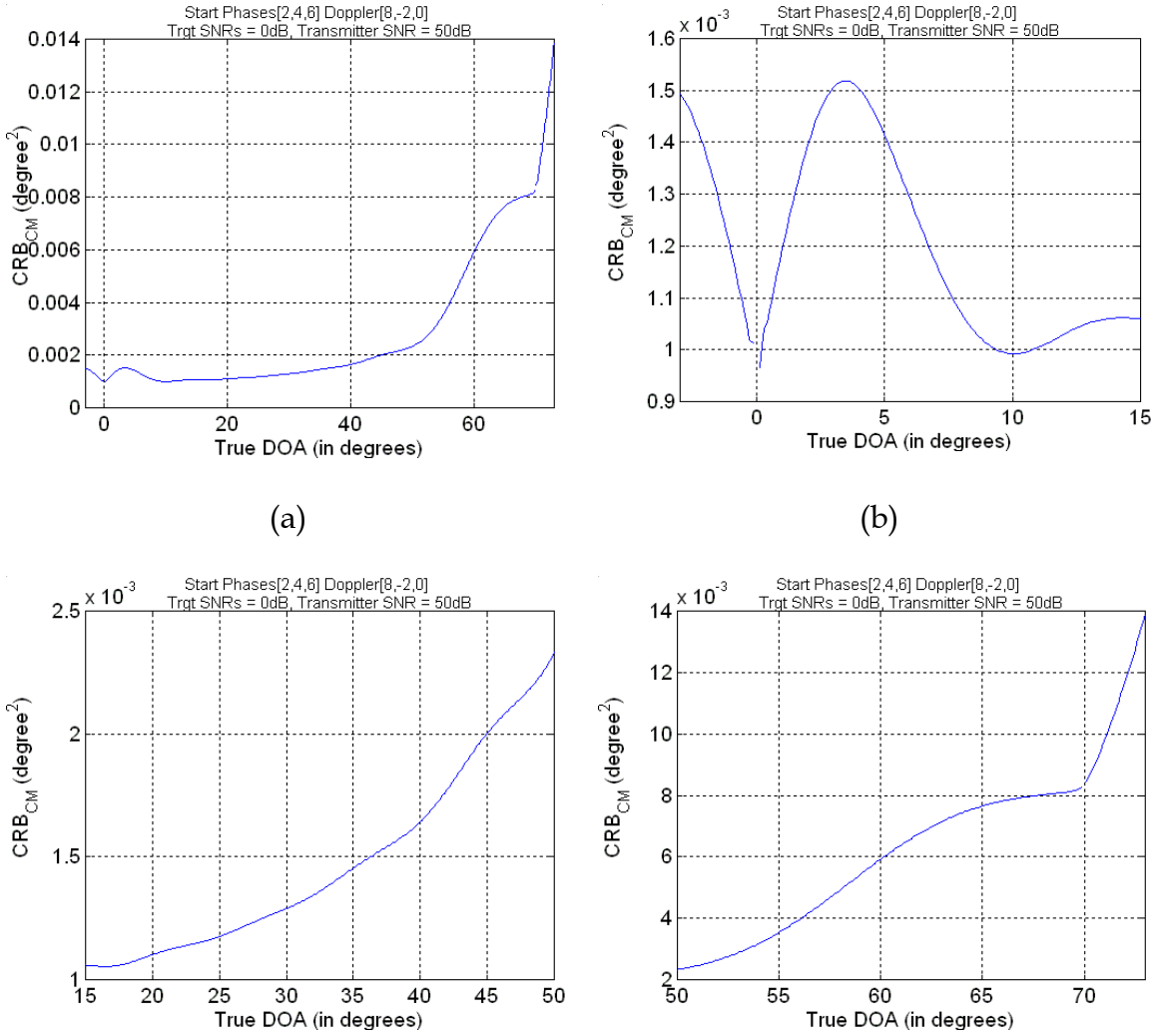

Figure 20. The CRB_{CM} of the moving signal source with a stationary signal source at 0° and a transmitter of opportunity at 70° when SNR of the moving and stationary signal sources are 0dB, and transmitter SNR 50dB; and Start Phases/Doppler Shifts of the moving, and stationary signal sources, transmitter are [2,4,6]/[8,-2,0] respectively .

Figure 16 (b) shows that the CRB_{CM} of the moving signal source for the two signal case is the same as Figure 20 (b). Figure 20 (b) shows, the CRB_{CM} of

the moving object near the stationary object when there is also a stationary object present out at 70°. This is because of the transmitter being located so far from the object of interest. In order to show the effect of a transmitter on the CRB_{CM} of the moving signal source in the vicinity of the stationary, the CRB_{CM} of the moving signal source is plotted in

Figure 21 considers the same conditions as in Figure 20, except that the transmitter of opportunity is located at 15° instead of 70°.

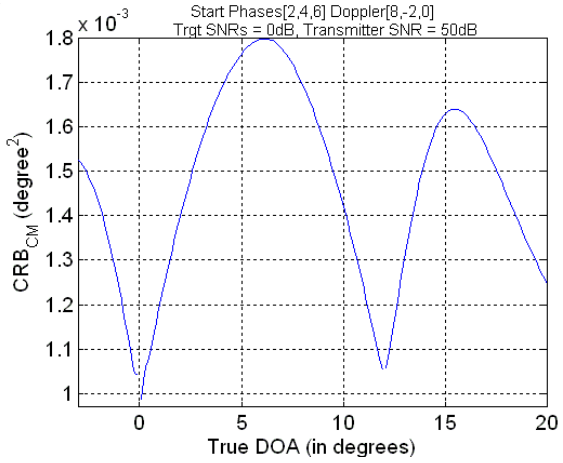

Figure 21. The CRB_{CM} of the moving signal source with a stationary signal source at 0° and a transmitter of opportunity at 12° when SNR of the moving and stationary signal sources are 0dB, and transmitter SNR 50dB; and Start Phases/Doppler Shifts of the moving, and stationary signal sources, transmitter are [2,4,6]/[8,-2,0] respectively .

When Figure 20 (d) is compared with Figure 19 (e) it is observed that the CRB_{CM} remains well below the CRB_{AS} when the moving object is in the transmitter region. Also comparing Figure 20 (b) with Figure 19 (b) shows that

bound of the moving signal source is lower when its estimator has the CM signal constraint. To make a long story short it can be rephrased as follows; the CRB_{CM} is a lower bound than CRB_{AS} when the phase parameters of the incoming signals have different characteristics, and the CRB_{CM} goes even lower when the phase parameters of each signal are less correlated.

4.4 Scenario 4: Moving Object vs. Different Transmitter of Opportunity (Interferer) Locations

This section demonstrates the case when there is one transmitter in the surveillance region. The CRB_{AS} and CRB_{CM} are presented below for one moving object signal whose DOA changes from -70° to 70° for different transmitter locations. The transmitter location in the azimuth plane is only changed from the DOA spectrum of –70° to 0° because the CRB is symmetric about the antenna broadside direction. This experiment should yield additional insight into antenna placement and orientation.

4.4.1 CRB_{AS} of the Moving Object for Different Transmitter Locations

As discussed earlier, AS DOA estimators are more susceptible to increases in the variance estimate when more than one signal is being received from the surveillance region. This is more pronounced when the signal of interest has less signal power compared with the others.

Figure 22 show the CRB_{AS} of a moving object when the transmitter is located at –70°, -50°, -30°, -15°, 0°.

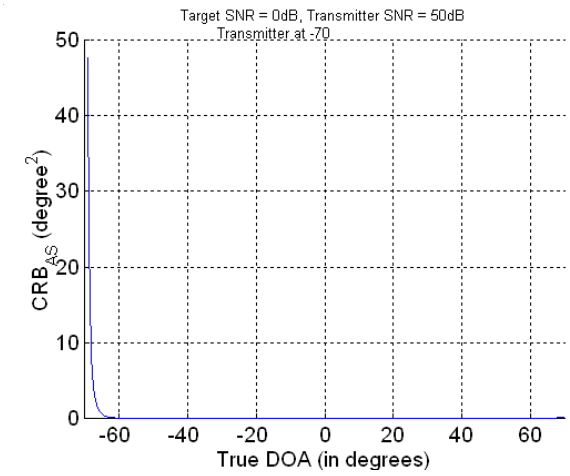

(a)

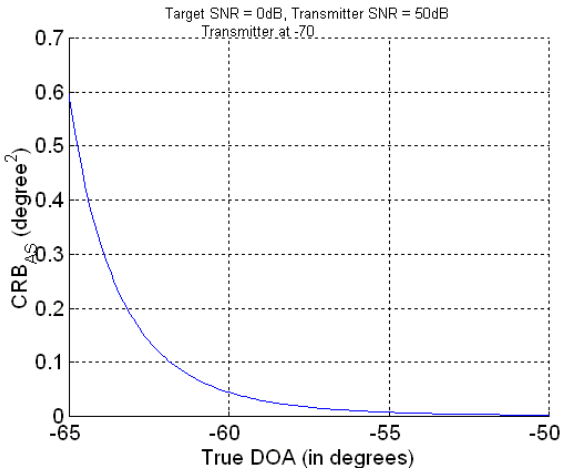

(b)

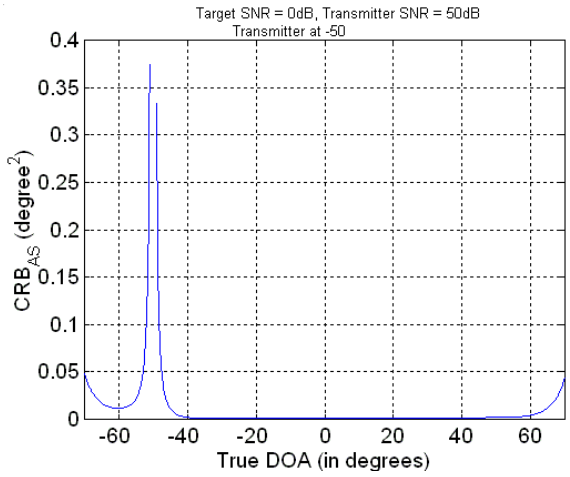

(c)

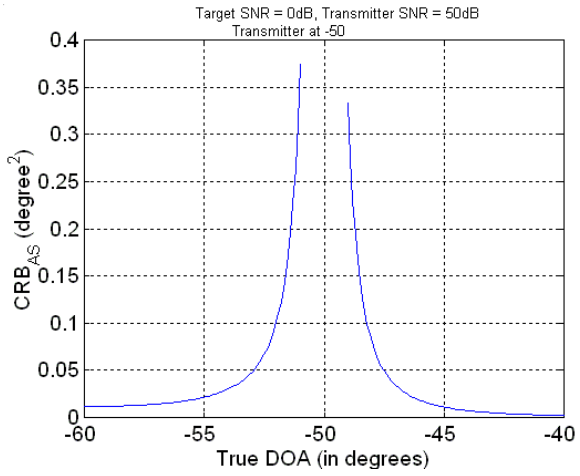

(d)

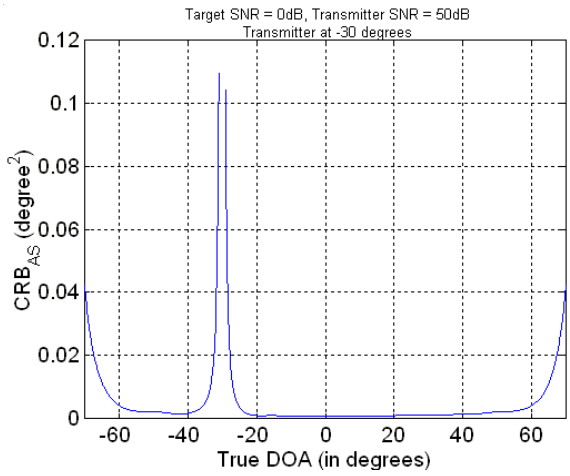
Target SNR = 0dB, Transmitter SNR = 50dB
Transmitter at -30 degrees
CRB_AS (degree^2)
True DOA (in degrees)

(e)

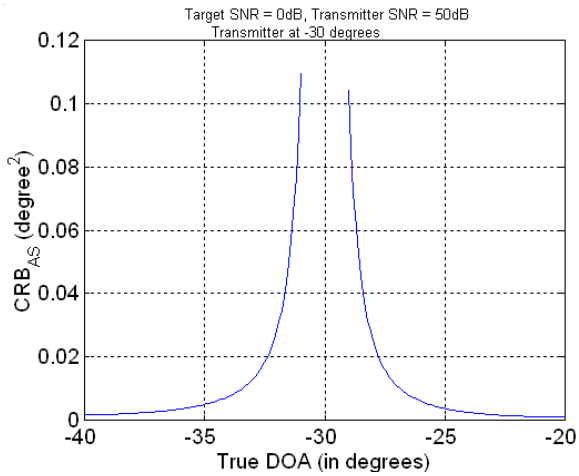
Target SNR = 0dB, Transmitter SNR = 50dB
Transmitter at -30 degrees
CRB_AS (degree^2)
True DOA (in degrees)

(f)

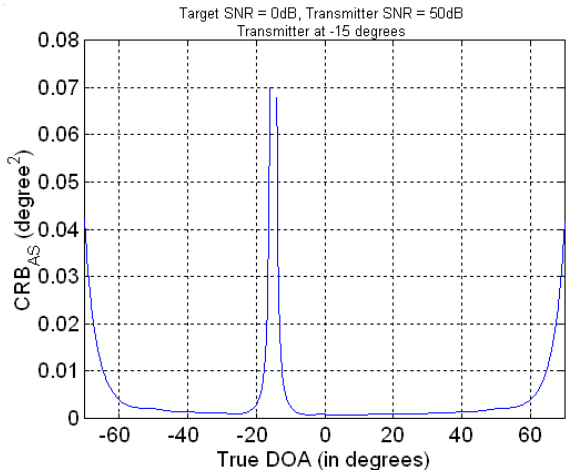
Target SNR = 0dB, Transmitter SNR = 50dB
Transmitter at -15 degrees
CRB_AS (degree^2)
True DOA (in degrees)

(g)

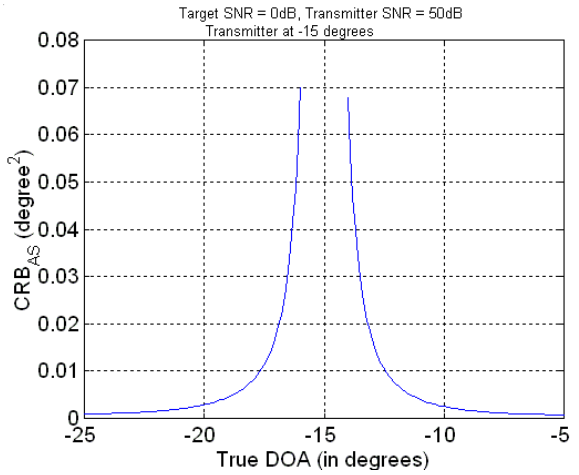
Target SNR = 0dB, Transmitter SNR = 50dB
Transmitter at -15 degrees
CRB_AS (degree^2)
True DOA (in degrees)

(h)

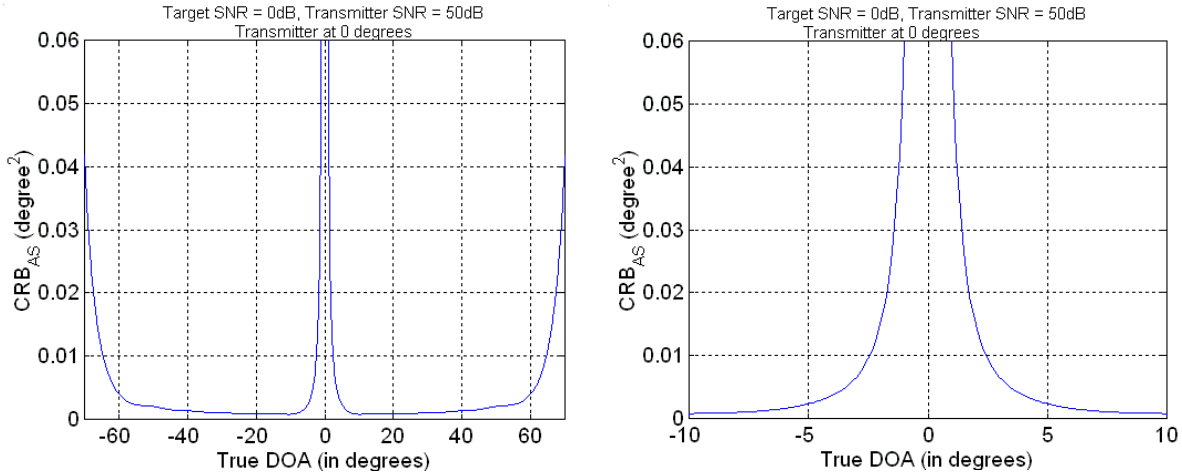

(i) (j)

Figure 22. The CRB_{AS} of the Moving Object with a transmitter of opportunity at different locations [–70°, -50°, -30°, -15°, 0°] when SNR of the moving is 0dB, and transmitter SNR 50dB.

The figures above show that the effect of the interfering transmitter signal on the CRB_{AS} decreases as the transmitter location shifts towards the antenna broadside. Therefore, having the transmitter closer to the antenna broadside direction enables less degradation in the bound. Of course, this results in greater DOA estimation error in the direction of the antenna. When the array antenna orientation can be arbitrarily chosen, placing the transmitter out of the coverage area results in the best accuracy for DOA estimation. If it is not possible to place the transmitter out of the coverage area, then the transmitter should be towards an edge of the array antenna where DOA estimation accuracy is already degraded due to system configuration. Although this results in greater errors

around the DOA of the interfering signal from the transmitter, the DOA for other angular regions remains free of interference and yields higher accuracy estimates.

4.4.2 CRB_{CM} of the Moving Object for Different Transmitter Locations

The CRB_{CM} has been found to be much lower than the CRB_{AS} in the presence of multiple signals. The results presented in this section still support this conclusion.

Figure 23 shows the CRB_{CM} of a moving object when the transmitter is located at –70°, -50°, -30°, -15°, 0°.

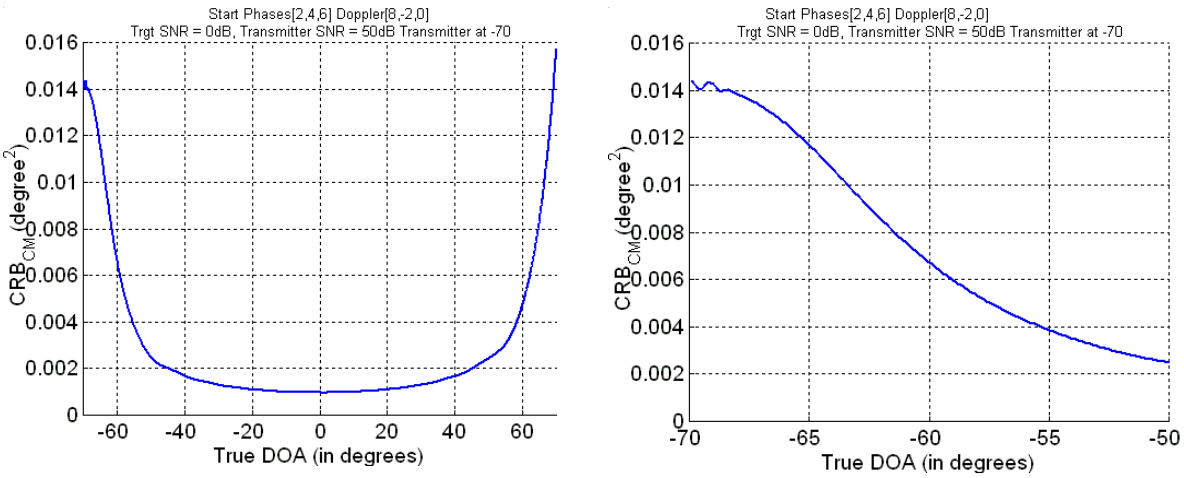

(a) (b)

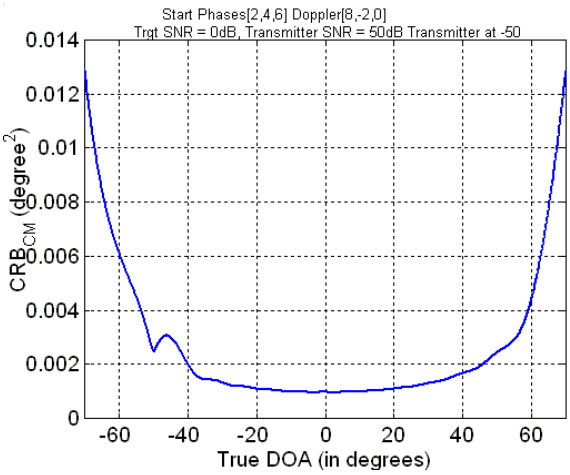
Start Phases[2,4,6] Doppler[8,-2,0]
Trgt SNR = 0dB, Transmitter SNR = 50dB Transmitter at -50
CRB_CM (degree^2)
True DOA (in degrees)

(c)

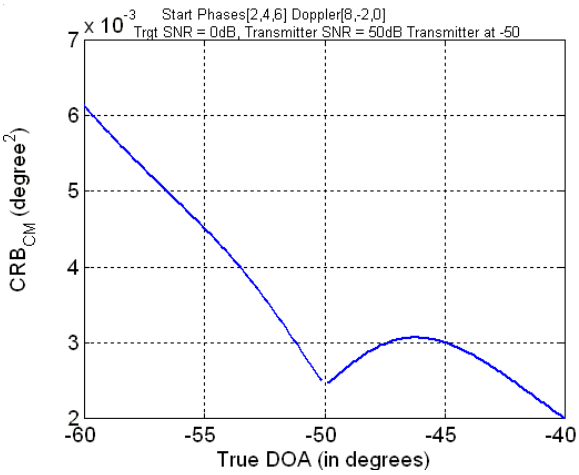
x 10^-3
Start Phases[2,4,6] Doppler[8,-2,0]
Trgt SNR = 0dB, Transmitter SNR = 50dB Transmitter at -50
CRB_CM (degree^2)
True DOA (in degrees)

(d)

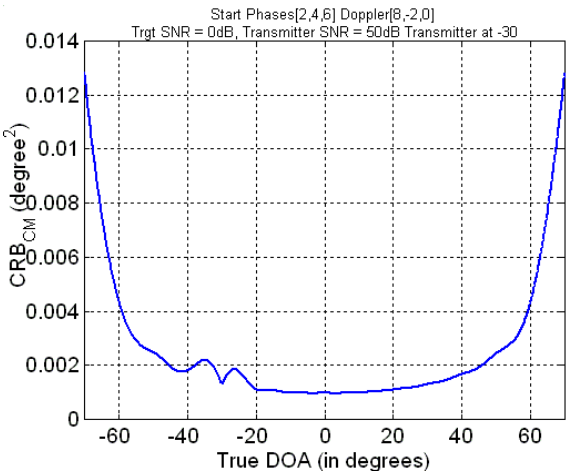
Start Phases[2,4,6] Doppler[8,-2,0]
Trgt SNR = 0dB, Transmitter SNR = 50dB Transmitter at -30
CRB_CM (degree^2)
True DOA (in degrees)

(e)

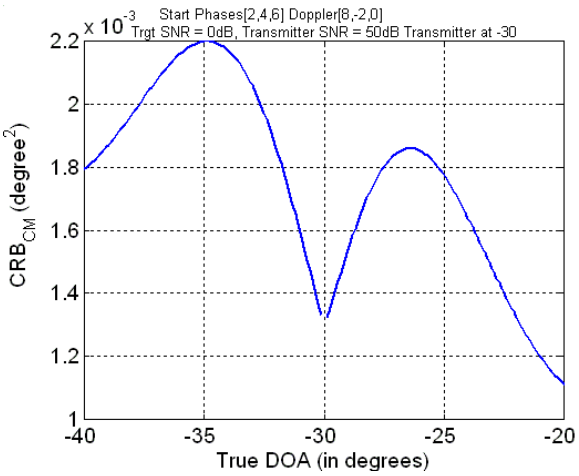
x 10^-3
Start Phases[2,4,6] Doppler[8,-2,0]
Trgt SNR = 0dB, Transmitter SNR = 50dB Transmitter at -30
CRB_CM (degree^2)
True DOA (in degrees)

(f)

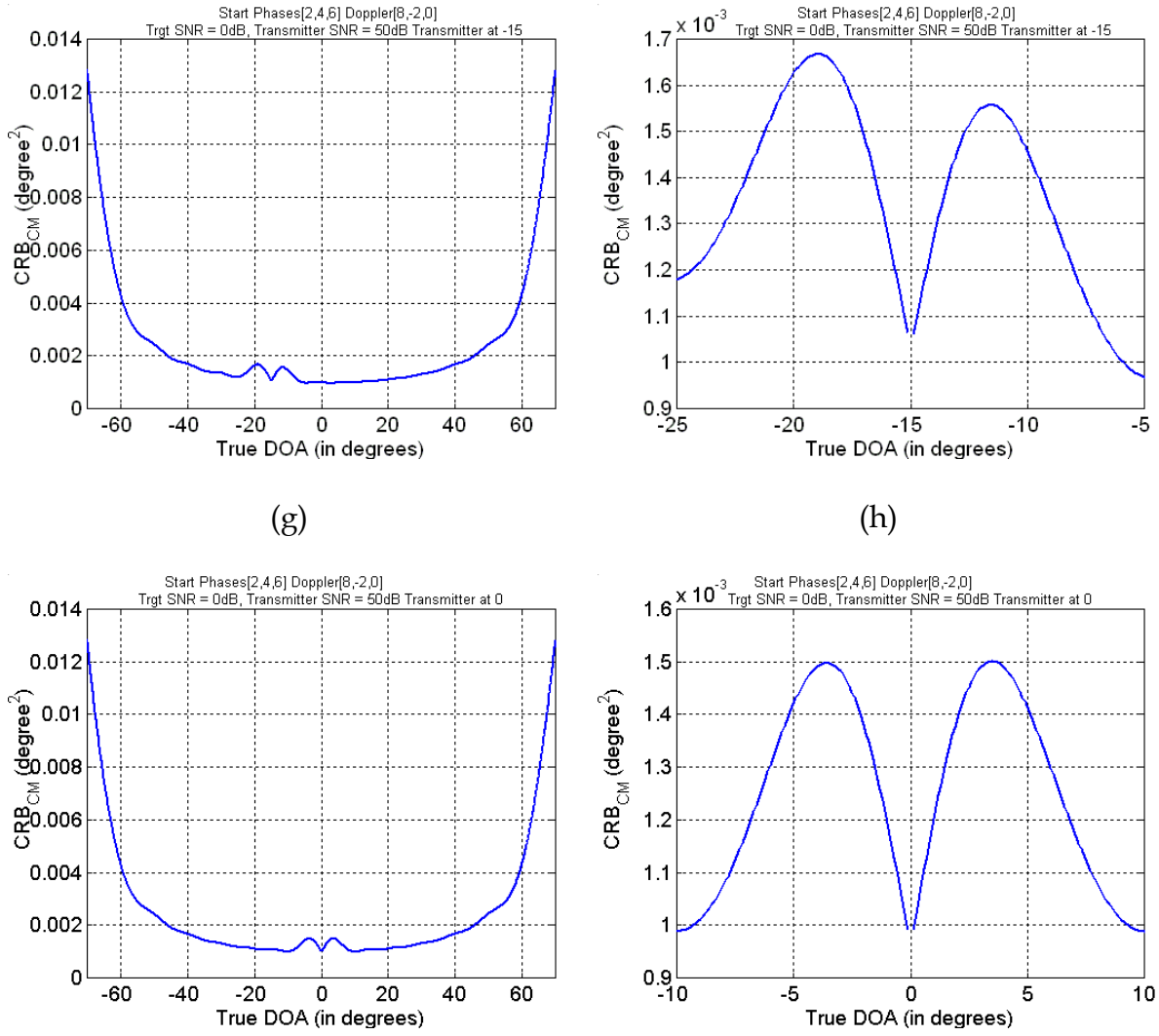

Figure 23. The CRB_{CM} of the Moving Object with a transmitter of opportunity at different locations [–70°, -50°, -30°, -15°, 0°] when SNR of the moving is 0dB, and transmitter SNR 50dB; and Start Phases/Doppler Shifts of the moving, and transmitter are [2,6]/[8,0] respectively.

There is a slight increase in CRB_{CM} when the object DOA is near the transmitter DOA. The CRB_{CM} almost keeps the form of the single object case but

there is a slight increase near the transmitter DOA when the object is in the same azimuth plane region.

In the CM case, it is still preferable to place the transmitter outside the surveillance region if possible. If the transmitter cannot be placed out of the surveillance region, but the antenna orientation can be varied, then the transmitter should be placed towards the edge of the array. By doing this, the DOA region near the antenna broadside direction, which provides the most accurate DOA estimates, is kept free from interference. It must be noted that the need to change the array antenna direction in the CM signal case is not as nearly pronounced as in the AS signal case.

5 . DISCUSSION

5.1 Conclusions

Performance of the Arbitrary Signal (AS) and Constant Modulus (CM) signal DOA estimators were evaluated using the Cramer-Rao Bound (CRB). The CRB theorem was found to be useful because it enables the analysis of the error variance for different cases. As discussed in Section 2.3.2, minimal error variance is desirable and the CRB provides a lower bound on this variance.

In the single object case, both AS and CM signal DOA estimators achieve the same bound. CM DOA estimators use the phase information of each incoming signal to separate signal sources from each other and DOA estimation is done separately for each signal. However, when only one signal is present in the environment, the CRB_{CM} is identical to the CRB_{AS}.

In the case of multiple signals, the CRB_{CM} is a lower bound around the region where the angular separation between two signals in azimuth gets smaller, even when one of the signals is strong interference from a transmitter. The CRB_{CM} is found to be slightly above the CRB for the single object case, including the case with the interfering transmitter. On the other hand, the CRB_{AS} for Arbitrary Signals increases greatly when the angular separation between two signals becomes small, and CRB_{AS} is also affected dramatically by interfering signals with large signal power, (such as the interfering transmitter signal). Hence, this research demonstrated that, in general, the bounds of the CM DOA

estimators are lower than the bounds for AS DOA estimators; CM DOA estimators are declared to have better performance.

As mentioned in Section 2.3, the CRB shows the performance of a Minimum Variance Unbiased (MVUB) estimator. In spectral estimation, the search for a MVUB estimator is a challenging task. Since the bounds for CM DOA estimators show good characteristics in scenarios closely representing real-world applications, the CM DOA estimators prove to be promising. Hence, in the search for the MVUB, giving consideration to CM Signal DOA estimators is highly encouraged.

5.2 Future Work

In this thesis a single Uniform Linear Array (ULA) configuration was studied and there was only one DOA estimate obtained from the array. Dividing the array into smaller sub-arrays results in degraded estimation performance [6]. On the other hand, combining all sub-array estimates and creating mutual coupling between the sub-arrays resulted in a new estimator with different performance. The change in overall DOA estimation performance should be studied and its performance compared to a non-divided array. As demonstrated in this thesis, the CRB provides an excellent tool for such a study.

As was demonstrated in Sections 4.2 and 4.3, the DOA CRB of a signal when other signals exist in the environment show different characteristics. The CRB was found to increase when the DOA of a signal gets close to the DOA of

other signals. This is especially true when there is correlation between the signals; the increase in the CRB becomes more significant. Correlation effects between two signals was implemented in this research using a correlation coefficient and the effect of the correlation level between the Arbitrary Signals on their CRB was shown. However, modeling correlation between CM signals is not as simple. In the thesis it was mentioned that worst case for CM signals occurs when the phase parameters of two signals coming from the same direction are exactly the same. This is the case when the phases of two signals are fully correlated. The changes in the CRB_{CM} with respect to correlation level of the two signals with close DOA angles should be studied by parameterizing the correlation level of the CM signals. This would possibly require a new derivation of the CRB for correlated CM signals.

One assumption that simplified the extent of the research is that the objects are zero altitude objects with DOA only changing in azimuth. Adding elevation to the individual objects and including their altitude in the calculations will reflect results that are more suited to real-world applications. Bounds for DOA error in elevation and azimuth can be achieved by using a planer array antenna model.

The numerical calculations of the CRB are based on the system described in Section 1.5, which is composed of a single ULA antenna configuration. As mentioned above, this can easily be extended to sets of smaller ULA antennas, although the composite estimate becomes somewhat more complicated.

However, ULA antenna configurations are only one of many. Cramer-Rao Bounds for other types of array configurations can also be determined and the advantages/disadvantages of different array types, shapes, radiating elements and element spacing can be studied.

Appendix A

PRF 1: $$E\left[\underline{e}^{H}(t)\,\underline{e}(t)\,\underline{e}^{H}(s)\,\underline{e}(s)\right]=\begin{cases} m^2\sigma^2 & \text{for } t \neq s \\ m(m+1)\sigma^2 & \text{for } t = s \end{cases}$$

When $t \neq s$, $\underline{e}(t)$ and $\underline{e}(s)$ are statistically independent from each other hence the expected value of their product can be written as the products of their expected values.

$$E\left[\underline{e}^{H}(t)\,\underline{e}(t)\,\underline{e}^{H}(s)\,\underline{e}(s)\right]=E\left[\underline{e}^{H}(t)\,\underline{e}(t)\right]E\left[\underline{e}^{H}(s)\,\underline{e}(s)\right]=\sum_{i=1}^{m}E\left[e_i^{*}(t)\,e_i(t)\right]\times\sum_{l=1}^{m}E\left[e_l^{*}(s)\,e_l(s)\right]$$
$$=\sum_{i=1}^{m}\sigma\times\sum_{l=1}^{m}\sigma=m^2\sigma^2$$

When $t = s$,

$$E\left[\underline{e}^{H}(t)\,\underline{e}(t)\,\underline{e}^{H}(t)\,\underline{e}(t)\right]=E\left[\left(\underline{e}^{H}(t)\,\underline{e}(t)\right)^2\right]=E\left[\left(\bar{\underline{e}}^{T}(t)\,\bar{\underline{e}}(t)+\tilde{\underline{e}}^{T}(t)\,\tilde{\underline{e}}(t)\right)^2\right]$$
$$=E\left[\left(\bar{\underline{e}}^{T}(t)\,\bar{\underline{e}}(t)\right)^2\right]+2E\left[\left(\bar{\underline{e}}^{T}(t)\,\bar{\underline{e}}(t)\right)\left(\tilde{\underline{e}}^{T}(t)\,\tilde{\underline{e}}(t)\right)\right]+E\left[\left(\tilde{\underline{e}}^{T}(t)\,\tilde{\underline{e}}(t)\right)^2\right]$$

Note that the real and imaginary parts are statistically independent.

$$E\left[\underline{e}^{H}(t)\,\underline{e}(t)\,\underline{e}^{H}(t)\,\underline{e}(t)\right]=E\left[\left(\bar{\underline{e}}^{T}(t)\,\bar{\underline{e}}(t)\right)^2\right]+2E\left[\bar{\underline{e}}^{T}(t)\,\bar{\underline{e}}(t)\right]E\left[\left(\tilde{\underline{e}}^{T}(t)\,\tilde{\underline{e}}(t)\right)\right]+E\left[\left(\tilde{\underline{e}}^{T}(t)\,\tilde{\underline{e}}(t)\right)^2\right]$$

$$\left.\begin{aligned} E\left[\bar{\underline{e}}^{T}(t)\,\bar{\underline{e}}(t)\right]&=E\left[\left(\tilde{\underline{e}}^{T}(t)\,\tilde{\underline{e}}(t)\right)\right]=\frac{m\sigma}{2} \\ E\left[\left(\bar{\underline{e}}^{T}(t)\,\bar{\underline{e}}(t)\right)^2\right]&=E\left[\left(\tilde{\underline{e}}^{T}(t)\,\tilde{\underline{e}}(t)\right)^2\right] \end{aligned}\right\}E\left[\underline{e}^{H}(t)\,\underline{e}(t)\,\underline{e}^{H}(t)\,\underline{e}(t)\right]=2E\left[\left(\bar{\underline{e}}^{T}(t)\,\bar{\underline{e}}(t)\right)^2\right]+\frac{m^2\sigma^2}{2}$$

$$E\left[\left(\bar{\underline{e}}^{T}(t)\,\bar{\underline{e}}(t)\right)^2\right]=E\left[\left(\sum_{i=1}^{m}\bar{e}_i^{\,2}(t)\right)^2\right]=E\left[\sum_{i=1}^{m}\bar{e}_i^{\,2}(t)\times\sum_{l=1}^{m}\bar{e}_l^{\,2}(t)\right]=\sum_{i=1}^{m}\sum_{\substack{l=1\\ l\neq i}}^{m}E\left[\bar{e}_i^{\,2}(t)\,\bar{e}_l^{\,2}(t)\right]+\sum_{i=1}^{m}E\left[\bar{e}_i^{\,4}(t)\right]$$
$$=\sum_{i=1}^{m}\sum_{\substack{l=1\\ l\neq i}}^{m}E\left[\bar{e}_i^{\,2}(t)\right]E\left[\bar{e}_l^{\,2}(t)\right]+m\,E\left[\bar{e}_i^{\,4}(t)\right]$$

$$\left.\begin{aligned} E\left[\bar{e}_i^{\,2}(t)\right] &= \frac{\sigma}{2} \\ E\left[\bar{e}_i^{\,4}(t)\right] &= \frac{3\sigma^2}{4} \end{aligned}\right\} E\left[\left(\underline{\bar{e}}^{T}(t)\,\underline{\bar{e}}(t)\right)^2\right] = (m-1)m\frac{\sigma^2}{4} + m\frac{3\sigma^2}{4} = (m+2)m\frac{\sigma^2}{4}$$

$$\Rightarrow E\left[\underline{e}^{H}(t)\,\underline{e}(t)\,\underline{e}^{H}(t)\,\underline{e}(t)\right] = m(m+2)\frac{\sigma^2}{2} + \frac{m^2\sigma^2}{2} = m(m+1)\sigma^2$$

PRF 2: $E\left[\underline{e}^{H}(t)\;\underline{e}(t)\;\underline{e}^{H}(s)\;\right]=0$

When t ≠ s, they are independent, and because the noise has zero mean, the proof is strait forward.

$$E\left[\underline{e}^{H}(t)\;\underline{e}(t)\;\underline{e}^{H}(s)\;\right]=E\left[\underline{e}^{H}(t)\;\underline{e}(t)\;\right]E\left[\underline{e}^{H}(s)\right]=0$$

When t = s, the expectation becomes the third order moment of a Gaussian random variable, which is zero.

PRF 3: $$\begin{bmatrix} \overline{\mathbf{H}} & -\widetilde{\mathbf{H}} \\ \widetilde{\mathbf{H}} & \overline{\mathbf{H}} \end{bmatrix}^{-1} = \begin{bmatrix} \overline{\mathbf{G}} & -\widetilde{\mathbf{G}} \\ \widetilde{\mathbf{G}} & \overline{\mathbf{G}} \end{bmatrix}$$

This equality can also be written as

$$\begin{aligned} \overline{\mathbf{H}}\overline{\mathbf{G}} + \widetilde{\mathbf{H}}\widetilde{\mathbf{G}} &= \mathbf{I} \\ \overline{\mathbf{H}}\widetilde{\mathbf{G}} + \widetilde{\mathbf{H}}\overline{\mathbf{G}} &= 0 \end{aligned}$$

which must hold true since $\mathbf{G} \overset{\Delta}{=} \mathbf{H}^{-1}$, and

$$\mathbf{I} = \mathbf{H}\mathbf{G} = \left(\overline{\mathbf{H}} + j\widetilde{\mathbf{H}}\right)\left(\overline{\mathbf{G}} + j\widetilde{\mathbf{G}}\right) = \left(\overline{\mathbf{H}}\overline{\mathbf{G}} - \widetilde{\mathbf{H}}\widetilde{\mathbf{G}}\right) + j\left(\overline{\mathbf{H}}\widetilde{\mathbf{G}} + \widetilde{\mathbf{H}}\overline{\mathbf{G}}\right).$$

Appendix B

$$CRB_{AS}(\underline{\theta}_R)=\frac{\sigma}{2}\left(\sum_{t=1}^{N}\mathrm{Re}\left[\mathbf{X}^H(t)\mathbf{D}^H\left[\mathbf{I}-\mathbf{A}\left(\mathbf{A}^H\mathbf{A}\right)^{-1}\mathbf{A}^H\right]\mathbf{D}\mathbf{X}(t)\right]\right)^{-1}$$ is given in (52).

Then the $\mathbf{J}_{ij}$ can be shown as,

$$J_{ij}=\frac{2}{\sigma}\mathrm{Re}\left\{d^H(\theta_{Ri})\left[\mathbf{I}-\mathbf{A}\left(\mathbf{A}^H\mathbf{A}\right)^{-1}\mathbf{A}^H\right]d(\theta_{Rj})\sum_{t=1}^{N}x_i^H(t)x_j(t)\right\}$$

$\mathbf{P}\overset{\Delta}{=}E\left[\underline{x}(t)\underline{x}^H(t)\right]$ and by definition $\lim_{N\to\infty}\frac{1}{N}\sum_{t=1}^{N}x_i^H(t)x_j(t)=P_{ji}$. Substituting P_{ij} into $\mathbf{J}_{ij}$ and rewriting Fisher Information matrix gives,

$$J=\frac{2}{\sigma}\mathrm{Re}\left\{D^H\left[\mathbf{I}-\mathbf{A}\left(\mathbf{A}^H\mathbf{A}\right)^{-1}\mathbf{A}^H\right]\mathbf{D}.*N\mathbf{P}^T\right\}.$$

Then the CRB_{AS} is obtained as given in Equation (53).

$$CRB_{AS}(\underline{\theta}_R)=\frac{\sigma}{2N}\left(\mathbf{Re}\left[\mathbf{D}^H\left[\mathbf{I}-\mathbf{A}\left(\mathbf{A}^H\mathbf{A}\right)^{-1}\mathbf{A}^H\right]\mathbf{D}.*\mathbf{P}^T\right]\right)^{-1}$$

Appendix C

$$\mathbf{P} \overset{\Delta}{=} E\left[\underline{x}\,\underline{x}^{H}\right]$$

When n = 2,

$$\mathbf{P} = \begin{bmatrix} E\left[x_1^2\right] & E\left[x_1 x_2\right] \\ E\left[x_1 x_2\right] & E\left[x_2^2\right] \end{bmatrix}$$

For convenience let's assume that $E\left[x_1^2\right]=1$, and $E\left[x_2^2\right] = \alpha\, E\left[x_1^2\right]$ so **P** can be written as,

$$\mathbf{P} = \begin{bmatrix} 1 & E\left[x_1 x_2\right] \\ E\left[x_1 x_2\right] & \alpha \end{bmatrix}$$

Correlation coefficient, ρ is equal to $\rho_{12} = \dfrac{E\left[x_1 x_2\right]}{\sigma_{x_1}\sigma_{x_2}}$. Since $\sigma_{x_2} = \sqrt{\alpha}\sigma_{x_1}$, and $\sigma_{x_1} = 1$; $E\left[x_1 x_2\right] = \rho_{12}\sigma_{x_1}\sigma_{x_2} = \rho_{12}\sqrt{\alpha}$. Substituting this into **P** gives,

$$\mathbf{P} = \begin{bmatrix} 1 & \rho_{12}\sqrt{\alpha} \\ \rho_{12}\sqrt{\alpha} & \alpha \end{bmatrix}$$

Appendix D

This appendix shows the CRB for a single signal over a DOA range of 70° to -70°, along with effects of different SNR levels. In Section 4.1, the CRB for a single signal is shown when SNR is 0dB. Here the CRB of a single signal is plotted for the SNR levels of 10, 20, -10dBs. In numerical representation of the SNR this corresponds to the increase of SNR from 0dB by 10, 100 and 1/10 respectively. There is an inverse relation between the SNR and CRB. When the SNR is increased by factors of 10, 100, and 1/10; CRB is reduced by factors of 1/10, 1/100, 10. This can be observed in the plots below. Please note that the shape remains the same but the magnitude on the axis where CRB is shown changes by the factors that have been mentioned above.

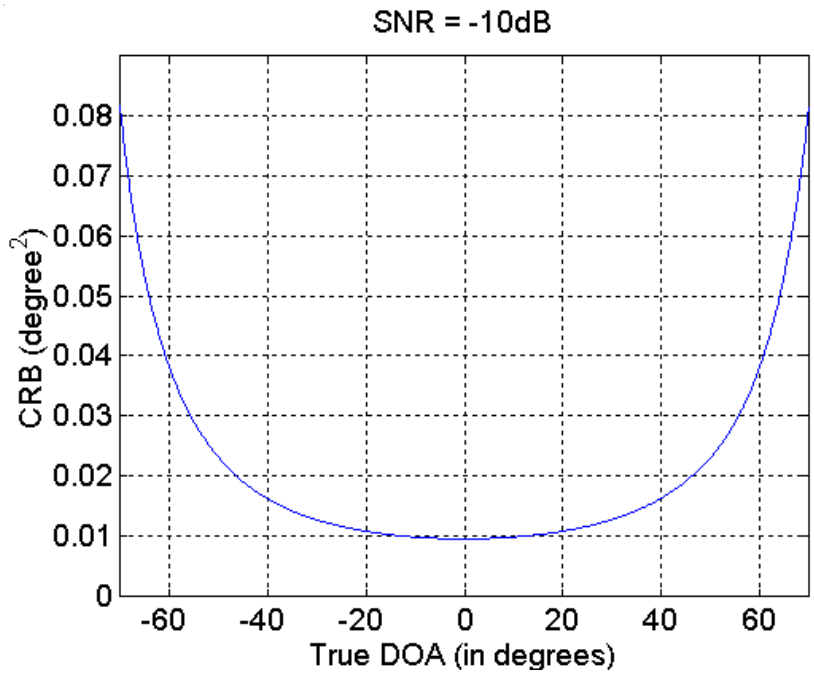

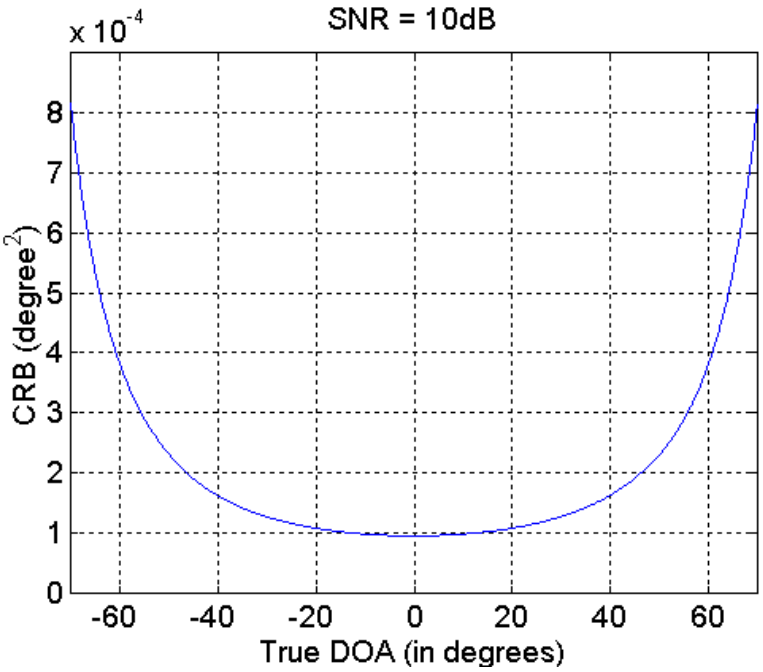
SNR = 10dB
x 10^-4
CRB (degree^2)
0
1
2
3
4
5
6
7
8
-60
-40
-20
0
20
40
60
True DOA (in degrees)

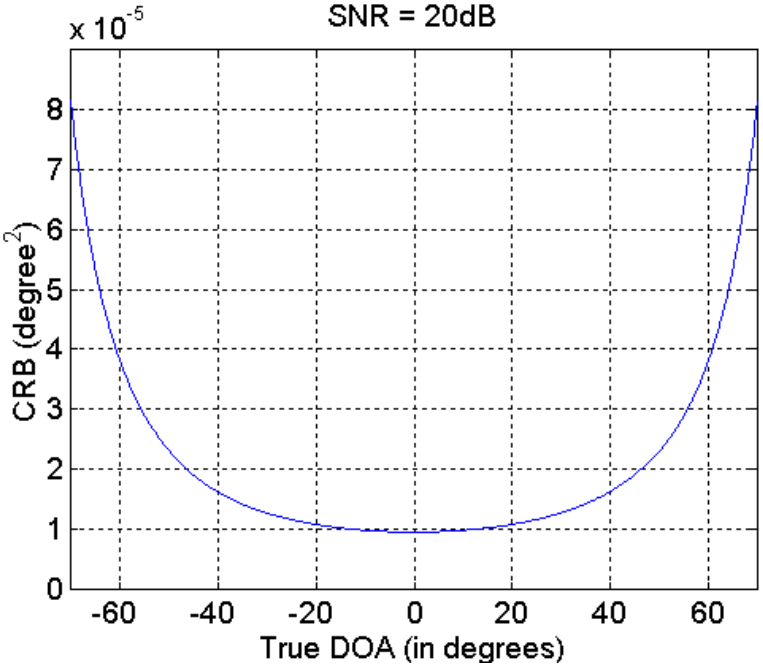
SNR = 20dB
x 10^-5
CRB (degree^2)
0
1
2
3
4
5
6
7
8
-60
-40
-20
0
20
40
60
True DOA (in degrees)

Appendix E

CRB_{AS} of the moving and the stationary signal sources are given in the figures below. As the correlation between the signal sources increases, the CRB_{AS} increase dramatically when two signal sources are close to one another in the azimuth plane. When the signal sources are further apart from each other in azimuth, then CRB_{AS} is still higher for the highly correlated signals case but it is not as pronounced as when angular signal separation of the signals is comparatively less.

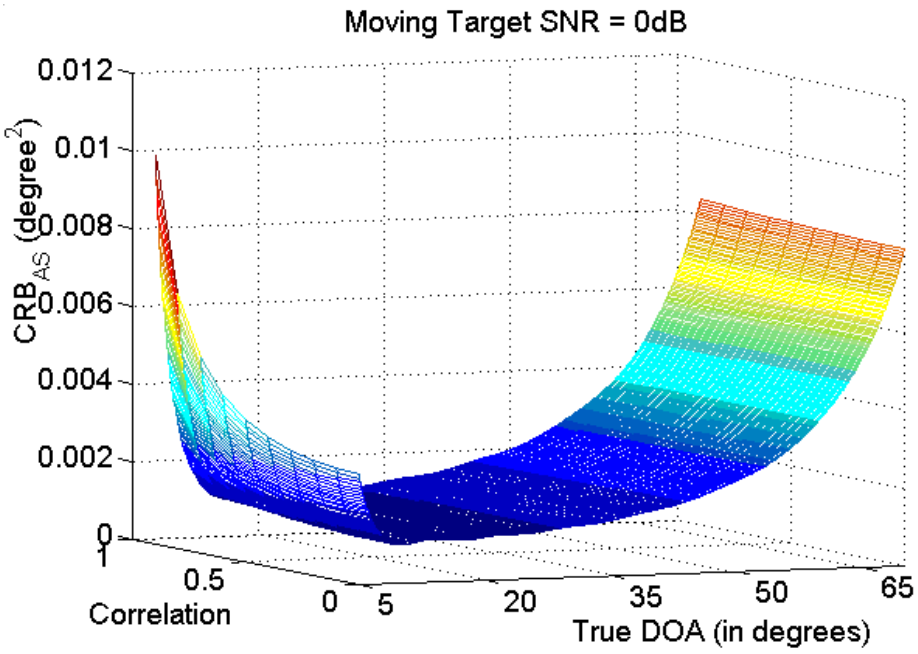

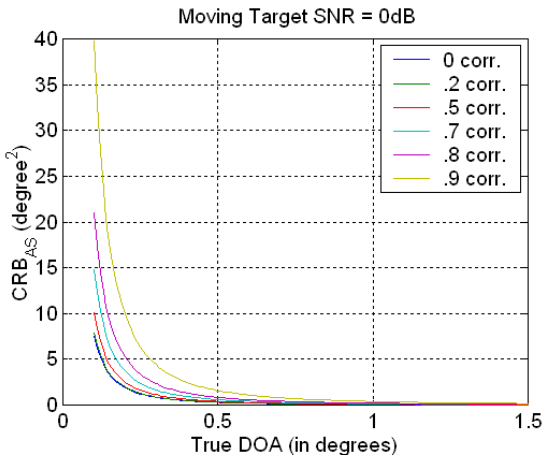

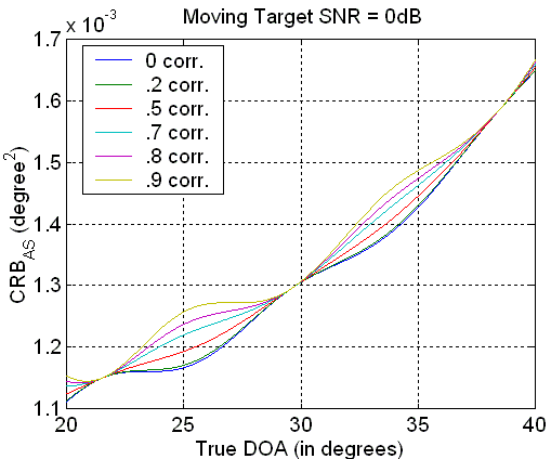

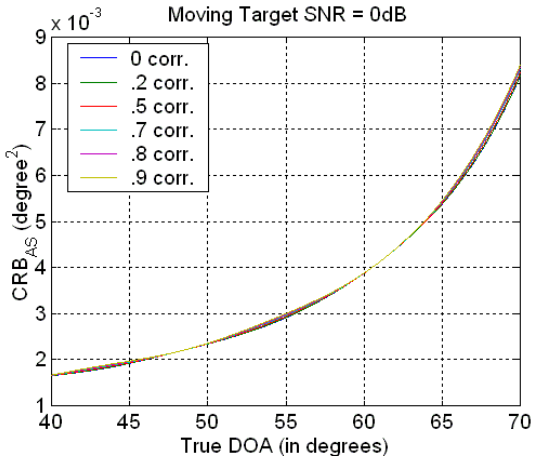

The CRB_{AS} of the moving signal source when there is a stationary signal source located at antenna broadside with 0dB SNR values for both.

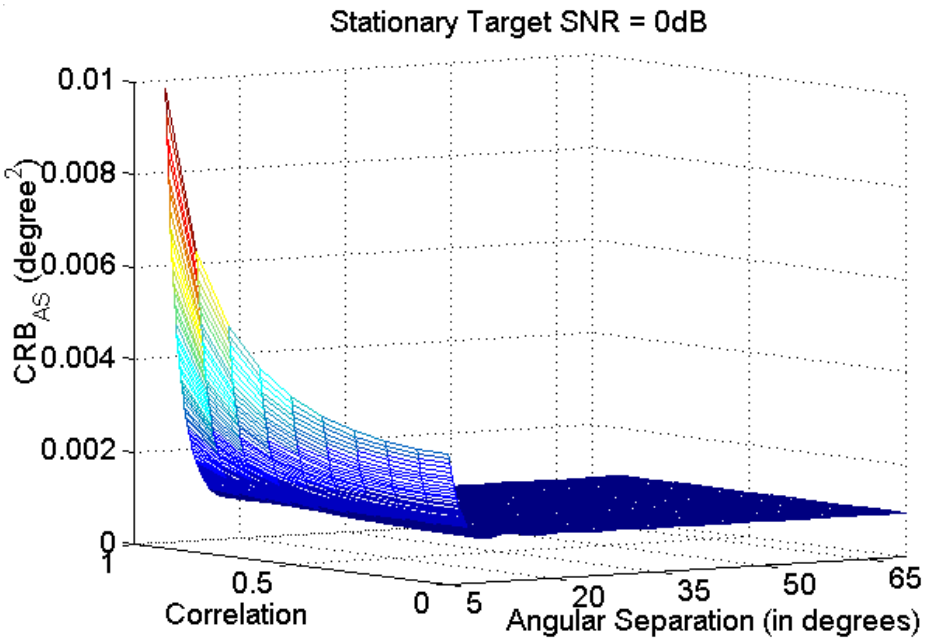

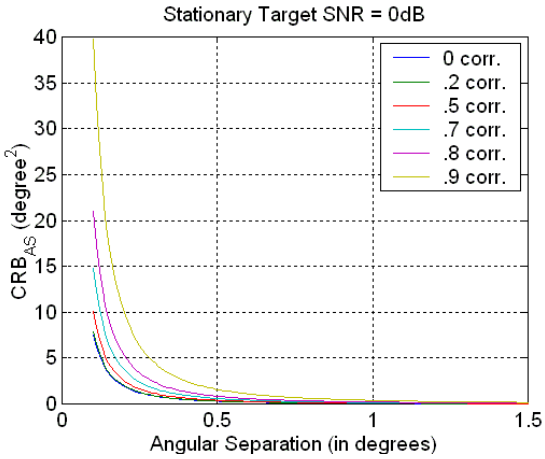

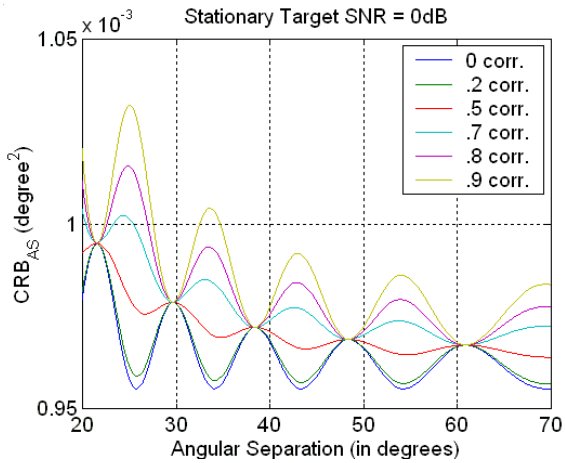

The CRB_{AS} of the stationary signal source located at the antenna broadside when there is a moving signal source getting closer to the stationary signal source in azimuth plane with 0dB SNR values for both.

BIBLIOGRAPHY

[1] Skolnik, Merrill I. Introduction to Radar Systems (3rd Edition). New York: McGraw Hill Co., 2001.

[2] Howland, Paul E. "A Review of Passive Sensor Technology," Surveillance Branch, NATO C3 Agency, Netherlands, 14 Sep 2000.

[3] Willis, Nicholas J. Bistatic Radar (2nd Edition). Maryland: Technology Service Corporation, 1995.

[4] Kay, Steven M. Fundamentals of Statistical Signal Processing. NJ: Prentice Hall, 1993.

[5] Scharf, Louis L. Statistical Signal Processing Detection, Estimation, and Time Series Analysis. Massachusetts: Addison-Wesley Publishing Co. Inc., 1991.

[6] Stoica, Petre, and Arye Nehorai. 'MUSIC, Maximum Likelihood, and Cramer-Rao Bound," *IEEE Transactions on Acoustics, Speech, and Signal Processing,* 37: 720-741 (May 1989)

[7] Van der Veen, Alle-Jan, and Arogyaswami Paulraj. "An Analytical Constant Modulus Algorithm," *IEEE Transactions on Signal Processing*, 44: (May 1996).

[8] Eaves, J. L. and E. K Reedy. *Principles of Modern Radar*. New York: Van Nostrand Reinhold, 1987.

[9] Maas, S. A. "Microwave Mixers in the 90s," *Microwave Journal*, 61-72 Mar 1990.

[10] Guerlac, H. E. *Radar in World War II*, Vols. I and II. New York: Tomask/American Institute of Physics, 1987.

[11] Skolnik, M. I. "*An analysis of Bistatic Radar*," IRE Transactions on Aerospace and Navigational Elektroniks, 19-27, Mar 1961.

[12] Price, A. *Instruments of Darkness – The Struggle For Radar Suppremacy.* William Kimber and Co. Ltd., 1967.

[13] Glaser, J. I. "*Some Results in the Bistatic Cross Section of Complex Objects," Proceedings of the IEEE,* 77, 5: 639-648 (May 1989).

[14] Willis, Nicholas J. "PCL Systems." Address to Air Force Institute of Technology (AFIT) Students and Faculty Members. AFIT, Wright-Patterson AFB, Ohio. June 2001.

[15] Veen, Alle J. “Blind Source Separation Based On Combined Direction Finding and Constant Modulus Properties,” Delft University of Technology, Netherlands.

[16] Howland, Paul E. *Television Based Bistatic Radar,* PhD thesis. School of Electronic and Electrical Engineering, University of Birmingham, England, Sep 1997 (B152TT).

[17] Stimson, George W. Introduction to Airborne Radar (2nd Edition). New Jersey: Scitech Publishing Inc., 1998.

[18] Balanis, Constantine A. Antenna Theory Analysis and Design (2nd Edition). New York:John Wiley & Sons Inc., 1997.

[19] Skolnik, Merrill I. Radar Handbook (2nd Edition). New York: McGraw Hill Co., 1990.

[20] Francos, Joseph M., and Benjamin Friedlander. “Bounds for Estimation of Complex Exponentials in Unknown Colored Noise,” *IEEE Transactions on Signal Processing*, 43: 2176- 2185 (September 1995).

[21] Stark, Henry, and John W. Woods. Probability, Random Processes, and Estimation Theory for Engineers (2nd Edition). New Jersey: Prentice Hall Inc., 1994.

[22] Gooch R., and J. Lundell. “The CM Array: An Adaptive Beamformer for Constant Modulus Signals,” *IEEE International Conference on Acoustics, Speech, and Signal Processing*, 2523-2526 (May 1986).

[23] Treicher, J.R. and M.G. Larimore. “New processing techniques based on constant modulus adaptive algoritm,” *IEEE Transactions on Acoustics, Speech, Signal Processing,* 33: 420-431 (April 1985).

[24] Leshem, Amir and Alle J. Van der Veen. “Direction-of-Arrival Estimation for Constant Modulus Signals,” *IEEE Transactions on Signal Processing,* 47:3125-3130 (November 1999).

[25] Sadler, Brian M., and Richard J. Kozick. “Bounds on Bearing and Symbol Estimation with Side Information,” *IEEE Transactions on Signal Processing,* 49: 822-834 (April 2001).

REPORT DOCUMENTATION PAGE

Form Approved
OMB No. 074-0188

1. REPORT DATE *(DD-MM-YYYY)*	2. REPORT TYPE	3. DATES COVERED *(From – To)*
15-03-2002	Master's Thesis	Jun 2001 – Mar 2002

4. TITLE AND SUBTITLE

STATISTICAL ERROR ANALYSIS OF A DOA ESTIMATOR FOR A PCL SYSTEM USING THE CRAMER-RAO BOUND THEOREM

5a. CONTRACT NUMBER

5b. GRANT NUMBER

5c. PROGRAM ELEMENT NUMBER

6. AUTHOR(S)

Say, Kerim, 1st Lt., TUAF

5d. PROJECT NUMBER

5e. TASK NUMBER

5f. WORK UNIT NUMBER

7. PERFORMING ORGANIZATION NAMES(S) AND ADDRESS(S)

Air Force Institute of Technology
Graduate School of Engineering and Management (AFIT/EN)
2950 P Street, Building 640
WPAFB OH 45433-7765

8. PERFORMING ORGANIZATION REPORT NUMBER

AFIT/GE/ENG/02M-23

9. SPONSORING/MONITORING AGENCY NAME(S) AND ADDRESS(ES)

NATO C3 Agency
Attn: Dr. Paul Howland
P.O Box174 Telephone No: +31-70 314-2476
The Netherlands e-mail: Paul.Howland@nc3a.nato.int

10. SPONSOR/MONITOR'S ACRONYM(S)

11. SPONSOR/MONITOR'S REPORT NUMBER(S)

12. DISTRIBUTION/AVAILABILITY STATEMENT

APPROVED FOR PUBLIC RELEASE; DISTRIBUTION UNLIMITED.

13. SUPPLEMENTARY NOTES

14. ABSTRACT

Direction of Arrival (DOA) estimation of signals has been a popular research area in Signal Processing. DOA estimation also has a significant role in the object location process of Passive Coherent Location (PCL) systems. PCL systems have been in open literature since 1986 and their applications are not as clearly understood as the DOA estimation problem. However, they are the focus of many current research efforts and show much promise.

The purpose of this research is to analyze the DOA estimation errors in a PCL system. The performance of DOA estimators is studied using the Cramer-Rao Bound (CRB) Theorem. The CRB provides a lower bound on the variance of unbiased DOA estimators. Since variance is a desirable property for measuring the accuracy of an estimator, the CRB gives a good indication about the performance of an estimator. Previous DOA estimators configured with array antennas used the array antenna manifold, or the properties of the array antenna structure, to estimate signal DOA. Conventional DOA estimators use arbitrary signal (AS) structures. Constant Modulus (CM) DOA estimators restrict the input signals to a family of constant envelope signals, and when there are multiple signals in the environment, CM DOA estimators are able to separate signals from each other using the CM signal property. CM estimators then estimate the DOA for each signal individually.

This research compares the CRB for AS and CM DOA estimators for a selected system. The CRB is also computed for this system when single and multiple and moving objects are present. The CRB_{AS} and CRB_{CM} are found to be different for the multiple signal case and moving object cases.

15. SUBJECT TERMS

Passive Radar, Passive Coherent Location System, Passive Sensor Location System, Bistatic Radar, Multistatic Radar, Cramer-Rao Bound, Direction of Arrival, DOA Estimator, Array Antennas, Statistical Error Analysis.

16. SECURITY CLASSIFICATION OF:			17. LIMITATION OF ABSTRACT	18. NUMBER OF PAGES	19a. NAME OF RESPONSIBLE PERSON
a. REPORT	b. ABSTRACT	c. THIS PAGE			Maj. Roger L. Claypoole, Jr., PhD.
U	U	U	UU	110	19b. TELEPHONE NUMBER (937) 255-3636, ext 4625; e-mail: Roger.Claypoole@afit.edu

Standard Form 298 (Rev. 8-98)
Prescribed by ANSI Std. Z39-18